THE ROLE OF CYPIN IN REGULATING SYNAPTIC CONTENT AND TRANSMISSION

By

ANA R. RODRIGUEZ

A dissertation submitted to the

Graduate School-New Brunswick

and

The Graduate School of Biomedical Sciences

Rutgers, The State University of New Jersey

In partial fulfillment of the requirements

For the degree of

Doctor of Philosophy

Graduate Program in Biomedical Engineering

Written under the direction of

Bonnie L. Firestein

And approved by

_____

_____

_____

_____

_____

_____

New Brunswick, New Jersey

October, 2016

ABSTRACT OF THE DISSERTATION

The Role of Cypin in Regulating Synaptic Content and Transmission

by ANA R. RODRIGUEZ

Dissertation Director:

Bonnie L. Firestein, Ph.D.

Proper synaptic transmission is essential for normal brain function and requires the precise spatial and functional assembly of molecular signal transduction machinery at synaptic sites and the correct morphology of dendrites and their branches. Defects in synaptogenesis and dendritogenesis are implicated in neurological and neurodevelopmental disorders. Cypin (**cy**tosolic **P**SD-95 **in**teractor) is a core regulator of dendrite branching and decreases the synaptic clustering of the scaffolding protein PSD-95 in rat hippocampal neurons. This dissertation will explore the functional implications of altering cypin levels on PSD-95 protein and synaptic function. We show that overexpression of cypin decreases synaptic PSD-95 protein levels, increases total PSD-95 protein levels, and increases the frequency of miniature excitatory postsynaptic currents (mEPSCs). We used microelectrode arrays to assess neuronal network dynamics after overexpression of cypin and uncovered changes in spiking variability that were not evident from the study of global network activity. The spike count variability of networks that overexpress cypin increases over time, and this variability is dependent on baseline activity levels. Moreover, attenuation of AMPAR-mediated synaptic transmission with the AMPAR antagonist CNQX (6-cyano-7-nitroquinoxaline-2,3-dione) shows that cypin overexpression results in a decrease in functional AMPARs, potentially interfering with

synaptic upscaling. Interestingly, we found that the alterations in synaptic transmission with overexpression of cypin are independent of cypin binding to PSD-95, whereas cypin-mediated changes in PSD-95 expression depend on cypin binding to PSD-95. Finally, we show that cypin interacts with the β7 subunit of the proteasome and interferes with its chymotryptic-like activity. Cypin overexpression results in increased ubiquitination of PSD-95, consistent with the observed increase in total PSD-95 levels. Taken together, our results suggest a proteasome-mediated role for cypin in the redistribution of PSD-95, and potentially, remodeling of the postsynaptic density associated with synaptic plasticity.

ACKNOWLEDGEMENTS

I would like to thank my advisor, Dr. Bonnie Firestein, for opening the doors of her lab to me and sharing her energy and enthusiasm for neuroscience with me from the very first day. Her guidance and support made my transition into her lab and the completion of my dissertation work possible, and I will always be grateful for the opportunity to work in her group. I would also like to thank my committee members: Dr. Ken Paradiso, Dr. David Meaney, Dr. Martin Yarmush, Dr. Kiran Madura, and Dr. Zhiping Pang. They have all been essential in the completion of this work in one way or another, and I thank them for their suggestions and thoughtful discussions over the years.

The members of the Firestein lab, past and present, made the last five years as enjoyable as possible and I thank them for that. Dr. Munjin Kwon and Dr. Kristina Hernández had the task of teaching this engineer how to think more like a biologist, and I couldn't have asked for better mentors in the lab. The many late nights and weekends spent in the lab were made so much better by their company and mentorship. Kristina and I became lab mates, desk mates, and inseparable friends during the time we shared in the Firestein lab, and I am very lucky to count with her support inside and outside of the lab. I would like to especially thank Kate O'Neill for being my partner in everything related to microelectrode arrays. We shared the frustrations, the failures, and the not so frequent successes, and I can't imagine having done this without her. I also want to acknowledge the animals that were used for this work. They are instrumental for the advancement of this field and without them, none of this is would be possible.

To my mom, dad, and brother for being the first ones to believe I could do this. Being far from them made this much harder and I've missed them deeply, but they made

sure that I felt their love and support every single day. They do more for me than I could ever ask for and I hope I'm able to repay it... at least with diplomas, which is my dad's favorite currency. I certainly couldn't have gotten this far without all the care packages full of Puerto Rican coffee. Their encouragement has meant more to me than I can possibly express and I can't thank them enough.

I also want to thank the rest of my family in Puerto Rico for always keeping me close, for sending pictures, cards, and happy thoughts. My best friend Gretchen certainly qualifies as family and has being an amazing cheerleader along the way. I feel so lucky to have her and am incredibly grateful for our friendship. I thank her for hopping on a plane for spontaneous weekend trips and always wanting to hear me practice my talks even if she has no idea what I'm talking about. I also want to thank the rest of my college friends – Chivi, Maqui, and Meran – for being there during the ups and downs of grad school and coming to visit as often as possible. I made great friends in grad school as well, and I'd especially like to thank Dr. Chris Utter, Dr. Andrea Gray, Dr. Mehdi Ghodbane, and Corina White for more venting sessions than I can count.

Lastly, I would like to thank my boyfriend Chris Dziedziak for his endless support and his beautiful family for allowing me to experience the love of a family away from home. Chris had the very difficult task of accompanying me towards the end of this grad school marathon and I can't thank him enough for everything he has done for me. He has being a daily source of support and cheered me on like I never imagined was possible. I can't thank him enough for all the ways he made me feel loved and cared for, and for believing in me blindly.

DEDICATION

To Mami Sandra y Papi Chú

TABLE OF CONTENTS

Chapter 1: Introduction

Communication between neurons occurs at highly specialized domains where information is processed, integrated, and propagated – the synapse. The majority of synapses occur at contacts between a presynaptic axon and a postsynaptic dendrite, most often at a dendritic spine. Axons and dendrites are highly specialized extensions and differ in morphology and function as well as in their cytoskeletal orientation. Axons transmit signals to other neurons, while dendrites have highly branched structures that are functionally specialized to receive and integrate inputs from presynaptic axons. Dendrite branching patterns and the extent of branching are directly associated with the amount and distribution of signals that a neurons receives and processes and depends upon intrinsic and extrinsic factors, such as neuronal activity (Kulkarni and Firestein 2012). Dendritic spines are membranous structures that protrude from dendrites, where they receive most of the excitatory synapses in the brain and allow individual synapses to be isolated from other synapses on the same neuron. Spines contain essential postsynaptic components, an actin cytoskeleton, and various organelles (Morgan Sheng and Hoogenraad 2007). They are highly heterogeneous structures, and their number, size, and shape change with connectivity between neurons and synaptic strength.

Proper synaptic transmission is essential for normal brain function and requires the precise assembly of molecular signal transduction machinery on both sides of the synapse as well as correct establishment of dendrites and their branches (Vetter et al. 2012). Defects in synaptogenesis and dendritogenesis lead to impaired synaptic transmission and are implicated in neurological and neurodevelopmental disorders, such

as schizophrenia, autism, and Alzheimer's disease (reviewed in: Kulkarni and Firestein 2012). For example, individuals with schizophrenia, a neuropsychiatric disorder characterized by cognitive impairment and significant altered perception, exhibit reduced dendrite branching and spine density in pyramidal neurons in the dorsolateral prefrontal cortex (Konopaske et al. 2014; Hernandez et al. 2016). This is thought to result in abnormal circuitry, disturbances in learning and memory, as well as a failure to use higher cognitive function to integrate experiences (Kulkarni and Firestein 2012).

Modifying the strength of synaptic transmission, commonly referred to as synaptic plasticity, is a fundamental mechanism for the storage and processing of information in the brain. Therefore, synaptic plasticity is essential during development and in learning and memory. Synaptic plasticity can be activity-dependent (Malenka and Bear 2004) and is mediated by the modification of synaptic proteins and a structural remodeling of the postsynaptic density (PSD), a specialized electron-dense structure at the postsynaptic membrane where receptors, scaffold proteins, and signaling molecules are highly concentrated (M Sheng 2001). Many of the proteins that make up the PSD of excitatory synapses are known to contain PDZ (**P**SD-95/**D**lg/**Z**O-1) domains, protein-protein interaction regions that interact with ligand proteins at their C-termini (Keith and El-Husseini 2008). These PDZ-containing proteins bind various types of synaptic proteins and organize and regulate the proteins at the excitatory synapse.

1.1 PSD-95 (**p**ost**s**ynaptic **d**ensity protein **95**)

Postsynaptic density protein 95 (PSD-95 or SAP-90) is a major scaffolding molecule found at the PSD of excitatory glutamatergic synapses. PSD-95 belongs to the

membrane-associated guanylate kinase (MAGUK) family of proteins and contains three N-terminal PDZ domains, an SH3 (Src-homology-3) domain, and a guanylate kinase (GK) homology domain. Other MAGUKs found at excitatory synapses include PSD-93, **s**ynapse **a**ssociated **p**rotein (SAP)102, and SAP97. The majority of excitatory synapses use glutamate as the neurotransmitter (Morgan Sheng and Hoogenraad 2007). PSD-95 is found in virtually every excitatory glutamatergic synapse and is associated with the trafficking and anchoring of glutamate receptors, particularly AMPA (alpha-amino-3-hydroxy-5-methyl-4-isoxazolepropionic acid), and NMDA (N-methyl-D-aspartate) receptors (Bredt and Nicholl 2003; Lin et al. 2004).

NMDA receptors (NMDARs) are calcium-permeable and play a central role in synaptic plasticity (Malenka and Bear 2004). NMDAR activation triggers a signaling cascade that results in an increase in the number of AMPA receptors (AMPARs) in the postsynaptic membrane, leading to long-term potentiation (LTP) of synaptic strength (Chater and Goda 2014). In contrast, weak and prolonged activation of NMDARs results in a decrease in postsynaptic AMPARs and long-term depression (LTD; Malenka and Bear 2004). PSD-95 interacts directly with NMDARs (Lin et al. 2004) and indirectly with AMPARs via the auxiliary protein stargazin (Schnell et al. 2002), and these interactions are important for proper receptor function. AMPARs are particularly mobile and diffuse rapidly between synaptic and extrasynaptic sites (Schnell et al. 2002). PSD-95 overexpression increases the number of AMPARs at synapses (Schnell et al. 2002), and PSD-95 knockout mice exhibit impaired AMPAR function (Béïque et al. 2006). Moreover, PSD-95 expression increases surface expression ad channel opening rates of NMDARs (Lin et al. 2004).

PSD-95 overexpression in cultured hippocampal neurons drives the maturation of synapses through an increase in size and number of dendritic spines and enhanced postsynaptic clustering and activity of glutamate receptors (A. E. El-Husseini et al. 2000; Schnell et al. 2002). Moreover, PSD-95 required to sustain the molecular organization of the PSD. Electron microscopy tomography showed that reduced PSD-95 after RNA interference knockdown results in loss of patches of vertical filaments in the PSD of hippocampal neurons (X. Chen et al. 2011). In addition, our laboratory showed that PSD-95 also has a non-synaptic role and acts as a stop signal for dendrite branching in hippocampal neurons (Charych et al. 2006).

1.2 Cypin

Cypin (**cy**tosolic **P**SD-95 **in**teractor) was originally identified as a protein that interacts with PSD-95 in rat brain and decreases its synaptic localization in hippocampal neurons (Firestein et al. 1999). Cypin terminates in a canonical PDZ-interacting sequence, –SSSV, and binds to the PDZ1 and PDZ2 domains of PSD-95. Cypin is found in the neck of synaptic spines and the shafts of dendrites but is normally absent from the postsynaptic density and spine head (Firestein et al. 1999). Cypin expression is evident as early as 4 days *in vitro* (DIV) in cultured hippocampal neurons and increases as neurons mature (Akum et al. 2004).

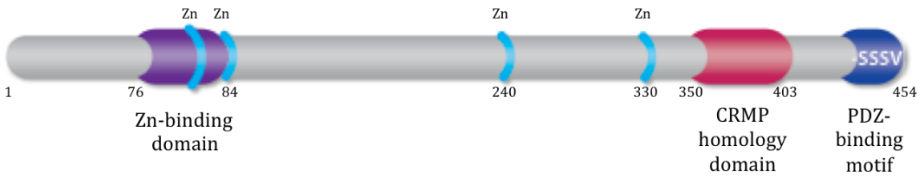

Figure 1-1. Schematic of cypin and its protein domains. Cypin is a 454-amino acid (aa) protein that contains a 9 aa zinc-binding motif necessary for its guanine deaminase activity, a CRMP homology domain, and a C-terminal PDZ-binding motif that associates with PSD-95 and other MAGUKs. Amino acids 240 and 330 are also involved in binding zinc.

Cypin is a guanine deaminase, and in addition to a C-terminal PDZ-binding motif, contains a zinc-binding motif and a CRMP (**c**ollapsin **r**esponse **m**ediator **p**rotein) homology domain, which mediates the binding of tubulin heterodimers to cypin **(Fig. 1-1**; Akum et al. 2004**).** Extensive research in our laboratory has identified cypin as a key regulator of dendrite branching in rat hippocampal neurons (Akum et al. 2004; Charych et al. 2006; M. Kwon et al. 2011; Tseng and Firestein 2011; O'Neill et al. 2015). Cypin binds tubulin heterodimers and promotes microtubule assembly, resulting in increased dendrite branching when cypin is overexpressed (Akum et al. 2004). Cypin knockdown decreases dendrite number. In addition, brain-derived neurotrophic factor (BDNF) and the small GTPase RhoA, two well-studied dendrite patterning regulators, act via cypin-dependent pathways (H. Chen and Firestein 2007; M. Kwon et al. 2011). BDNF increases proximal dendrite branching in rat hippocampal neurons via cAMP response element-binding protein (CREB)-dependent transcriptional regulation of cypin (M. Kwon et al. 2011). In contrast, activation of RhoA results in decreased dendrite branching by regulating translation of cypin (H. Chen and Firestein 2007).

1.3 Microelectrode arrays (MEAs) for the study of neuronal network dynamics

In vitro neuronal networks are widely used as an experimental model system to study the mechanisms that govern neuronal circuitry dynamics and information processing. Microelectrode arrays (MEAs) have become a useful tool to study the electrical activity of neuronal networks and answer physiologically relevant questions at the network level. MEAs contain a large number of evenly spaced electrodes embedded in the bottom of the dish, where brain slices or monolayers of dissociated neuronal cultures are established and maintained (Hales, Rolston, and Potter 2010). These neuronal networks have been found to conserve many of the properties that distinguish neurons *in vivo,* such as connectivity, excitation/inhibition ratio, and plasticity (Eytan et al. 2004; Wagenaar, Pine, and Potter 2006). Moreover, cultures in MEAs respond to pharmacological treatments in similar concentration ranges to those used in *in vivo* studies (Gramowski, Schiffmann, and Gross 2000; Morefield et al. 2000; Gullo et al. 2014), making them valuable tools in the screening of pharmacological or toxicological compounds (Kutzing, Luo, and Firestein 2011; Kutzing, Luo, and Firestein 2012).

Using MEA technology to examine changes in the electrical activity of neuronal networks also offers advantages over other more traditional electrophysiological techniques. MEA recordings are non-invasive, which allows the user to perform multiple and long-term recordings that shed light into the dynamic function of networks of neurons. Because the cultures are easy to monitor and can survive for extended periods of time, it is possible to obtain information from the same cells, or groups of cells, at distinct points in time (Gross et al. 1995). In addition, the multiple recording sites make it possible

to address interactions between neurons at multiple different locations within the network (Wagenaar, Pine, and Potter 2006).

Perhaps the greatest advantage of MEA technology in recent years has been the wide variety of analyses that continue to be developed, improved, and shared to study multiple processes and paradigms of interest at the single unit and network level (Quiroga, Nadasdy, and Ben-Shaul 2004; Churchland et al. 2010; Fikret E Kapucu et al. 2012; Harris et al. 2016). Combined measurements of neuronal spiking, bursting, and population-wide synchronization with parameters that describe the temporal dynamics and variability of neuronal activity have been used successfully to answer questions related to neuronal circuit establishment and maturation in different systems (Vogel 2005; Gullo et al. 2012). For example, MEAs were used to distinguish between inhibitory and excitatory neurons on the basis of the distinct variability in their spiking activity (Becchetti et al. 2012) and developmental changes in spike waveform properties (Weir et al. 2014). Hence, MEAs represent a valuable tool to obtain spatiotemporal information from neuronal circuits.

1.4 Thesis overview

Cypin is a major regulator of dendrite branching and influences the synaptic clustering of the scaffolding protein PSD-95. This dissertation will explore the functional implications of altering cypin levels on PSD-95 protein and synaptic function. In Chapters 2 and 3, we use microelectrode array technology to investigate the changes in neuronal circuit dynamics that result from alteration in cypin levels. We use measurements that describe both the population-wide activity of the networks as well as changes in spike

waveforms and the temporal distribution of activity. In Chapter 4, we examine the effects of altering cypin levels on PSD-95 protein expression and synaptic transmission. In particular, we study changes in AMPAR-mediated activity using MEAs. Finally, in Chapter 5 we investigate a new role for cypin as a proteasome interactor.

Chapter 2: Evaluation of the effect of cypin overexpression on overall network activity parameters

2.1 Introduction

The structure and function of neuronal networks undergo constant modification and development (Tau and Peterson 2010). A wide range of cues determine the cellular and morphological characteristics of a neuron and the circuits they ultimately form. Regulation of dendrite formation, branching, and patterning is crucial for the establishment of proper neuronal circuitry (Vetter et al. 2012; Kulkarni and Firestein 2012). Our laboratory has identified cypin as a core regulator of dendritic arborization in hippocampal neurons and has shown that overexpression of cypin during the active dendrite branching period results in increased branching (Akum et al. 2004; Charych et al. 2006; M. Kwon et al. 2011; O'Neill et al. 2015). In addition, cypin was originally identified as a protein that interacts with the scaffolding protein PSD-95 and decreases its clustering at synapses (Firestein et al. 1999). Cypin has a clear role in the development of dendrite branches and is known to bind to PSD-95 (Firestein et al. 1999), affecting PSD-95 expression levels; however, its role in regulating synaptic dynamics is currently unclear.

Multi-site electrophysiological recordings have been used extensively to characterize neuronal networks physiologically. Currently, microelectrode arrays (MEAs) are the standard technology used to study spatiotemporal changes in neuronal network dynamics (reviewed in (Massobrio et al. 2015; Obien et al. 2015)). This is of particular benefit when studying the response of neuronal circuitry to toxicological or pharmacological compounds, as MEAs allow for monitoring activity before and after

treatments in the same neuronal culture (Chiappalone et al. 2007; Fikret Emre Kapucu et al. 2016). For example, our laboratory has used MEAs in an *in vitro* model of traumatic brain injury to study the effects of glutamate-mediated neurotoxicity that takes place as part of the chemical insult post-mechanical injury (Kutzing, Luo, and Firestein 2011; Kutzing, Luo, and Firestein 2012). The results of these studies suggest that exposing cortical neurons to different concentrations of excess glutamate results in functionally different injury profiles.

Studying network dynamics using MEAs allows for the monitoring of specific parameters that characterize the spontaneous or evoked activity of neuronal networks. The activity pattern of a neuronal network typically involves isolated spikes accompanied by bursts – periods of high electrical activity when multiple locations within the circuit display numerous action potentials during a short period of time (Raichman and Ben-Jacob 2008). An enhancement in burst strength and synchronization in a neuronal network can result as a response to learning stimulations (Chao and Chen 2005). Thus, these parameters and analysis tools allow us to study how changing molecular and cellular components of a network affect its functionality and dynamics. In addition, establishing MEA models of neurological diseases can be used to better understand how neuronal communication is altered in these disorders (Gullo et al. 2014). In one such study, Gambazzi and colleagues used lentiviral gene transfer to establish a cortical neuron model of Huntington's disease and found that these neurons exhibited a deficit in spike and burst rates, while the duration of bursts remained unchanged (Gambazzi et al. 2010).

The parameters used to describe network dynamics vary between studies, but there is a subset of measurements that are extensively employed in the field. For example,

the overall spike (G J Brewer et al. 2009; Biffi et al. 2013) and burst rates (Wagenaar, Pine, and Potter 2006; Fikret E Kapucu et al. 2012), as well as network synchronization (Eisenman et al. 2015; Selinger, Pancrazio, and Gross 2004; Chiappalone et al. 2007), are used in the majority of MEA studies that describe global network activity levels. In this chapter, we use these analyses to understand the functional consequence of cypin overexpression in networks of hippocampal neurons. MEA technology and widely-used analysis parameters that describe the overall activity of neuronal networks allow us to indirectly study whether changes in dendritic arborization and PSD-95 trafficking via cypin overexpression affect the dynamics of neuronal circuits.

2.2 Materials and Methods

2.2.1 Cell culture

Neuronal cultures were prepared from hippocampi of Sprague-Dawley rat embryos at 18 days of gestation. The hippocampi were mechanically dissociated by pipetting slowly through the bore of a fire-polished Pasteur pipette. MEAs (Multi Channel Systems, Germany) were coated with 0.5 mg/ml poly-D-lysine (PDL; Sigma) for at least 1 hour, washed three times with sterile water, and then coated with 10 µg/ml laminin (Sigma) for at least 30 minutes, and cultures were established at a density of $1x10^6$ cells/MEA. Cultures were maintained in NbActiv4 medium (BrainBits, LLC) at 37 °C and 5% CO_2. Half medium changes were performed every other day. All animals were cared for ethically in accordance with Institutional Animal Care and Use Committee (IACUC) standards.

2.2.2 Lentiviral particle production and transduction

The lentiviral plasmids were constructed by subcloning cDNAs encoding wild type cypin and cypin lacking the PDZ binding motif (cypinΔPDZ) into the control EGFP-expressing FG12 vector (gift from Dr. Chris Pröschel, University of Rochester School of Medicine). Lentiviral particles were generated by transfecting HEK293TN cells (ATCC) using the calcium phosphate precipitation method with one of the lentiviral plasmids, the packaging plasmid psPAX2, and the envelope plasmid pMD2.G (VSV-G). The medium was replaced 24 hours post-transfection and the medium containing viral particles was collected 48 hours later, concentrated using PEG-it virus precipitation solution (System Biosciences) according to the manufacturer's instructions, and stored at -80 °C until use. HEK293TN cells were maintained and transfected in Dulbecco's Modified Eagle Medium (DMEM; Life Technologies) containing 10% fetal bovine serum (Atlanta Biologicals). Neuronal cultures grown on MEAs were transduced on day *in vitro* (DIV) 10 with lentiviral supernatant and half of the culture medium was changed 36 hours later and every other day from then on. Successful transduction was confirmed through fluorescence microscopy.

2.2.3 Microelectrode Array Recordings

Standard MEAs containing 60 planar electrodes (59 recording electrodes and 1 internal reference electrode), each with a 10 μm diameter and an inter-electrode spacing of 200 μm (60MEA200/10iR-Ti-gr; Multi Channel Systems, Germany), were used for all experiments. Baseline recordings were performed on DIV10 immediately before lentiviral transduction, on DIV17, and on DIV21. Prior to each recording, the culture medium was saved and replaced with recording solution (144 mM NaCl, 10 mM KCl, 1 mM $MgCl_2$, 2 mM $CaCl_2$, 10 mM HEPES, 2 mM Na-pyruvate, 10 mM glucose, pH 7.4), and the MEA was

placed into the cell culture incubator for 5 minutes to allow it to reach equilibrium. After each recording, the cultures were washed twice with fresh culture medium before adding the saved conditioned medium. Each MEA was covered with a semipermeable lid (ALA MEA-MEM; ALA Scientific) during handling and recordings to prevent contamination from airborne pathogens.

Spontaneous electrical signals were monitored and recorded for 5 minutes using the data acquisition commercial software MC_Rack (Multi Channel Systems) as described previously by our group (Kutzing, Luo, and Firestein 2011). The temperature of the cultures was maintained at 37 °C on a heat-controlled stage and the signals were sampled at 20 kHz with an MEA1060-Inv-BC amplifier (Multi Channel Systems).

2.2.4 Signal Processing

The raw data were imported into MATLAB (MathWorks, Inc.) using MEA-Tools, an open-source toolbox. The signals were filtered through a 4^{th} order Butterworth filter (20-2,000 Hz) and a notch filter to remove 60 Hz electric hum. The electrodes that exhibited irregular activity or excessive noise were excluded from the analysis. The MATLAB routines used for signal processing and data analysis discussed in this section were developed by Kate O'Neill, in part based on previous work from our group (Kutzing, Luo, and Firestein 2011).

2.2.4.1 Spike Detection

Spikes were detected using an adaptive threshold. Briefly, a spike was defined as a signal with voltage exceeding a positive or negative threshold, chosen to be 4.5 standard deviations times the background noise for a 10 second window for each recording channel.

To ensure that spikes were counted only once on an electrode, spikes were detected at their maximum absolute value and interspike intervals (ISIs) had to be longer than 2 ms. When spike rate is reported, it refers to the number of spikes divided by the recording time (300 seconds). Active electrodes were defined as those whose firing rate was ≥ the 75th percentile of the distribution.

2.2.4.2 Burst Detection

Bursts were defined as an episode of densely packed spikes occurring in a channel. For a period of high activity to be classified as a burst, its core had to be composed of at least 4 spikes with a maximum ISI between two consecutive spikes of 100 ms (Chiappalone et al. 2007). Additional spikes within 200 ms of the burst core or 1/3 times the electrode firing rate were included as part of the burst train. When burst rate is reported, it refers to the number of bursts divided by the recording time (300 seconds).

2.2.4.3 Synchrony of Firing

We measured the synchrony of firing (SF) to assess how the bursting behavior of an electrode is correlated to that of the other bursting electrodes. Briefly, SF was defined as the number of times a pair of electrodes (x and y) fired together within the same burst (B_{xy}) normalized to the maximum number of times they could fire together ($B_{x|y}$; the number of bursts recorded from the higher bursting electrode of the two; Kutzing et al. 2011).

$$SF = \frac{B_{xy}}{B_{x|y}}$$

The mean synchrony of firing between all electrodes in a culture was calculated and reported.

2.2.5 Statistics

All data are presented as mean values ± standard error of the mean, with *n* indicating the number of MEAs. All statistical analyses were performed using Prism 7.0 (GraphPad, La Jolla, CA) with $p<0.05$ representing statistical significance.

2.3 Results

2.3.1 Hippocampal neurons cultured on MEAs exhibit spontaneous electrical activity

To study the consequence of altering cypin levels in neuronal network activity, we first cultured primary rat hippocampal neurons on MEAs **(Fig. 2-1A, B)**. We chose to maintain these hippocampal cultures in NbActiv4 medium, a serum-free cell culture medium that promotes higher spike rates in neuronal networks by enhancing synaptogenesis, not solely by promoting the growth of astroglia (Gregory J. Brewer et al. 2008). Our neuronal culture protocol was optimized to achieve healthy hippocampal cultures that remain electrically active for at least three weeks in culture.

We monitored and recorded the spontaneous electrical activity of the networks starting at DIV10 using the data acquisition software MC_Rack. Since we previously reported that cypin alters distal dendrite branching at this timepoint (Akum et al. 2004; O'Neill et al. 2015), DIV10 represents an appropriate timepoint to begin our network activity experiments. We found that network-wide robust spiking and bursting behavior

was evident **(Fig. 2-1C, D)** at this point in functional development of the networks, and DIV10 was chosen as the baseline timepoint for all future experiments.

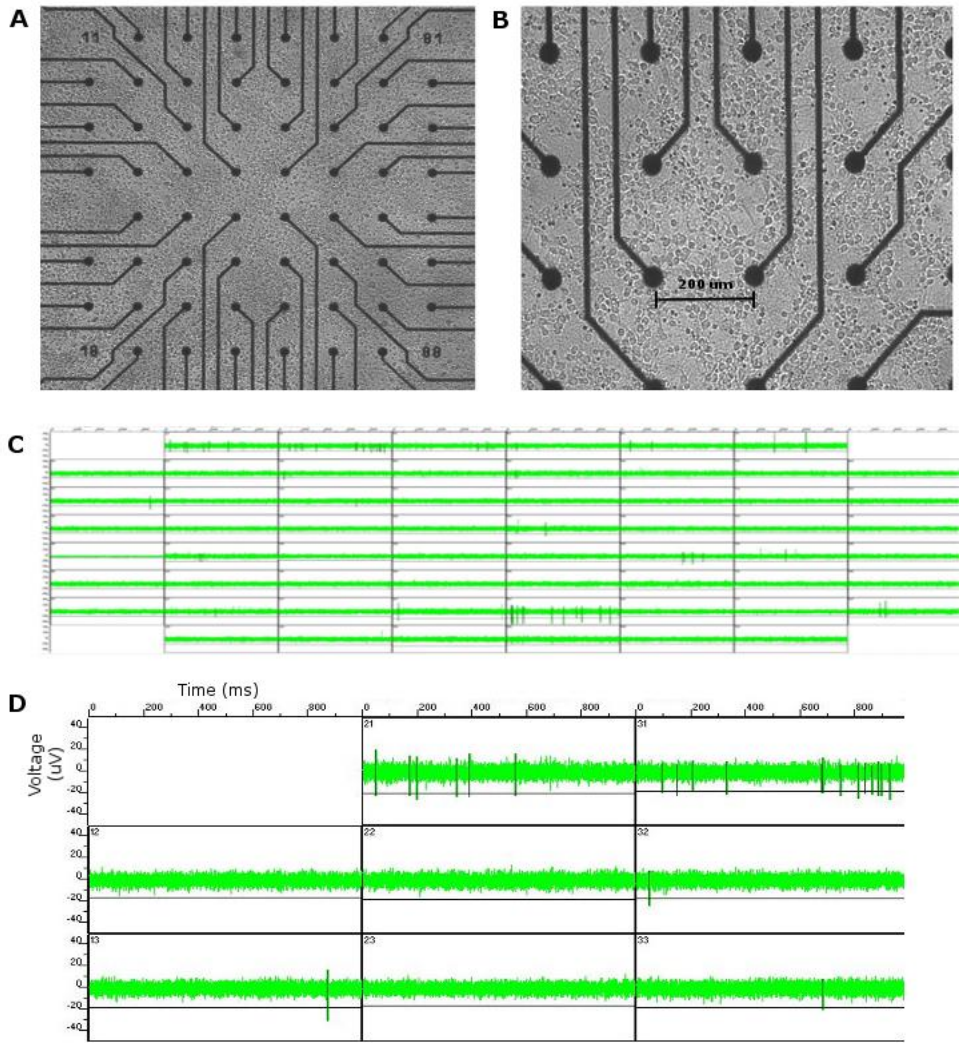

Figure 2-1. Hippocampal neurons grown on MEAs exhibit spontaneous electrical activity. (A) Recording area of an MEA at DIV10 (4X). Hippocampal neurons were cultured on MEAs for up to three weeks. (B) Zoomed in image of hippocampal neurons on electrode contacts. There is an inter-electrode spacing of 200 µm. (C,D) Neuronal networks at DIV10 exhibit spontaneous activity consisting of isolated

spikes and organized bursting events, as displayed on MC_Rack software during a recording.

To confirm that the recorded activity was transmitted synaptically, we recorded the electrical activity of the networks in the presence of a combination of synaptic blockers: 5 µM 6-cyano-7-nitroquinoxaline-2,3-dione (CNQX), 20 µM bicuculline, and 20 µM (2R)-amino-5-phosphonovaleric acid (APV) **(Fig. 2-2)**. The cocktail of synaptic blockers was added to the recording medium for the duration of the 5 minute equilibration prior to recording. This treatment resulted in a dramatic decrease in the overall spiking activity of the networks, confirming that the recorded activity resulted from action potentials induced by synaptic transmission.

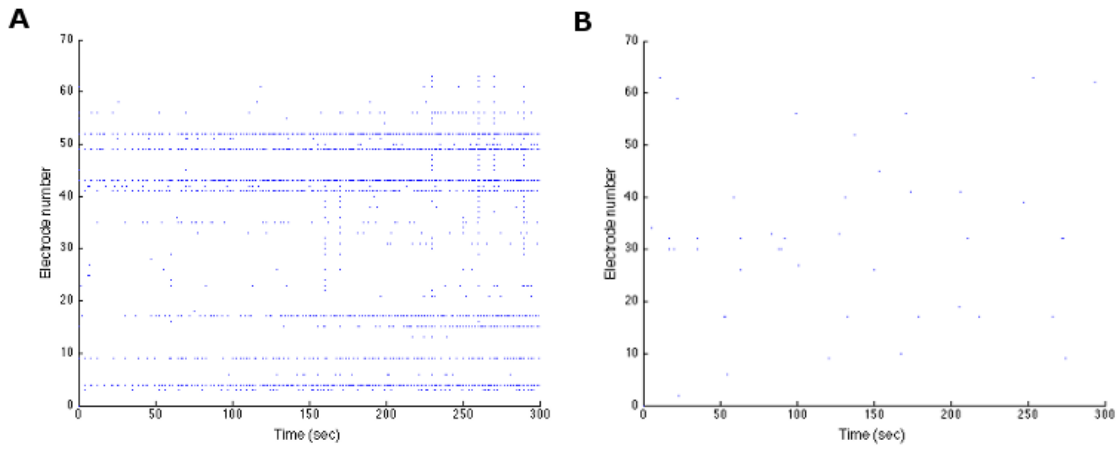

Figure 2-2. Recorded activity on MEAs is transmitted synaptically. (A) The cultures show a high level of activity prior to exposure to synaptic blockers at DIV14. Each dot represents a recorded spike. (B) Treatment with synaptic blockers almost completely abolishes the spontaneous electrical activity of the networks.

2.3.2 Lentiviral gene transfer in dense neuronal cultures on MEAs

The high cell density necessary to achieve robust network activity on MEAs represented a challenge when selecting a method to overexpress cypin in our cultures and assess the effects on neuronal network dynamics. We have extensive experience in transfection using a variety of methods, including nucleofection (Carrel et al. 2009), lipofection (Akum et al. 2004; Charych et al. 2006; M. Kwon et al. 2011; Sweet et al. 2011; O'Neill et al. 2015), and the calcium phosphate transfection method (Munjin Kwon and Firestein 2013; Tseng and Firestein 2011) in standard neuronal cultures. While these methods offer many advantages concerning ease of use, reproducibility, and cell survival, their inherent drawback lies in the fact that transfection efficiency in primary neurons is not high enough to study protein expression differences in a reliable manner. Lentiviruses are known to integrate stably into the host-cell genome of dividing and non-dividing cells (Karra and Dahm 2010; Geraerts et al. 2006). Therefore, they represent an attractive and efficient vehicle for stable gene transfer in neurons.

We constructed lentiviral vectors, produced lentiviral particles, and infected dense hippocampal cultures on MEAs at DIV10 immediately after baseline recording. Concentrated lentiviral particles were added to the culture medium, and the medium was replaced 36 hours later to avoid excessive toxicity. GFP expression was evident 4 days after transduction. **Figure 2-3** shows representative images of successfully transduced hippocampal cultures on MEAs. All transduced MEAs were visually inspected under a fluorescence microscope to confirm successful transduction based on GFP expression. When GFP expression was not extensive, the cultures were excluded from subsequent analyses.

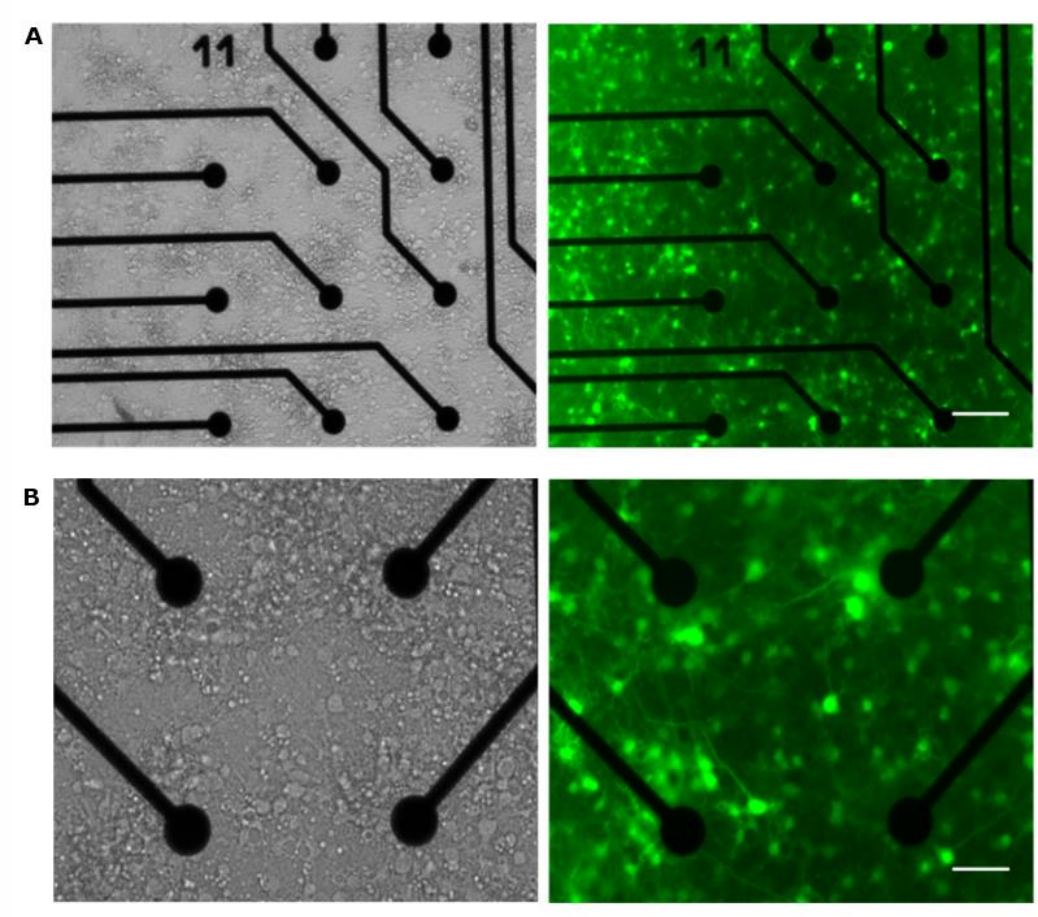

Figure 2-3. Transduced cultures on MEAs exhibit a high proportion of GFP-positive neurons. (A) Brightfield and fluorescence images (100X) of transduced MEA cultures at DIV17. Scale bar is 100 µm. (B) Higher magnification (200X) confirms that a high fraction of the cultured neurons express GFP. Scale bar is 50 µm.

Sister cultures were maintained in 6-well plates. We isolated protein from cell lysates of these cultures at DIV21 and subjected the samples to Western blot analysis to confirm transfection and expression efficiencies (see Chapter 4). Reproducible transduction efficiencies and protein expression confirmed that this method was the best gene transfer tool for the purposes of this project.

2.3.3 The effect of cypin overexpression on the spiking activity of neuronal networks

Hippocampal neurons were cultured on MEAs and transduced with lentivirus on DIV10 to overexpress GFP-tagged cypin or cypin lacking the PDZ binding motif (cypinΔPDZ). Cultures overexpressing only GFP were used as controls. The electrical activity of the neuronal networks was monitored and recorded on DIVs 17 and 21. Our cultures exhibited extensive GFP expression by DIV17 **(Fig. 2-3)**, a time at which MEA networks have been shown to have mature connections and a balance of inhibitory and excitatory synapses (Köller et al. 1990; Chiappalone et al. 2007).

We found that the overall spiking activity of the cultures decreased by DIV17 and remained at this lower level until DIV21, regardless of condition; networks that overexpressed cypin demonstrated a significantly lower decrease in spike rate when compared to control networks **(Fig. 2-4)**. This global decrease in activity is consistent with the notion that during the establishment and maturation of synapses within neural circuits, connections undergo continuous modification and refinement (Tau and Peterson 2010; Biffi et al. 2013). Early synaptic connections tend to be brief and frequent and give way to the more stable connections characteristic of mature circuits. Spontaneous average firing rates are negatively correlated with the extent of clustering (i.e., connection) in a network (Litwin-Kumar and Doiron 2012). Elimination of the PDZ-binding motif does not eliminate the effect of cypin overexpression (**Fig. 2-4**). Therefore, it is plausible that cypin overexpression promotes decreased functional connectivity within the neurons in a network and that this is not dependent on PSD-95 or PSD-95 family members binding.

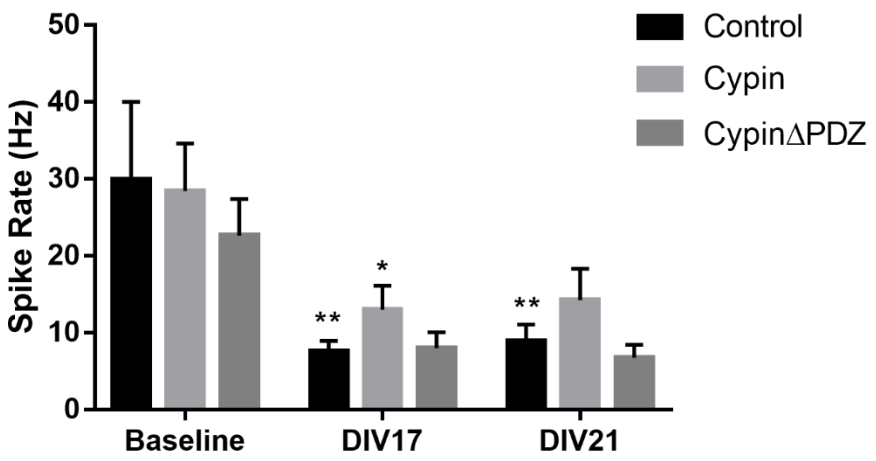

Figure 2-4. Spike Rate decreases over time for all conditions. We found that the rate of spiking activity decreased over time for control networks (p < 0.01) with respect to its baseline. Networks that overexpress cypin show no decrease in spike rate at DIV21 (*p < 0.05 for DIV17 and p = 0.0774 at DIV21) when compared to its baseline. The spike rate of networks that overexpress cypinΔPDZ demonstrate no decrease in spike rate on both DIV 17 and 21. Statistics were calculated by two-way ANOVA followed by Tukey's multiple comparisons test vs. baseline for each condition (*n* = 12 for control, 14 for cypin and 11 for cypinΔPDZ). Extreme outliers were removed when identified by Grubb's test with α = 0.05.**

We calculated the average number of active spiking electrodes to confirm that the reductions in detected activity were not due to a failure of our system to detect signals at later timepoints. Active electrodes were defined when spike rate was ≥ the 75th percentile of the distribution of spike rates for a particular culture. We found that the average number of active electrodes was similar for all timepoints and all conditions **(Fig. 2-5)**, suggesting that the observed decrease in activity was due to developmental changes in the network and/or our experimental manipulations.

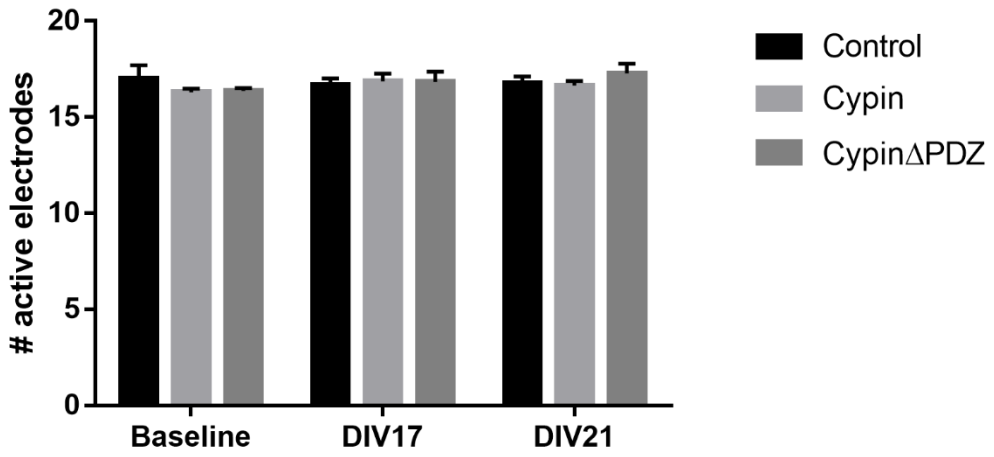

Figure 2-5. The number of active spiking electrodes is consistent between conditions. The average number of active electrodes was similar for all timepoints and experimental conditions. No statistical differences were observed as determined by two-way ANOVA followed by Tukey's multiple comparisons test (*n* = 12 for Control, 14 for Cypin and 11 for CypinΔPDZ).

Although the number of active electrodes proved to be a stable measurement, we observed high trial-to-trial variability associated with spiking data. This has been previously reported by others (Fikret E Kapucu et al. 2012; Litwin-Kumar and Doiron 2012; Fikret Emre Kapucu et al. 2016) and was visually evident when monitoring the activity during recordings as well as when displaying the spike rate distribution of individual cultures. To determine if the initial level of spiking activity dictates how active a culture remains over time, we classified the cultures depending on the initial average number of spikes detected: low baseline (<2,000 spikes), intermediate baseline (2-10,000 spikes), and high baseline (>10,000 spikes) **(Fig. 2-6)**. Since 2,000 spikes is a low activity threshold, we also analyzed intermediate and high baselines (>2,000 spikes) in combination to further elucidate if low baselines influence the observed global variability.

Overall average spike rate of the networks decreased over time regardless of the condition (**Fig. 2-6A**, corresponding to **Fig. 2-4** results). Spike rates decreased dramatically by DIV17 and stabilized until DIV21. Cultures with baselines under 2,000 spikes **(Fig. 2-6B)** exhibited little to no change in the average spike rates over time for all conditions with the exception of an increase in spiking for control networks on DIV17. Coincidentally, that specific timepoint displayed the highest level of variability between control cultures. When considering the group of cultures with baselines of >2,000 spikes **(Fig. 2-6C)**, it becomes evident that these networks behave almost identically to the overall group including the low baseline cultures (ALL, **Fig. 2-6A)**. These data imply that low baseline cultures do not make a large contribution to the overall spike rate reduction observed when considering the full distribution of spike rates. In contrast to data for all spikes and >2,000 spikes (**Fig. 2-6A, C**), the spike rate of networks with intermediate baselines that overexpress cypin remain relatively unchanged over time while networks overexpressing GFP and cypinΔPDZ show the observed trend towards a decrease in spike rate over time. Finally, cultures with initial high spike rates **(Fig. 2-6E)** show significant reductions in activity by DIV17 and DIV21 regardless of the condition.

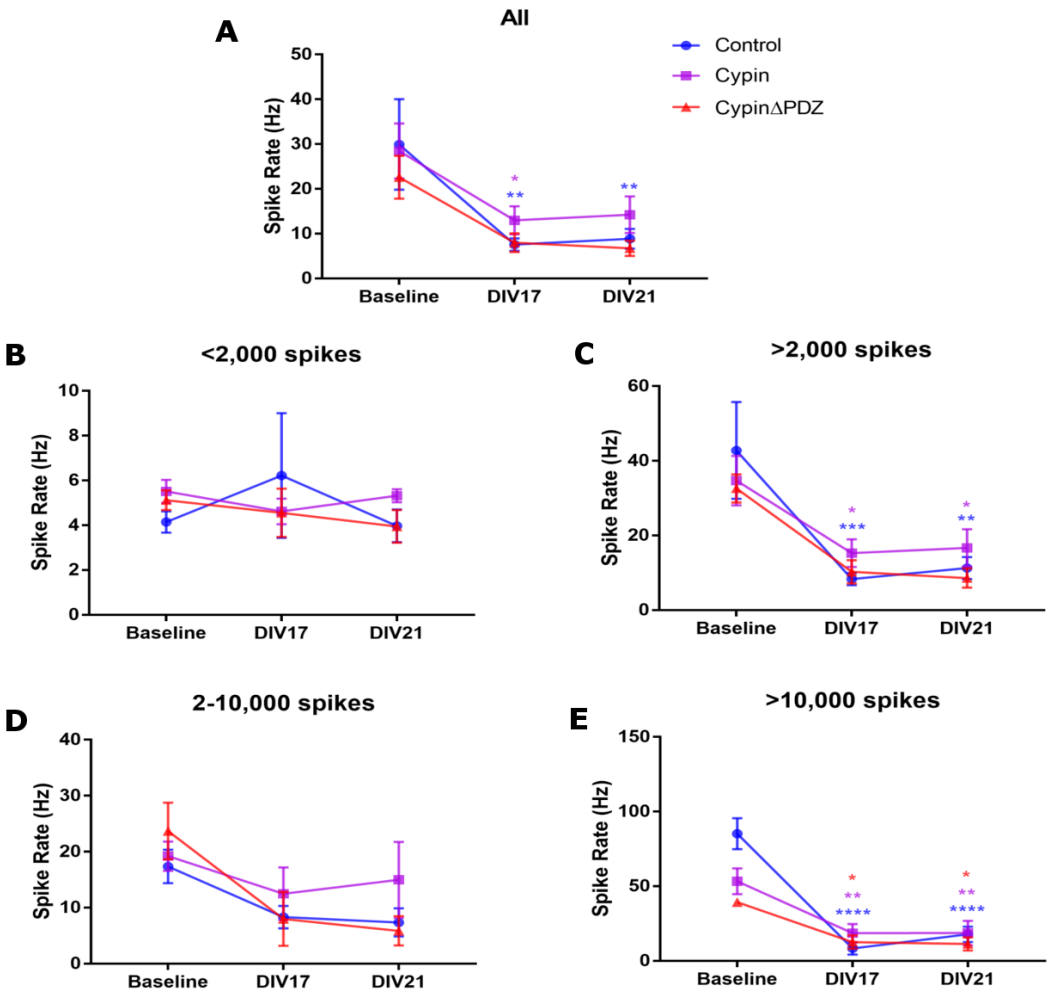

Figure 2-6. Changes in spike rate based on baseline activity levels. The extent of spike rate decrease is dependent on initial level of activity. (A) Spike rates decreased dramatically by DIV17 and stabilize until DIV21 (*n* = 12 for Control, 14 for Cypin and 11 for CypinΔPDZ). (B) Spike rates exhibit little to no change for cultures with low baselines (*n* = 4 for Control, 3 for Cypin and 4 for CypinΔPDZ). (C) Low baseline cultures do not contribute to the overall spike rate reduction (*n* = 8 for Control, 11 for Cypin and 7 for CypinΔPDZ). (D) Network activity of cultures with intermediate baselines shows little to no change after cypin overexpression (*n* = 5 for Control, 6 for Cypin and 3 for CypinΔPDZ). (E) Spike rates decrease for all

conditions in networks with high baselines (*n* = 3 for Control, 5 for Cypin and 4 for CypinΔPDZ). Statistics were calculated with respect to each group's baseline by two-way ANOVA followed by Tukey's multiple comparisons test (*p < 0.05, **p < 0.01, ***p < 0.001, ****p < 0.0001). Extreme outliers were removed when identified by Grubb's test with α = 0.05.

In summary, the spike rate of cultures with initially low baselines were not affected by network development or cypin overexpression. In contrast, cultures with high baselines show the greatest reductions in spike rates over time for all conditions. Our data suggest that when cypin is overexpressed in cultures with intermediate baselines, the spike rate, and potentially the functional connectivity, remain unchanged. Interestingly, the average spike rate of networks that overexpress cypinΔPDZ only changes at higher baselines. One possible explanation is that networks of neurons overexpressing cypin and cypinΔPDZ take longer to mature, hence demonstrating smaller decreases in firing. Our data suggest that cypin overexpression has different effects on network activity and that the effects are dependent on the initial spike rate.

2.3.4 The effect of cypin overexpression on the bursting activity of neuronal networks

Bursts, or periods of organized high frequency spiking, are characteristic of developing and mature neuronal networks (Wagenaar, Pine, and Potter 2006; Biffi et al. 2013). We measured the level of spontaneous bursting activity that occurred in our networks over time and found that burst rates did not decrease significantly over time **(Fig. 2-7)**. It is important to note that the variability of the baseline responses renders the

results more difficult to interpret, although bursting levels do not depend on initial bursting (data not shown) as spiking levels do.

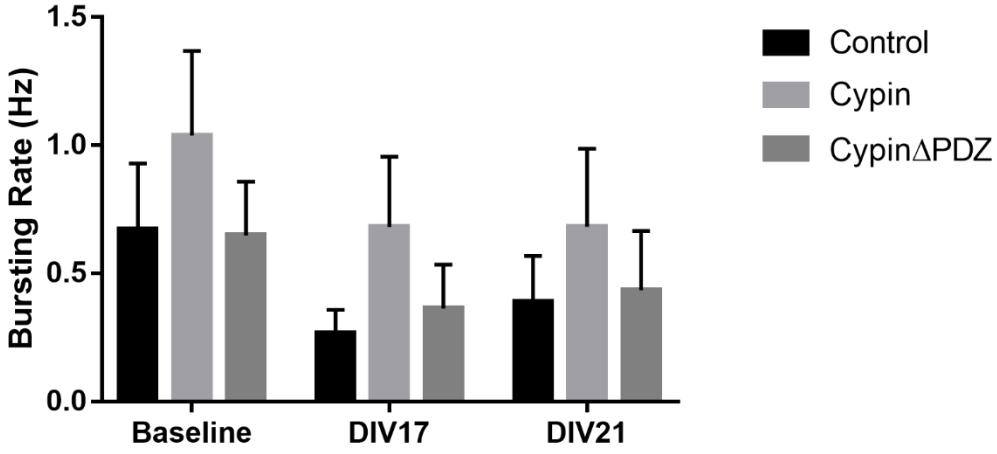

Figure 2-7. Spontaneous bursting rate does not significantly change over time. Cypin or cypinΔPDZ overexpression results in no significant changes to bursting activity. No statistical differences were observed as determined by two-way ANOVA followed by Tukey's multiple comparisons test (*n* = 12 for Control, 14 for Cypin and 11 for CypinΔPDZ). Extreme outliers were removed when identified by Grubb's test with α = 0.05.

We calculated the average number of active bursting electrodes with burst rates ≥ the 75th percentile of the distribution of bursting rates for a particular culture. We found that the average number of active electrodes was similar between conditions at DIVs 10 and 21 (**Fig. 2-8**). The average number of active electrodes remained unchanged for networks overexpressing cypin between DIV10 and DIV21.

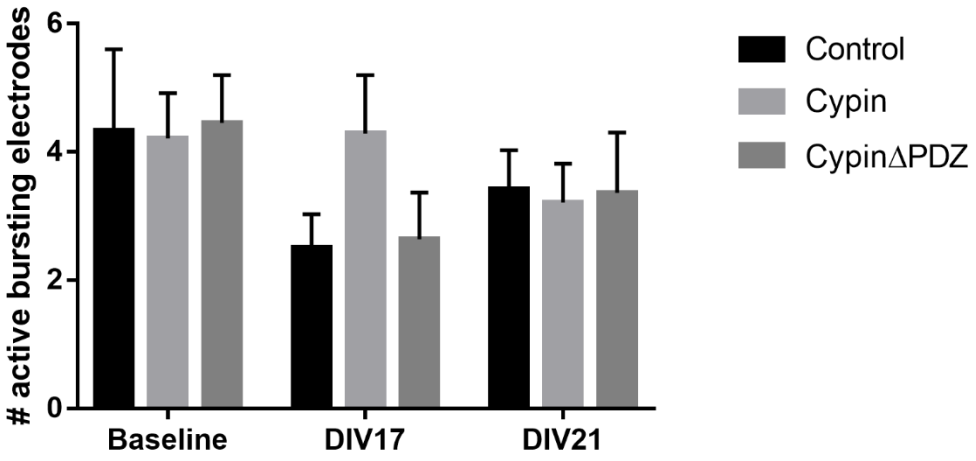

Figure 2-8. The number of active bursting electrodes. The average number of active electrodes remained consistent for cypin networks over time. No statistical differences were observed as determined by two-way ANOVA followed by Tukey's multiple comparisons test (*n* = 12 for Control, 14 for Cypin and 11 for CypinΔPDZ).

To further investigate the bursting behavior of the networks, we calculated the average burst duration **(Fig. 2-9)** and the average number of spikes that made up each burst **(Fig. 2-10)**. It is interesting to note that although the baseline bursting behavior was highly variable between conditions, the temporal length of the bursts remained constant over time **(Fig. 2-9)**. These data suggest that the burst duration is not dependent on the level of bursting in our cultures.

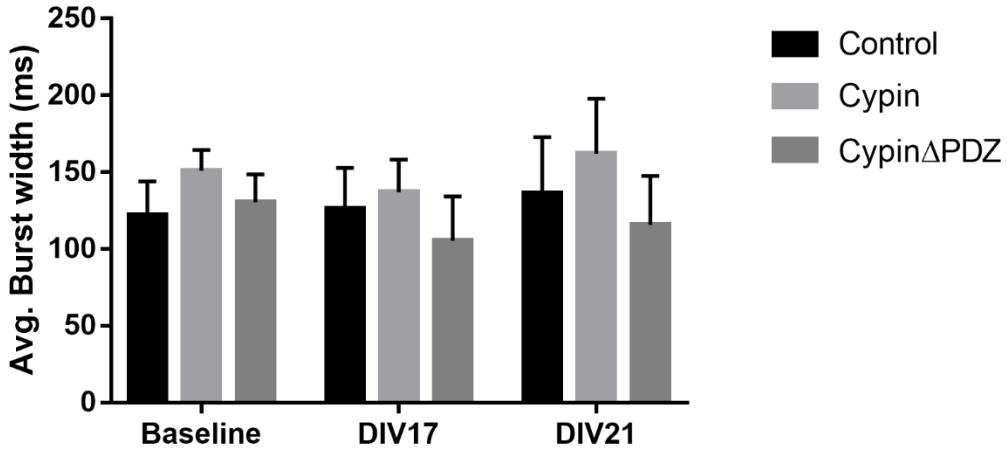

Figure 2-9. Average burst width. The temporal length of bursting events is constant over time. No statistical differences were observed as determined by two-way ANOVA followed by Tukey's multiple comparisons test (*n* = 12 for Control, 14 for Cypin and 11 for CypinΔPDZ).

Similarly, the average number of spikes per burst remained consistent between conditions **(Fig. 2-10)**. There was a statistically significant increase observed by DIV21 in networks overexpressing cypin, corresponding with the trend observed for temporal duration of the bursts. Spike composition and burst duration do not appear to be directly related to burst rate; however, our data suggests that bursting behavior is more robust in networks that overexpress cypin than in other experimental conditions.

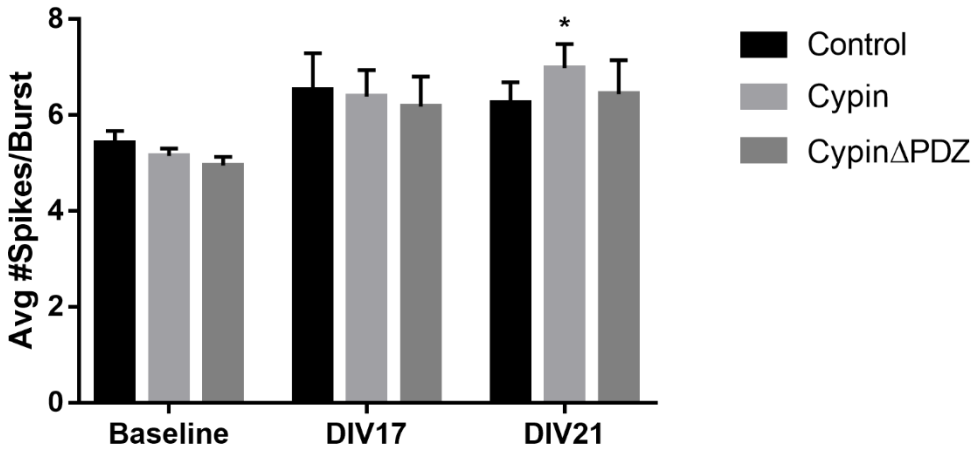

Figure 2-10. The average number of spikes per burst is consistent between conditions and timepoints; however, there is an increase (*p<0.05) in the average number of spikes that make up bursts in networks that overexpress cypin in DIV21 when compared to its baseline. Statistics were calculated by two-way ANOVA followed by Tukey's multiple comparisons test (*n* = 12 for Control, 14 for Cypin and 11 for CypinΔPDZ). Extreme outliers were removed when identified by Grubb's test with α = 0.05.

2.3.5 Changes in synchrony of firing after cypin overexpression

To further understand whether the detected activity was organized, we calculated the synchrony of firing of bursting events. For this, we calculated the synchrony between every pair of electrodes and then calculated the mean between all the bursting pairs. As with bursting activity, we found that the initial synchrony of firing was highly variable between conditions **(Fig. 2-11)**. The synchrony of firing in control and cypinΔPDZ networks demonstrated little to no change over time even though their respective baselines were not similar. It remains a possibility that this is a result of averaging small increases and decreases in synchronization. It is interesting to note that cypin networks

exhibited the highest baseline bursting levels of all conditions but are not necessarily the most synchronized at that timepoint. This suggests that synchronized firing is not directly related to the amount of bursts exhibited by our networks.

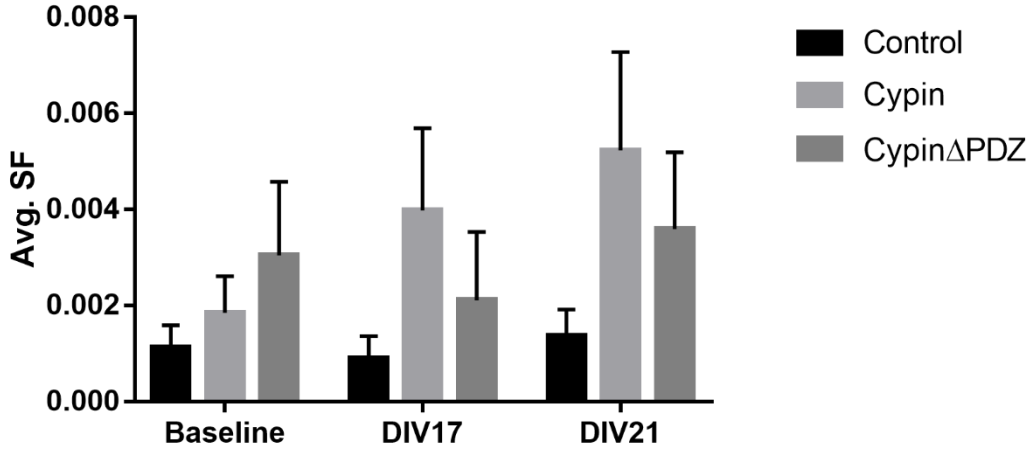

Figure 2-11. The effect of cypin overexpression on synchronized firing. Networks overexpressing GFP, cypin and cypinΔPDZ display little to no change in synchrony. No statistical differences were observed as determined by two-way ANOVA followed by Tukey's multiple comparisons test (*n* = 12 for Control, 14 for Cypin and 11 for CypinΔPDZ). Extreme outliers were removed when identified by Grubb's test with α = 0.05.

2.4 Discussion

In this chapter, we used MEAs to examine the functional consequence of overexpressing cypin or the mutant cypinΔPDZ in hippocampal neuronal networks. We successfully established hippocampal cultures on MEAs and validated the analysis parameters previously used by our group to study functional changes in cortical networks

(Kutzing, Luo, and Firestein 2011). We found that hippocampal neurons exhibited robust spiking and bursting activity by DIV10, similar to what has been reported by others (Biffi et al. 2013). Since cypin promotes enhanced dendrite branching at this timepoint, we chose to transduce and alter cypin levels. Although lentiviral transduction has been shown to produce low toxicity in neuronal cultures (Geraerts et al. 2006), it is necessary to note that transduction may have produced a mild injury to our cultures and could have affected electrical activity. For the purposes of this analysis, we assume that since all cultures were transduced in the same manner, any adverse effects resulting from transduction affected all the cultures equally. Only cultures that were GFP-positive, visually healthy, and exhibited detectable spontaneous activity were used for further analysis.

We maintained sister cultures that were seeded and transduced in parallel to MEA cultures. Western blot analyses of protein lysates from these cultures confirmed cypin overexpression. Due to the high density of these cultures, we could not perform dendrite branching analysis. However, we have published extensively on the increased dendrite branching observed after cypin overexpression (Akum et al. 2004; M. Kwon et al. 2011; Charych et al. 2006; O'Neill et al. 2015) and infer that our cultures on MEAs also exhibited enhanced branching.

We measured the overall rate of spiking of the cultures immediately before transduction (baseline), 7 days later (DIV17), and 11 days later (DIV21). We observed that the overall rate of isolated spikes decreased by DIV17 for all conditions and stabilized until DIV21 and that this was not dependent on the number of electrodes that remained active. As networks mature, their firing rate is known to plateau (Tau and Peterson 2010; Biffi et al. 2013), which could explain the lack of change in activity from DIV17 to DIV21. The fact

that networks that overexpressed cypin and cypinΔPDZ demonstrated a lower degree of reduction in activity could be due to an enhanced ability to receive inputs due to increased dendrite branching (Charych et al. 2006). Moreover, a computational model of networks with clustered connections based on anatomical evidence showed that highly clustered networks demonstrate dynamic transitions between episodes of high and low firing rate (Litwin-Kumar and Doiron 2012). Due to the high cell density of our cultures, we hypothesize that this could occur in our system and that changes in activity that occur over short periods of time could be masked by averaging. We address these possibilities in in the next chapter.

A more detailed examination of the temporal change in spike rate revealed that cypin overexpression has slightly different effects on network activity and that this is dependent on the initial spike rate and independent of PSD-95 or PSD-95 family member binding. It is interesting to note that even when grouping the MEAs based on their average baseline activity, the inherent trial-to-trial variability is still evident (refer to baseline activity in **Fig. 2-6E** for example).

Bursting events are characteristic of neuronal networks and they represent periods of spatiotemporally organized activity. We found that the networks displayed no changes to bursting activity over time. We further characterized the bursting behavior of the networks by calculating the average burst width and the average number of spikes per burst. We found that the average temporal length of the bursts remained unchanged between conditions and over time, suggesting that burst length is not dependent on the rate of bursting. These data agree with a study by Gambazzi and colleagues showing that

the frequency of bursting events, and not the duration, is dependent on the overall activity of the network (Gambazzi et al. 2010).

We observed an increase in the average number of spikes per burst over time for all conditions, with networks overexpressing cypin exhibiting the highest participation of spikes in bursts. Overall, our data suggest that bursting behavior is unchanged in networks that overexpress cypin. However, variability is quite high, potentially masking any effects of cypin overexpression. In fact, when we calculated the overall average synchrony of firing of bursting events, we observed a trend towards an average increased synchronized firing of cypin networks over time that was not observed in control or cypinΔPDZ networks. It is important to note that this synchrony of firing describes instances when any two electrodes exhibited a bursting event at the same time and is thus possible to mask or exaggerate subtle effects by averaging.

Overall, the global network effects observed as a consequence of overexpressing cypin and cypinΔPDZ were subtle. We do not reject the possibility that, in addition to the high variability between trials, changes in our global parameters could be short-lived or not large since they include the full network. Given the high cell density and long time between transduction and recording, it is possible that compensatory mechanisms come into play and the network reaches homeostasis.

2.5 Acknowledgements

I would like to thank Kate O'Neill for her contribution in developing the MATLAB routines used for data analysis.

Chapter 3: Analysis of spiking variability after cypin overexpression

3.1 Introduction

One of the major goals of the neuroscience community is to understand the basic elements and functioning of neuronal network circuits. However, high variability in the spontaneous activity of neurons and in neuronal responses to stimuli represents a significant challenge for neuronal information processing (Moreno-Bote 2014). Numerical simulations have shown that spiking neurons emit chaotic and non-repetitive signals that are sensitive to small perturbations (Litwin-Kumar and Doiron 2012; Kuebler and Thivierge 2014). Analysis becomes increasingly challenging when simultaneously measuring the activity of many neurons, as is the case of microelectrode array recordings. Nevertheless, MEAs continue to be the gold standard to study how networks of neurons behave since MEAs allow for the recording of network activity without disrupting the natural functioning of the network, and various modifications that can be implemented to both the design and processing of MEAs and analysis of the obtained signals.

Development of methods to quantify spiking variability has gained significant attention in the field as it is now understood that the mean rate of activity provides an incomplete, yet valuable, characterization of neuronal network responses (Ponce-Alvarez, Kilavik, and Riehle 2010; Churchland et al. 2010; Kuebler and Thivierge 2014). Studying spiking variability provides a fuller understanding of how activity changes over time and exposes activity patterns that arise and might be masked when averaging. This analysis has proven valuable in studies that range from *in vitro* networks (Gullo et al. 2012; Becchetti et al. 2012) to animal studies (Churchland et al. 2010; Lei et al. 2011; White,

Abbott, and Fiser 2012) to computational models (Christodoulou and Cleanthous 2011; Litwin-Kumar and Doiron 2012; Moreno-Bote 2014). For example, a study by Churchland and colleagues (Churchland et al. 2010) showed a decline in the firing rate variability of neuronal responses in various areas of the feline cortex after the presentation of stimuli. Interestingly, they found that this stimulus-driven variability decrease was not dependent on the level of mean firing rate.

The most widely used statistics to measure spiking variability are the Fano factor (FF; Eden & Kramer 2010) and the coefficient of variation of interspike intervals (CV; Christodoulou & Bugmann 2001). The Fano factor measures the dispersion of the spike count distribution and is defined as the ratio of the variance to the mean of the number of spikes emitted in a fixed time interval. This statistic can be used to compare how the observed variability compares to that of a purely random, Poisson, process. For a Poisson process, the Fano factor is theoretically equal to 1 and Fano factors above 1 are said to denote higher variability in the firing rate (Eden and Kramer 2010; Kuebler and Thivierge 2014). In an example of how the Fano factor has been a valuable tool, Becchetti and colleagues demonstrated that the Fano factor was a reliable measure to distinguish between excitatory and inhibitory neurons in an MEA study of neocortical cultures from mice expressing GFP in GABAergic cells (Becchetti et al. 2012).

In contrast, the coefficient of variation (CV) of interspike intervals measures spiking variability in terms of precise spike timing. The CV is defined as the ratio of the standard deviation to the mean of the interspike intervals (William R Softky 1992). Similar to the Fano factor, neurons with spike trains that behave like a Poisson process are expected to have a CV equal to 1 and high CV values denote higher variability in spike

timing. In fact, cortical neurons have highly irregular interspike intervals (W R Softky and Koch 1993). Many factors have been proposed to be responsible for this high variability, with a balance of excitation and inhibition (Shadlen and Newsome 1994) and temporally-modulated synaptic inputs (Knoblauch 2012) being among the most prominent ones.

Finally, spike sorting algorithms allow us to uncover details about the individual signals that comprise the overall activity of a network. Each electrode in a microelectrode array will more than likely record activity from multiple neurons, especially in the case of high density cultures. Different neurons can fire in response to different stimuli, and thus, it is valuable to determine specific information about the spikes (Hernan Gonzalo Rey, Pedreira, and Quian Quiroga 2015). Each spike has a particular shape, and this is dependent on the morphology of the dendritic tree of the neuron, the distance from the neuron to the electrode, the coupling between the neuron and the electrode, and the properties of the recording medium (Gold et al. 2006; Fendyur et al. 2011; Hernan Gonzalo Rey, Pedreira, and Quian Quiroga 2015). The importance and value of spike sorting is best illustrated by a study where patients with epilepsy had electrodes implanted into the hippocampus and were presented with visual stimuli (Hernan G. Rey et al. 2015). Spike sorting based on waveform shape revealed that a subset of the neurons were selective to specific and individual stimuli regardless of an absence of firing rate changes.

In this chapter, we use multiple parameters mentioned above to study spiking variability after cypin overexpression in neuronal circuits. We applied these tools at the network level and uncovered changes that were not possible to isolate when only considering the mean rates of firing and synchronized bursting.

3.2 Materials and Methods

3.2.1 Cell culture

Neuronal cultures were prepared from hippocampi of Sprague-Dawley rat embryos at 18 days of gestation. The hippocampi were mechanically dissociated by pipetting slowly through the bore of a fire-polished Pasteur pipette. MEAs (Multi Channel Systems, Germany) were coated with 0.5 mg/ml poly-D-lysine (PDL; Sigma) for at least 1 hour, washed three times with sterile water, and then coated with 10 µg/ml laminin (Sigma) for at least 30 minutes, and cultures were established at a density of $1x10^6$ cells/MEA. Cultures were maintained in NbActiv4 medium (BrainBits, LLC) at 37 °C and 5% CO_2. Half medium changes were performed every other day. All animals were cared for ethically in accordance with Institutional Animal Care and Use Committee (IACUC) standards.

3.2.2 Lentiviral particle production and transduction

The lentiviral plasmids were constructed by subcloning cDNA encoding wild type cypin or cypin lacking the PDZ binding motif (cypinΔPDZ) into the control FG12 vector containing EGFP for expression (gift from Dr. Chris Pröschel, University of Rochester School of Medicine). Lentiviral particles were generated by transfecting HEK293TN cells (ATCC) using the calcium phosphate precipitation method with one of the lentiviral plasmids, the packaging plasmid psPAX2, and the envelope plasmid pMD2.G (VSV-G). The medium was replaced 24 hours post-transfection, and the medium containing viral particles was collected 48 hours later, concentrated using PEG-it virus precipitation solution (System Biosciences) according to the manufacturer's instructions, and stored at -80 °C until use. HEK293TN cells were maintained and transfected in Dulbecco's Modified Eagle Medium (DMEM; Life Technologies) containing 10% fetal bovine serum (Atlanta

Biologicals). Neuronal cultures grown on MEAs were transduced on day *in vitro* (DIV) 10 with lentiviral supernatant, and half of the culture medium was changed 36 hours later and every other day from then on. Successful transduction was confirmed through fluorescence microscopy.

3.2.3 Microelectrode Array Recordings

Standard MEAs containing 60 planar electrodes (59 recording electrodes and 1 internal reference electrode), each with a 10 μm diameter and an inter-electrode spacing of 200 μm (60MEA200/10iR-Ti-gr; Multi Channel Systems, Germany), were used for all experiments. Baseline recordings were performed on DIV10 immediately before lentiviral transduction, on DIV17, and on DIV21. Prior to each recording, the culture medium was saved and replaced with recording solution (144 mM NaCl, 10 mM KCl, 1 mM $MgCl_2$, 2 mM $CaCl_2$, 10 mM HEPES, 2 mM Na-pyruvate, 10 mM glucose, pH 7.4), and the MEA was placed into the cell culture incubator for 5 minutes to allow it to reach equilibrium. After each recording, the cultures were washed twice with fresh culture medium before adding the saved conditioned medium. Each MEA was covered with a semipermeable lid (ALA MEA-MEM; ALA Scientific) during handling and recordings to prevent contamination from airborne pathogens.

Spontaneous electrical signals were monitored and recorded for 5 minutes using the data acquisition commercial software MC_Rack (Multi Channel Systems) as described previously by our group (Kutzing, Luo, and Firestein 2011; Kutzing, Luo, and Firestein 2012). The temperature of the cultures was maintained at 37 °C on a heat-controlled stage and the signals were sampled at 20 kHz with an MEA1060-Inv-BC amplifier (Multi Channel Systems).

3.2.4 Signal Processing

The raw data were imported into MATLAB (MathWorks, Inc.) using MEA-Tools, an open-source toolbox. The signals were filtered through a 4th order Butterworth filter (20-2,000 Hz) and a notch filter to remove 60 Hz electric hum. The electrodes that exhibited irregular activity or excessive noise were excluded from the analysis. The MATLAB routines used for signal processing and data analysis discussed in this section were developed by Kate O'Neill, in part based on previous work from our group (Kutzing, Luo, and Firestein 2011).

3.2.4.1 Spike Detection

Spikes were detected using an adaptive threshold. Briefly, a spike was defined as a signal with voltage exceeding a positive or negative threshold, chosen to be 4.5 standard deviations times the background noise for a 10 second window for each recording channel. To ensure that spikes were counted only once on an electrode, spikes were detected at their maximum absolute value and interspike intervals (ISIs) had to be longer than 2 ms. When spike rate is reported, it refers to the number of spikes divided by the recording time (300 seconds). Active electrodes were defined as those whose firing rate was ≥ the 75th percentile of the distribution.

3.2.5 Measurements of Spiking Variability

3.2.5.1 Fano Factor

The spike count variability was measured by the Fano factor (FF). This parameter is used extensively (Churchland et al. 2010; White, Abbott, and Fiser 2012; Scaglione et al. 2011; Gullo et al. 2012) to broaden the understanding of neuronal network activity patterns;

it is defined as the ratio of the variance to the mean of the spike count in a given time interval (Eden and Kramer 2010):

$$FF = \frac{\sigma^2(spike\ count)}{mean(spike\ count)}$$

For every 300 seconds recording, we calculated a FF every 10 seconds and averaged all FF to obtain the mean Fano factor of the entire network. We process our data 10 seconds at a time, and this allowed us to incorporate the FF calculation into our analysis in a straightforward manner. For a random process with a Poisson distribution, the Fano factor is theoretically 1 (Eden and Kramer 2010; Gambazzi et al. 2010). In contrast, regular spike rates exhibit a FF equal to 0. High Fano factors are characteristic of irregular spiking (Churchland et al. 2010; Litwin-Kumar and Doiron 2012).

3.2.5.2 Interspike Interval

The interspike interval (ISI) is a measurement of the period of time between two consecutive spikes (W R Softky and Koch 1993; Kuebler and Thivierge 2014). ISI distributions provide valuable information about the temporal spiking patterns produced by neuronal networks. We calculated ISIs for every spike (minus one) per electrode to generate the distribution of ISIs for each of the 59 recording electrodes. We computed the average of the ISIs of all electrodes and obtained the mean ISI for each entire network.

3.2.5.3 Coefficient of Variation

The coefficient of variation (CV) is a standard measurement of the ISI variability (Vogel 2005). It is defined as the ratio of the standard deviation to the mean of the ISI (W R Softky and Koch 1993; Kuebler and Thivierge 2014):

$$CV = \frac{\sigma(ISI)}{mean(ISI)}$$

We calculated CVs for every electrode to generate the distribution of CVs for each of the 59 recording electrodes. We computed the average of all CVs to obtain the mean CV for each entire network. For a random process with a Poisson distribution, the CV is 1. CV tends to 0 for regular spike trains and is larger than 1 for irregular firing (W R Softky and Koch 1993).

3.2.6 Spike Sorting

We applied Wave clus, a spike sorting algorithm (Quiroga, Nadasdy, and Ben-Shaul 2004), to obtain information about individual neurons within our networks. Spike sorting extracts features from each spike and clusters them in classes that best reflect their shape. To do so, Wave clus calculates the wavelet transform for each spike and uses a set of the obtained wavelet coefficients as input for a clustering algorithm based on k-nearest neighbor interactions (Blatt, Wiseman, and Domany 1996). Using the wavelet transform instead of principal component analysis (PCA) to extract the shape information is advantageous because it allows for more specific discerning of spike features (Quiroga, Nadasdy, and Ben-Shaul 2004; Hernan Gonzalo Rey, Pedreira, and Quian Quiroga 2015).

We first detected individual spikes as described above. For each detected spike, we collected a spike time stamp and a waveform cutout spanning 1 ms before and 2.2 ms after the spike absolute maxima **(Fig. 3-1)**. The obtained waveform cutouts were sorted using the unsupervised Wave clus algorithm. After automatic clustering, we performed the suggested minor manual tuning (Quian Quiroga 2004) to improve the sorting accuracy.

All detected spikes for each condition and timepoints were included in the spike sorting analysis.

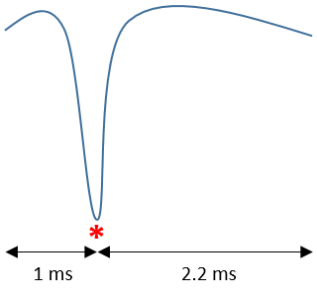

Figure 3-1. Spike cutout schematic. Spike waveform cutouts spanning 1 ms (19 data points) prior and 2.2 ms (44 data points) after the absolute maximum value of the spike (represented by *) were stored and sorted. All spikes were aligned by setting their maximum at data point 20.

3.2.7 Statistics

All data are presented as mean values ± standard error of the mean (s.e.m.), with *n* indicating the number of MEAs. All statistical analyses were performed using Prism 7.0 (GraphPad, La Jolla, CA) with $p<0.05$ representing statistical significance.

3.3 Results

3.3.1 Cypin overexpression increases spike count variability

We calculated the Fano factor as a measure of the variability in the spike count over periods of 10 seconds. We found that networks exhibited steady average Fano factors of 3.03 – 3.10 at baseline, suggesting that the firing rate of the networks is inherently irregular at this timepoint (**Fig. 3-2**). Cypin overexpression significantly increased the

Fano factor by DIV21. These data suggest that although the mean spike rate of networks that overexpress cypin decreases over time, as shown in Chapter X, mean variability in firing rate increases.

High Fano factors have been observed in other systems (Churchland et al. 2010), and it is not uncommon for an MEA study to report this level of spike count variability (Weir et al. 2014). Highly clustered networks exhibit high Fano factors, raising the possibility that overexpression of cypin causes subsets of connected neurons in a network to become better connected functionally (Litwin-Kumar and Doiron 2012). This introduces slow fluctuations in firing rate accompanied by high spiking variability. Fano factors can be calculated for any given time window at the discretion of the researcher and determined based on the system under study. It is important to note that Fano factors increase as a function of time window length (Vogel 2005; White, Abbott, and Fiser 2012; Litwin-Kumar and Doiron 2012), and 10 seconds is considered a large time window for this measurement.

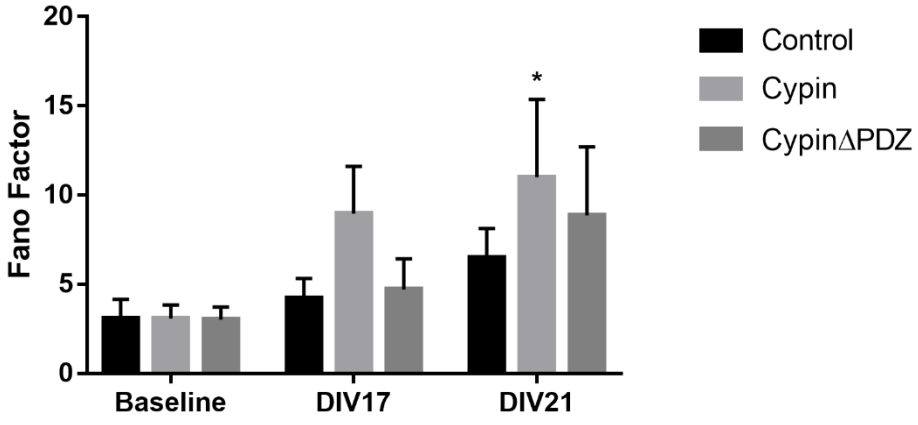

Figure 3-2. Spike count variability increases over time in networks that overexpress cypin. The FF increases after cypin overexpression (*p < 0.05 for DIV21), and this

increase is not dependent on PSD-95 binding. Statistics were calculated by two-way ANOVA followed by Tukey's multiple comparisons test (*n* = 12 for control, 14 for cypin and 11 for cypinΔPDZ). Extreme outliers were removed when identified by Grubb's test with α = 0.05.

3.3.2 Influence of spike rate on variability

We sought to determine whether variability in spike count is dependent on the spike rate. The relationship between spike rate and spike count variability for each network is summarized in **Fig. 3-3**. For each culture, the Fano factor is plotted versus the spike rate. Hence, each line represents data from a single culture over time with one data point each for baseline, DIV17, and DIV21. High variability occurs in this relationship within each condition over time and between conditions (**Fig. 3-3**). In fact, we found that the distribution of Fano factors is significantly different in the control condition between baseline and DIV21 (Mann-Whitney U test, $p < 0.05$) and for the cypin condition between baseline and DIV17 (Mann-Whitney U test, $p < 0.01$). The remaining Fano factor distributions did not show significant differences over time. We calculated the average non-parametric Spearman's rank correlation coefficients (Spearman's rho) for each condition and found no significant correlations between FF and spike rate. The high trial-to-trial variability renders this relationship difficult to interpret, yet differences in spike rate have been shown to influence spike count variability (Vogel 2005).

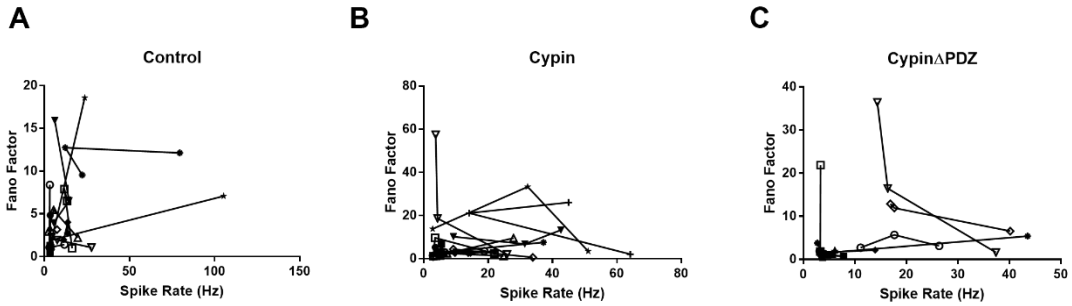

Figure 3-3. The Fano factor dependence on spike rate is highly variable. Networks overexpressing (A) GFP (Control; Spearman's rho = -0.1818 ± 0.2053; *n* = 12), (B) cypin (Spearman's rho = 0.07692 ± 0.2107; *n* = 14) and (C) cypinΔPDZ (Spearman's rho = 0.05556 ± 0.2693; *n* = 11) exhibited high trial-to-trial variability in the relationship between spike count variability and spike rate.

We then studied the relationship between these two parameters at different levels of initial spiking rate to determine if the baseline activity level influences Fano factor over time **(Fig. 3-4)**. Because of the wide spread of data points along both axes, the mean ± s.e.m. is displayed. We classified the cultures depending on the initial average number of spikes detected – low baseline (<2,000 spikes), intermediate baseline (2-10,000 spikes), and high baseline (>10,000 spikes) – and studied how the average Fano factor is influenced by level of firing over time. We also analyzed intermediate and high baselines (>2,000 spikes) in combination to further elucidate if low baselines influence the observed global variability in spike count. For each condition, the average Fano factor is plotted versus the average spike rate across the three timepoints; therefore, each line represents the average data of all the cultures in a particular condition over time. Note that each line has 3 data points: a circle (baseline), a square (DIV17), and a triangle (DIV21).

To quantify the dependence of the spike count variability on the mean spike rate, we calculated the Spearman's correlation coefficients for each condition at each timepoint and compared them using Fisher's Z-transformation (Myers and Sirois 2006). We found that the coefficient of correlation of networks that overexpress cypin changed significantly ($p < 0.01$, $n = 6$) from baseline (Spearman's rho = -0.4286) to DIV21 (Spearman's rho = 0.6571) for intermediate baselines **(Fig. 3-4D).** This suggests that for intermediate baselines, there is a negative relationship between variability and rate that significantly evolves into a positive relationship by DIV21 when cypin is overexpressed. Moreover, we found that the coefficient of correlation of networks that overexpress cypin changed significantly ($p < 0.01$, $n = 5$) from baseline (Spearman's rho = 0.5) to DIV17 (Spearman's rho = 1.0) for high baselines **(Fig. 3-4E).** This is accompanied by a strong trend ($p = 0.0561$, $n = 5$) towards a decrease between DIV17 and DIV21 (Spearman's rho = 0.8). These data suggest that at high baselines, there is a positive relationship between Fano factor and spike rate that gets stronger by DIV17, before it becomes negative by DIV21. We found no significant changes in coefficients of correlation for networks overexpressing GFP or cypinΔPDZ for any initial spike rate level, suggesting that cypin mediates its effects, at least in part, by binding to PSD-95 or PSD-95 family members.

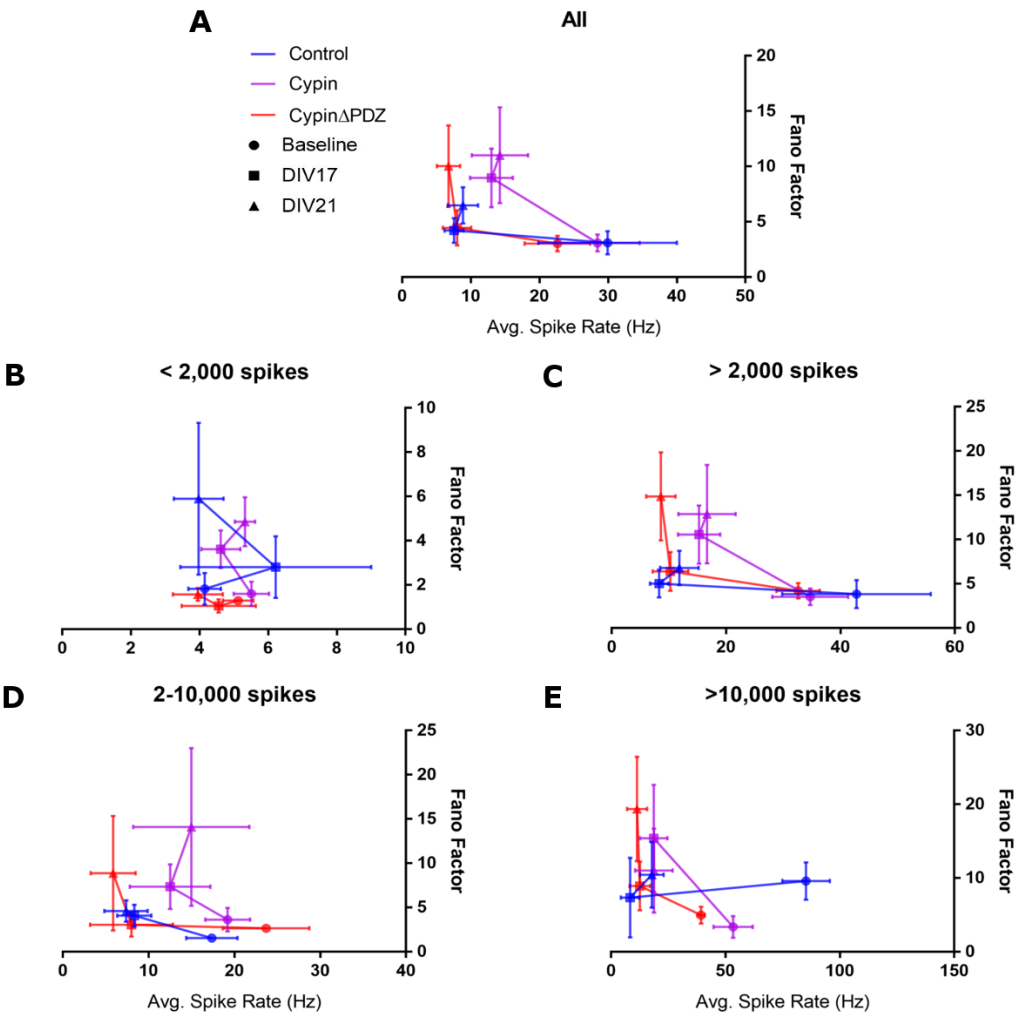

Figure 3-4. Dependence of the FF on the initial average spike rate. The average Fano factor is plotted versus the average spike rate for (A) all networks analyzed (*n* = 12 for control, 14 for cypin and 11 for cypinΔPDZ), (B) networks with low initial spike rates (*n* = 4 for control, 3 for cypin and 4 for cypinΔPDZ) (C) networks with intermediate and high initial spike rates (*n* = 8 for control, 11 for cypin and 7 for cypinΔPDZ) (D) networks with intermediate initial spike rates (*n* = 5 for control, 6 for cypin and 3 for cypinΔPDZ), and (E) networks with high initial spike rates (*n* = 3 for control, 5 for cypin and 4 for cypinΔPDZ). Each line has 3 data points: a circle (baseline), a square (DIV17), and a triangle (DIV21).

3.3.3 The average interspike interval increases after cypin overexpression

We calculated the average latency between consecutive spikes (interspike interval, ISI) across the entire networks and found that cypin overexpression significantly increases this latency by DIV21 **(Fig. 3-5)**. This increase in ISI occurs at the same timepoint as the increase in mean FF, suggesting that at DIV21, networks that overexpress cypin have higher spike count variability and that the spikes happen further apart in time from each other. There is also a decrease at DIV21 in average spike rate for networks overexpressing cypin (Fig. 2-4). This raises the possibility that a prolonged refractory period between spikes is responsible for the reduced spike rate at DIV21 (Vogel 2005).

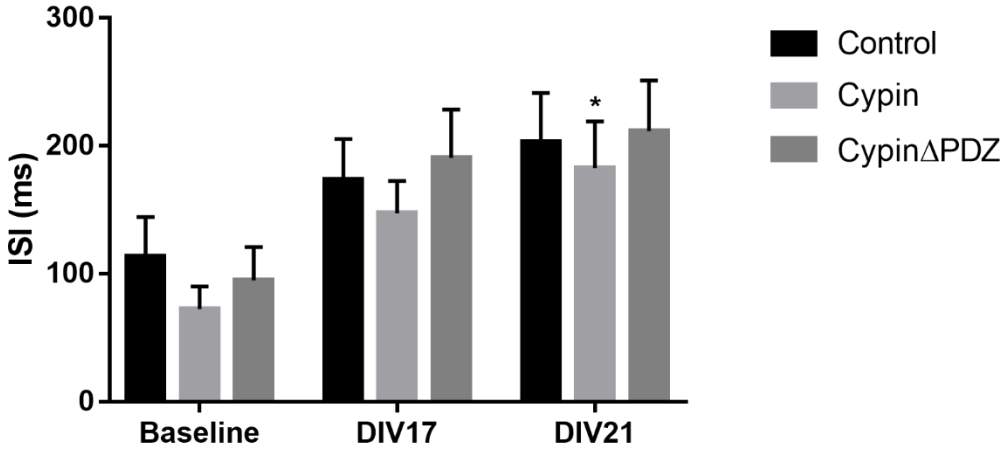

Figure 3-5. The mean ISI increases when cypin is overexpressed. Statistics were calculated by two-way ANOVA followed by Tukey's multiple comparisons test (*n* = 12 for control, 14 for cypin and 11 for cypinΔPDZ).

3.3.4 Variability of Interspike Intervals

We calculated the coefficient of variation (CV) of the interspike intervals as a measure of the variability of the ISI distribution. We found that the CV does not change significantly for any of the conditions over time **(Fig. 3-6)**. Similar to the mean Fano factor, we observed that the mean CV at baseline (ranging from 1.56 to 1.88) describes inherently irregular spike trains (Christodoulou and Bugmann 2001) that remain irregular over time. Taken together, our results show that cypin overexpression increases the variability in the spike count while not affecting the variability in latency between spikes.

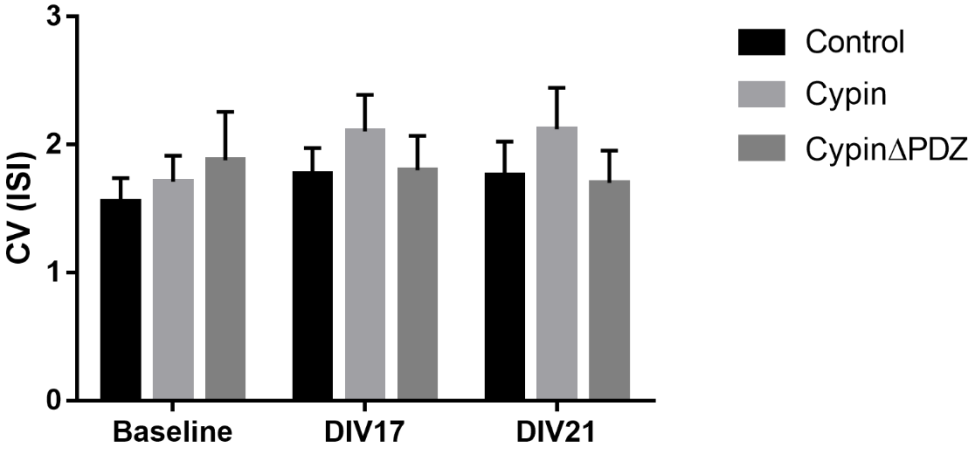

Figure 3-6. Coefficient of variation is constant over time. No statistical differences were observed as determined by by two-way ANOVA followed by Tukey's multiple comparisons test (*n* = 12 for control, 14 for cypin and 11 for cypinΔPDZ). Extreme outliers were removed when identified by Grubb's test with α = 0.05.

3.3.5 Changes in spike waveforms

We used the spike sorting algorithm Wave clus to determine whether waveform shape differences are observed in networks after cypin overexpression. Spike sorting is

important when studying multisite recordings because it allows us to decipher information of the individual neurons that make up the signals detected by each recording site (Harris et al. 2016). To gain insight into more detailed differences present in these networks, we compared the shapes of the spontaneous potentials detected by our networks over time **(Fig. 3-7)**.

Our results show that field potentials generated by spontaneous activity of the networks are composed of spikes of different shapes after cypin is overexpressed and that this change may be dependent on binding to PSD-95 or PSD-95 family members (**Fig. 3-7**). At baseline, networks exhibit field potentials are comprised of mostly of negative peaks, as shown previously in the literature for recordings from planar MEAs (Fendyur et al. 2011). Networks in all conditions appear to gain new spike waveforms by DIV17, with networks overexpressing cypin showing the most dramatic change. For more mature networks (DIV21), networks that overexpressed GFP or cypinΔPDZ show distributions that resemble their corresponding baseline distributions. However, networks overexpressing cypin retained waveforms present at DIV17 and exhibited a proportion of negative triphasic spikes that was not observed in either GFP-expressing or cypinΔPDZ-expressing networks. Negative spike shapes have been previously associated with axonal recordings (Fendyur et al. 2011), making it plausible that overexpression of cypin increases the amount of recordable spikes from axons and excitable soma.

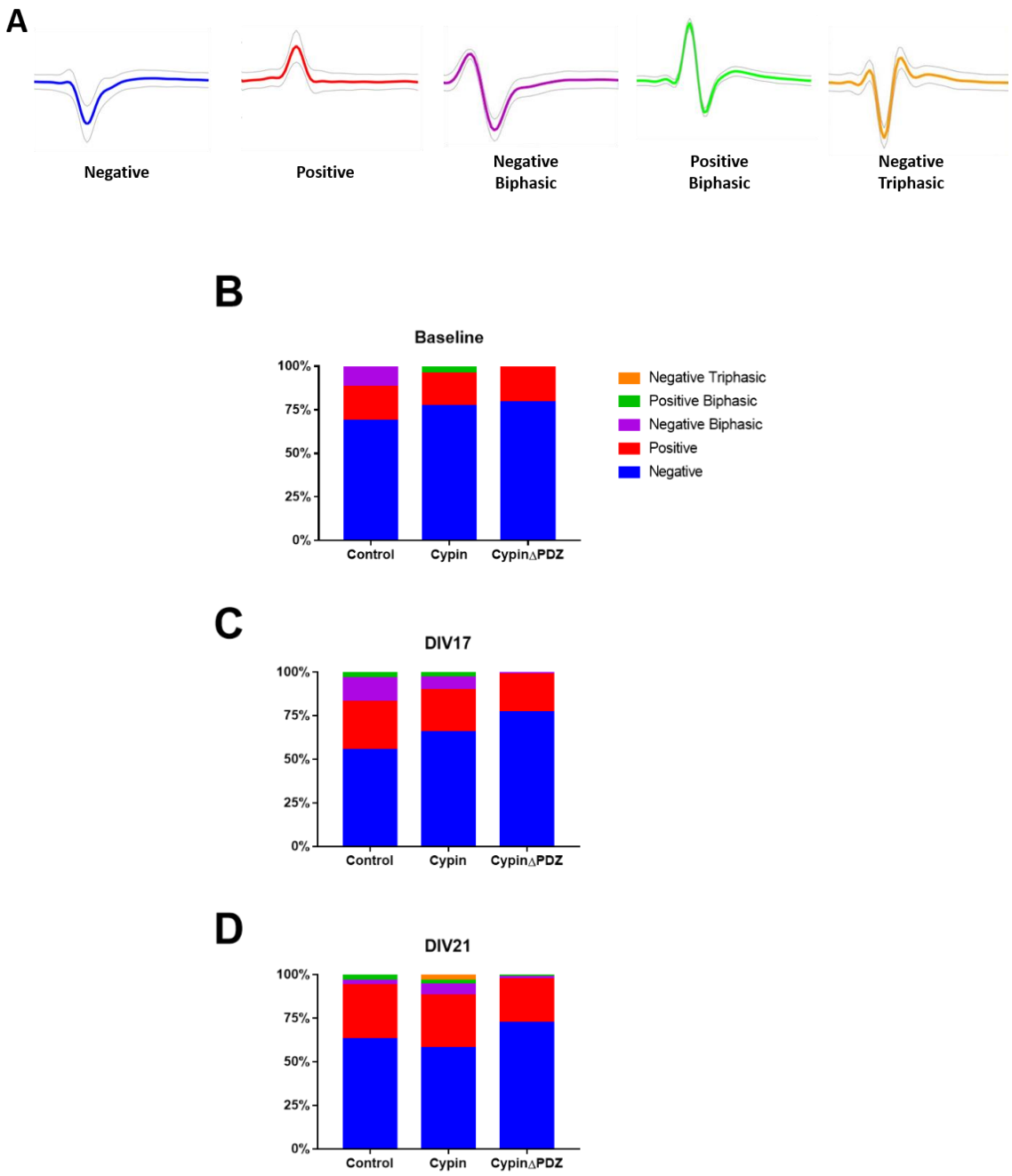

Figure 3-7. Categorization of the spike waveforms detected before and after transduction. (A) Representative average spike waveforms observed. Spike waveform distribution at (B) baseline, (C) DIV17, and (D) DIV21 was determined

using Wave_clus. The waveform data for all spikes for a given condition were pooled at each timepoint.

3.4 Discussion

In this chapter, we used Fano factor as a measure of the spiking variability in neuronal networks after cypin overexpression. We found that networks that overexpress cypin exhibit higher spike count variability by DIV21. In contrast, the spike count variability of networks overexpressing GFP or cypinΔPDZ did not change significantly over time. Our networks displayed high Fano factors even at baseline, which could be a result of the chosen time window at which the Fano factor was calculated (White, Abbott, and Fiser 2012) and the high cell density of our cultures. Computational models have correlated an increase in spike count variability with higher clustering between neurons in a network (Litwin-Kumar and Doiron 2012). In addition, Churchland and colleagues showed that the Fano factor decreases as the mean firing rate increases in a multiunit recording and confirmed that this reflects an underlying variance in the firing rate since at higher spiking rates, refractory periods regularize spiking (Churchland et al. 2010). We hypothesize that at DIV21, networks that overexpress cypin undergo more dramatic firing fluctuations as some clusters within the network transition to and from low to high activity levels, causing the overall spike count variability to increase.

We further investigated the relationship between Fano factor and spike rate in our system. As with other parameters, we found high trial-to-trial variability when looking at how the Fano factor for each culture changes over time. However, when we classified the cultures based on their initial spike rate, we found that only networks that overexpress

cypin show significant changes in the correlation between spike count variability and spike rate for intermediate (baseline to DIV21) and high baselines (baseline to DIV17). These results support our previously stated hypothesis that networks that overexpress cypin exhibit more dramatic fluctuations in firing as changes in variability appear to depend on spike rate, whereas no dependence on spike rate was found for variability in networks overexpressing GFP or cypinΔPDZ.

Similar to what has been reported in dissociated cortical cultures (W R Softky and Koch 1993), we found that our hippocampal networks exhibited high coefficients of variation (CV > 1), even at baseline. Although we observed a significant increase in the interspike interval from baseline to DIV21 in networks overexpressing cypin, no changes were observed in network coefficient of variation. Since our analysis includes all detected spikes, one explanation for this is that the presence of bursting spikes masks effects in the variability of interspike intervals. In addition, the presence of bursts is linked to high coefficients of variation (Knoblauch 2012), suggesting that networks with higher bursting rates potentially exhibit lower mean ISIs and higher mean CVs.

We sought to uncover differences in our networks at the individual spike level. To do so, we performed spike sorting based on the shapes of the waveforms detected. Neuronal networks coupled to planar electrodes on MEAs are known to fire mostly negative spikes, accompanied by a lower proportion of positive spikes (Fendyur et al. 2011). Our results are consistent with this throughout the 21 days in culture. We found that by DIV17, networks in all conditions gained one new type of spike waveform, with cypin-overexpressing networks showing the greatest shift in distribution. By DIV21, networks that overexpress cypin exhibit a new type of spike waveform, the negative triphasic spike,

which is not present in any of the other conditions. In fact, networks that overexpress GFP or cypinΔPDZ show a distribution of spikes that resembles their respective baselines, and GFP-overexpressing networks show a decrease in spike waveform distribution complexity. Thus, the changes in spike waveforms observed after cypin overexpression are dependent on PSD-95 family member binding.

The polarity and shape of spike waveforms are dependent on many factors, such as morphology of the dendritic tree, the distance between the spiking neuron and the recording electrode, the coupling between neurons and electrodes, and the properties of the recording medium (Gold et al. 2006). Hence, we assume that the observed changes in spike waveforms in our networks are not random and resulted from a combination of overexpression of our proteins of interest and regular network development. Neuron-electrode coupling and distance as well as recording medium composition are factors that would affect all conditions equally. It is plausible that the enhanced dendritic arbor present in cypin-overexpressing networks is responsible for some or all of the spike waveform changes observed. In fact, negative triphasic spikes have been shown to be characteristic of recordings from dendritic segments of interneurons (Csicsvari et al. 1999).

Overall, studying spike variability after cypin overexpression as a complement to our studies of mean activity rates uncovered specific network changes that are often masked by averaging. We find that cypin overexpression increases the spike count variability, the mean network interspike interval, and the complexity of the spike waveforms fired, and it does so in a PSD-95 family member-binding dependent manner.

3.5 Acknowledgements

I would like to thank Kate O'Neill for her contribution in developing the MATLAB routines used for spike detection and waveform cutout acquisition.

Chapter 4: Effect of altering cypin levels on PSD-95 protein levels and synaptic function

4.1 Introduction

Proper synaptic transmission is essential for normal brain function and requires the precise spatial and functional assembly of molecular signal transduction machinery at synaptic sites and the correct morphology of dendrites and their branches (Vetter et al. 2012). The postsynaptic density (PSD), an electron-dense region that characterizes the membranes of postsynaptic neurons, is a dynamic and complex structure. The composition of the PSD has been widely studied, and it has been proposed that the PSD serves as a network composed of scaffolding and cytoskeletal proteins that localize signaling molecules, receptors, and ion channels at the synapse (M Sheng 2001). Therefore, the organization of these proteins is critical for the regulation of synaptic transmission and synaptic plasticity. Defects in dendritogenesis and synaptogenesis contribute to neurological and neurodevelopmental disorders (Kulkarni and Firestein 2012).

PSD-95 is a member of the membrane-associated guanylate kinase (MAGUK) family of proteins and is found at the PSD of excitatory glutamatergic synapses (A. E. El-Husseini et al. 2000), where it has been associated with the trafficking and anchoring of all three classes of glutamate receptors – kainate, alpha-amino-3-hydroxy-5-methyl-4-isoxazolepropionic acid (AMPA), and N-methyl-D-aspartate (NMDA) type glutamate receptors. Cypin (**cy**tosolic **P**SD-95 **in**teractor) was originally identified as a highly abundant PSD-95-binding protein in brain extracts (Firestein et al. 1999). Overexpression

of cypin in rat hippocampal cultures disturbs postsynaptic localization of PSD-95 and SAP102 (**s**ynapse **a**ssociated **p**rotein 102), a related neuronal MAGUK protein (Firestein et al. 1999). In mature hippocampal cultures, both PSD-95 and SAP102 are targeted and clustered in dendrites at discrete spots that are likely to reflect postsynaptic sites. When cypin is overexpressed in culture, a significant reduction of PSD-95 and SAP102 clusters is observed. Immunostaining for the presynaptic marker synaptophysin demonstrated that the total number of synaptic sites is not altered and that cypin specifically regulates the synaptic targeting of associated MAGUK proteins.

Numerous studies show that changes in PSD-95 expression drive the maturation of dendritic spines and influence synaptic targeting and trafficking of glutamate receptors, resulting in alterations in the electrical activity of glutamatergic synapses (A. E. El-Husseini et al. 2000; Migaud et al. 1998; Bredt and Nicholl 2003; Béïque et al. 2006; Keith and El-Husseini 2008; Yudowski et al. 2013). Overexpression of PSD-95 in hippocampal slice cultures specifically recruits AMPA receptors (AMPARs) to synapses and enhances AMPAR-mediated excitatory postsynaptic currents (EPSCs) with no change in NMDAR-mediated EPSCs (Schnell et al. 2002). Moreover, impaired AMPAR function occurs in PSD-95 knockout mice (Béïque et al. 2006). This disruption in activity is specifically due to the fact that a significant proportion of synapses lack functional AMPARs, independent of spine morphology, supporting the need to understand both the structural and functional implications of altering levels of PSD-95 and its interactors in hippocampal neurons.

In this chapter, we investigate the effect of altering cypin levels on dendrite branching, PSD-95 protein levels, and synaptic function. We examine the result of overexpression of cypin or a cypin mutant that cannot bind to PSD-95 or its family

members (cypinΔPDZ), on dendrite branching at a developmental timepoint that our group has not studied before. We knocked down cypin and overexpressed cypin or cypinΔPDZ and measured the effect on total and subcellular PSD-95 protein levels. We further study the functional consequence of this alteration by recording miniature excitatory postsynaptic currents (mEPSCs) from hippocampal neurons after overexpression and knockdown of cypin. Finally, we use microelectrode array technology to assess whether cypin overexpression affects AMPAR-mediated activity in neuronal networks by recording the spontaneous activity of neuronal circuits in the presence of the AMPAR antagonist 6-cyano-7-nitroquinoxaline-2,3-dione (CNQX).

4.2 Materials and Methods

4.2.1 Cell culture

Neuronal cultures were prepared from hippocampi of Sprague-Dawley rat embryos at 18 days of gestation as described previously (M. Kwon et al. 2011). The hippocampi were mechanically dissociated by pipetting slowly through the bore of a fire-polished Pasteur pipette. Cells were plated on 12 mm glass coverslips or 6-well plates coated with 0.5 mg/ml poly-D-lysine (PDL; Sigma). Cultures were maintained in Neurobasal medium (Gibco) supplemented with B27 (Gibco) and GlutaMAX (Gibco) at 37 °C and 5% CO_2. All animals were cared for ethically in accordance with Institutional Animal Care and Use Committee (IACUC) standards.

4.2.2 Lentiviral particle production and transduction

The lentiviral plasmids were constructed by subcloning cDNA encoding wild type cypin or cypin lacking the PDZ binding motif (cypinΔPDZ) into the control FG12 vector containing EGFP for expression. For knockdown, shRNAs against cypin were subcloned into the pHUUG vector (vectors were gift from Dr. Chris Pröschel, University of Rochester School of Medicine). Lentivirus containing shRNAs against glutathione S-transferase (GST) were used as control. Lentiviral particles were generated by transfecting HEK293TN cells (ATCC) using the calcium phosphate precipitation method with one of the lentiviral plasmids, the packaging plasmid psPAX2, and the envelope plasmid pMD2.G (VSV-G). The medium was replaced 24 hours post-transfection, and the medium containing viral particles was collected 48 hours later, concentrated using PEG-it virus precipitation solution (System Biosciences) according to the manufacturer's instructions, and stored at -80 °C until use. HEK293TN cells were maintained and transfected in Dulbecco's Modified Eagle Medium (DMEM; Life Technologies) containing 10% fetal bovine serum (Atlanta Biologicals). Neuronal cultures were transduced with lentiviral supernatant on day *in vitro* (DIV) 10 when grown on MEAs and 6-well plates or on DIV14 when grown on glass coverslips. Half of the culture medium was changed 36 hours later and every other day from then on. Successful transduction was confirmed through fluorescence microscopy.

4.2.3 Western Blotting

Neurons were scrape-harvested on DIV21 into RIPA buffer (50 mM Tris-HCl pH 7.4, 150 mM NaCl, 1 mM EGTA, 1% NP-40, 0.25% sodium deoxycholate, 0.1% SDS, 1 mM PMSF). Cells were lysed by passing them through a 25½-gauge needle approximately 10 times. The lysates were placed on a nutator for 30 minutes at 4 °C, followed by a 15 minute

spin at 13,000×*g* to pellet insoluble material. Proteins were resolved on a 10% SDS-polyacrylamide gel and transferred to a PVDF membrane. The blot was probed with the indicated antibodies. Blots were scanned, and the intensities of the bands of interest were quantified using ImageJ software (NIH).

4.2.4 Cell culture on MEAs

MEAs (Multi Channel Systems, Germany) were coated with 0.5 mg/ml poly-D-lysine (PDL; Sigma) for at least 1 hour, washed three times with sterile water, and then coated with 10 µg/ml laminin (Sigma) for at least 30 minutes. Cultures were established at a density of $1x10^6$ cells/MEA and maintained in NbActiv4 medium (BrainBits, LLC) at 37 °C and 5% CO2. Half medium changes were performed every other day.

4.2.5 CNQX treatment

Increasing amounts of the competitive AMPAR antagonist CNQX, ranging between 1 – 10 µM and diluted in recording solution, were added to the cultures, and activity was recorded for 5 minutes after equilibration was reached. After each recording, the cultures were washed twice with fresh culture medium. The networks recovered for at least 15 minutes between each CNQX treatment.

4.2.6 Subcellular Fractionation

On DIV21, neurons from two wells of a 6-well plate for each condition were scrape-harvested into 150 µl of homogenization buffer (HB; 320 mM sucrose, 4 mM HEPES, 1 mM EGTA, 1 mM PMSF). Subcellular structures were fractionated as we previously described (Firestein et al. 1999; M. Chen et al. 2005). The cell membranes were disrupted by passing cells through a 25½-gauge needle approximately 10 times. The homogenate was

centrifuged at 1,000×*g* for 10 minutes at 4 °C. The supernatant (S1) was collected and centrifuged at 12,000×*g* for 15 minutes at 4 °C. The pellet (P2) was resuspended and washed in 100 µl of HB and centrifuged at 13,000×*g* for 15 minutes at 4 °C. The resulting pellet (P2'), representing a crude synaptosomal fraction, was lysed by osmotic shock and homogenized by pipetting up and down multiple times. The homogenate was spun at 33,000×*g* for 20 minutes at 4 °C to yield supernatant LS1 and pellet LP1 (heavy membranes). LS1 was spun at 251,000×*g* for 2 hours at 4 °C. The resulting supernatant (LS2) contained soluble proteins, while the pellet (LP2) contained synaptic vesicle proteins. Each fraction was stored at -20 °C in protein loading buffer.

4.2.7 Assessment of Dendritic Spine Number

Cultured hippocampal neurons were co-transfected with plasmids encoding RFP (to visualize spines) and GFP, GFP-cypin, or GFP-cypinΔPDZ on DIV14 using the calcium phosphate method. Neurons were fixed on DIV 17 and immunostained for GFP and RFP. Images of dendritic segments were taken with a 60x plan apochromat oil immersion objective (NA 1.4) using a Yokogawa CSU-10 spinning disk confocal head attached to an inverted fluorescence microscope (Olympus IX50). X-, Y-, and Z-resolution was set as 0.067 µm, 0.067 µm and 0.1 µm, respectively, to define dendritic spines. Spines were counted along dendritic segments starting from 20 µm to 80 µm from the soma. For each cell, segments were quantified and averaged. Spines were manually counted from at least 12 neurons for each experimental condition, and analysis was performed with the experimenter blinded to the condition.

4.2.8 Assessment of Dendrite Number

Cultured hippocampal neurons were transfected on DIV7 using Lipofectamine LTX with Plus reagent (Invitrogen) according to the manufacturer's instructions. Neurons were fixed on DIV12 with 4% paraformaldehyde in PBS for 15 minutes, washed 3 times with PBS, and then incubated in blocking solution (2% normal goat serum, 0.1% Triton X-100, and 0.02% sodium azide in PBS) for 1 hour. All antibodies used were diluted in blocking solution. Neurons were incubated for 1 hour at room temperature or overnight at 4 °C with primary antibodies: GFP (DSHB-12A6) to identify transfected cells and MAP2 (BD Biosciences) to identify neurons. They were then washed with PBS 3 times and incubated for 1 hour at room temperature with appropriate secondary antibodies. Coverslips were mounted onto glass slides with Fluoromount-G (Southern Biotechnology). Transfected cells were visualized by immunofluorescence on an EVOS FL microscope at 20X (Thermo Fisher Scientific).

Semi-automated Sholl analysis was performed as described previously (Langhammer et al. 2010; Kutzing et al. 2010; O'Neill et al. 2015). Briefly, images of hippocampal neurons were traced using the NeuronJ plugin for ImageJ (NIH). The tracing files were converted to SWC files using MATLAB (Mathworks) for further manipulation. NeuronStudio was then used to define the connectivity pattern between the segments and the morphological data were exported to Excel using MATLAB. The experimenter was blinded to the condition when performing dendrite analysis. The axon was excluded based on MAP2 immunostaining absence.

4.2.9 Electrophysiology

Whole cell patch-clamp recordings were obtained from the soma of hippocampal neurons as described previously (Hernandez et al. 2016). Recordings were performed on

DIV21. The external solution contained (in mM): 140 NaCl, 5 KCl, 2 $CaCl_2$, 2 $MgCl_2$, 10 HEPES, and 10 glucose (pH 7.4 adjusted with NaOH; 290–310 mOsmol). Recording electrodes (3–5 MΩ) contained a K^+-based internal solution composed of (in mM): 126 K-gluconate, 4 KCl, 10 HEPES, 4 ATP-Mg, 0.3 GTP-Na_2, 10 phosphocreatine, and 10 QX-314 bromide (pH 7.2; 280–300 mOsmol). Action potentials were blocked with 1 μM tetrodotoxin (TTX; Tocris, R & D Systems) to record miniature excitatory postsynaptic currents (mEPSCs). The membrane potential was held at –70 mV throughout all experiments. Data were amplified and filtered at 2 kHz by a patch-clamp amplifier (Multiclamp 700B), digitalized (DIGIDATA 1440A), stored, and analyzed by pCLAMP (Molecular Devices). Data were discarded when the input resistance changed >20% during recording. Recordings were performed by Przemyslaw Swiatkowski.

4.2.10 Microelectrode Array Recordings

Standard MEAs containing 60 planar electrodes (59 recording electrodes and 1 internal reference electrode), each with a 10 μm diameter and an inter-electrode spacing of 200 μm (60MEA200/10iR-Ti-gr; Multi Channel Systems, Germany), were used for all experiments. Baseline recordings were performed on cultures on DIV10 immediately before lentiviral transduction and on DIV14. Prior to each recording, the culture medium was saved and replaced with recording solution (144 mM NaCl, 10 mM KCl, 1 mM $MgCl_2$, 2 mM $CaCl_2$, 10 mM HEPES, 2 mM Na-pyruvate, 10 mM glucose, pH 7.4), and the MEA was placed into the cell culture incubator for 5 minutes to allow it to reach equilibrium. After each recording, the cultures were washed twice with fresh culture medium before adding saved conditioned medium. Each MEA was covered with a semipermeable lid (ALA MEA-

MEM; ALA Scientific) during handling and recordings to prevent contamination from airborne pathogens.

Spontaneous electrical signals were monitored and recorded for 5 minutes using the data acquisition commercial software MC_Rack (Multi Channel Systems) as described previously by our group (Kutzing, Luo, and Firestein 2011; Kutzing, Luo, and Firestein 2012). The temperature of the cultures was maintained at 37 °C on a heat-controlled stage and the signals were sampled at 20 kHz with an MEA1060-Inv-BC amplifier (Multi Channel Systems).

4.2.11 Signal Processing

The raw data were imported into Matlab (MathWorks, Inc.) using MEA-Tools, an open-source toolbox. The signals were filtered through a 4^{th} order Butterworth filter (20-2,000 Hz) and a notch filter to remove 60 Hz electric hum. The electrodes that exhibited irregular activity or excessive noise were excluded from the analysis. The Matlab routines used for signal processing and data analysis discussed in this section were developed by Kate O'Neill, in part based on previous work from our group (Kutzing, Luo, and Firestein 2011).

4.2.11.1 Spike Detection

Spikes were detected using an adaptive threshold. Briefly, a spike was defined as a signal with voltage exceeding a positive or negative threshold, chosen to be 4.5 standard deviations times the background noise for a 10 second window for each recording channel. To ensure that spikes were counted only once on an electrode, spikes were detected at their maximum absolute value and interspike intervals (ISIs) had to be longer than 2 ms.

When spike rate is reported, it refers to the number of spikes divided by the recording time (300 seconds). Active electrodes were defined as those whose firing rate was ≥ the 75th percentile of the distribution.

4.2.12 Spike Sorting

We applied Wave clus, a spike sorting algorithm (Quiroga, Nadasdy, and Ben-Shaul 2004), to obtain information about individual neurons within our networks. Spike sorting extracts features from each spike and clusters them in classes that best reflect their shape. To do so, Wave clus calculates the wavelet transform for each spike and uses a set of the obtained wavelet coefficients as input for a clustering algorithm based on k-nearest neighbor interactions (Blatt, Wiseman, and Domany 1996). Using the wavelet transform instead of principal component analysis (PCA) to extract the shape information is advantageous because it allows for more specific discerning of spike features (Quiroga, Nadasdy, and Ben-Shaul 2004; Hernan Gonzalo Rey, Pedreira, and Quian Quiroga 2015).

We first detected individual spikes as described above. For each detected spike, we collected a spike time stamp and a waveform cutout spanning 1 ms before and 2.2 ms after the spike absolute maxima. The obtained waveform cutouts were sorted using the unsupervised Wave clus algorithm. After automatic clustering, we performed the suggested minor manual tuning (Quian Quiroga 2004) to improve the sorting accuracy. All detected spikes for each condition and timepoints were included in the spike sorting analysis.

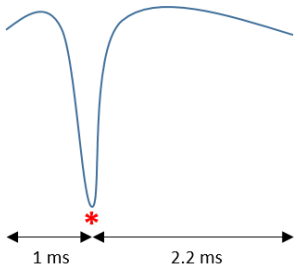

Figure 4-1. Spike cutout schematic. Spike waveform cutouts spanning 1 ms (19 data points) prior and 2.2 ms (44 data points) after the absolute maximum value of the spike (represented by *) were stored and sorted. All spikes were aligned by setting their maximum at data point 20.

4.2.13 Statistics

All data are presented as mean values ± standard error of the mean (s.e.m.), with *n* indicating the number of MEAs. All statistical analyses were performed using Prism 7.0 (GraphPad, La Jolla, CA) with $p<0.05$ representing statistical significance.

4.3 Results

4.3.1 Cypin increases proximal and distal dendrite branching

We overexpressed cypin or cypin lacking the PDZ-binding motif (cypinΔPDZ) in rat hippocampal neurons from DIV 7-12, a period of active proximal and distal branching (Dotti, Sullivan, and Banker 1988; Charych et al. 2006), and assessed their effect on dendrite branching. Total Sholl analysis suggests that overexpression of either cypin or cypinΔPDZ promotes proximal and distal dendrite branching during this developmental

timepoint **(Fig. 4-2A)**. Cypin overexpression resulted in a significant increase in dendritic branches at 0-54 μm from the soma, while cypinΔPDZ significantly increased branching at 0-48 μm from the soma (**Fig. 4-2B**). As a result, the total number of dendrites was significantly increased by DIV12 **(Fig. 4-2C)** in both conditions. Interestingly, we observed that this increase observed in Total Sholl analysis is dendrite order-specific. Overexpression of cypin significantly increased the number of tertiary **(Fig. 4-2F)**, but not primary or secondary dendrites **(Fig. 4-2D, E)**. In contrast, neurons that overexpress cypinΔPDZ show a trend towards an increase in primary and tertiary dendrites. In a recent study, our group (O'Neill et al. 2015) showed the cypin overexpression between DIV 6-10 results in an increase in both primary and tertiary dendrites. Our data suggest that the observed increase in primary dendrites is transient and that the primary dendrites promoted by cypin are pruned by DIV12. In addition, the changes in the dendritic arbor promoted by cypin at this timepoint do not appear to be dependent on binding to PSD-95 or PSD-95 family members, as both have very similar effects on arborization.

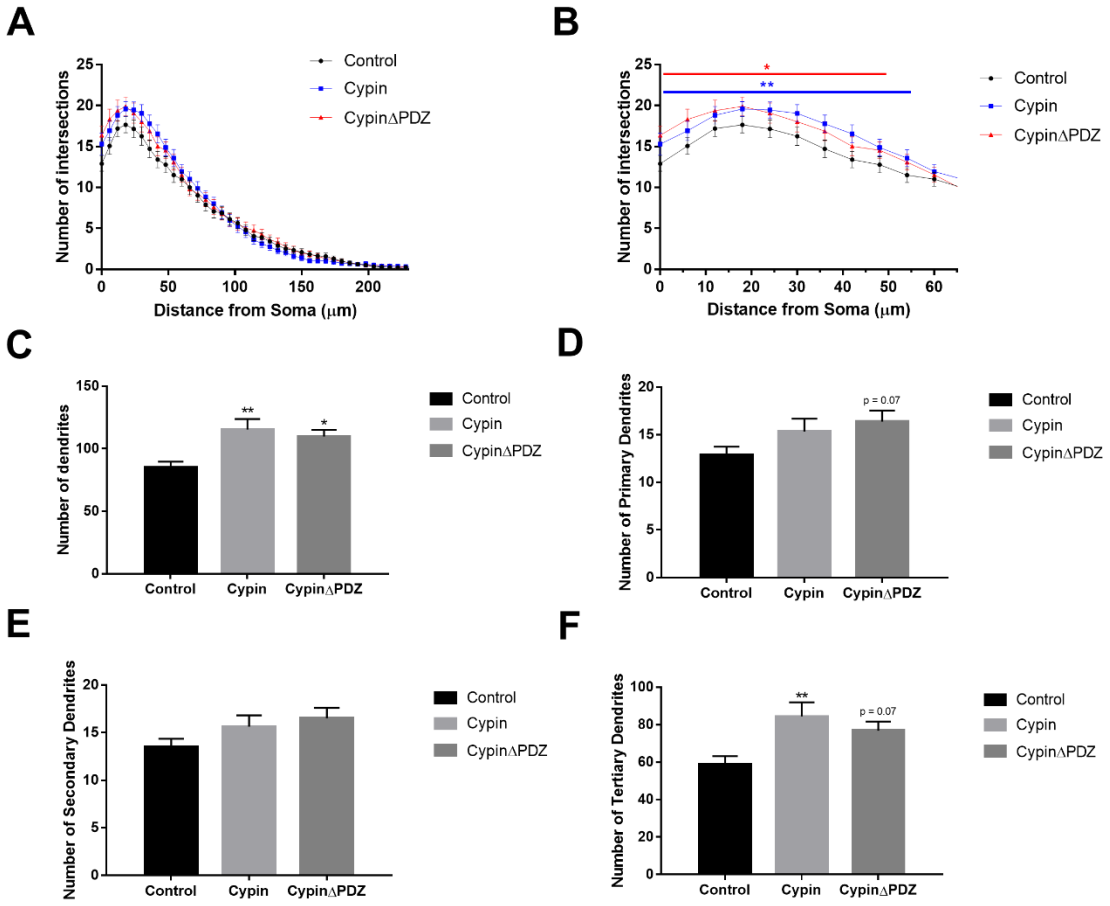

Figure 4-2. Cypin overexpression from DIV7-12 increases proximal and distal dendrite branching. (A) Total Sholl analysis shows increased dendrite branching when cypin or cypinΔPDZ are overexpressed. (B) Sholl analysis within 60 μm of the soma shows that cypin overexpression increases branching at 0-54 μm from the soma (p < 0.01), while cypinΔPDZ increases branching at 0-48 μm from the soma (*p < 0.05). (C) Overexpression of cypin or cypinΔPDZ increase the total number of dendrites. Overexpression of cypin or cypinΔPDZ does not result in significant increased (D) primary or (E) secondary dendrites. (F) Cypin overexpression increases the number of tertiary dendrites. Statistics were calculated by (A-B) two-way ANOVA followed by Tukey's multiple comparisons test (C-F) one-way ANOVA**

followed by Dunnett's multiple comparison test (*n* = 40 for control, 42 for cypin and 34 for cypinΔPDZ).

4.3.2 Cypin alters total PSD-95 protein levels

We examined whether alterations in cypin protein levels affect total PSD-95 protein levels in culture. Hippocampal neurons were transduced at DIV10 with lentiviral particles to overexpress GFP-tagged cypin or cypinΔPDZ. Cypin overexpression resulted in increased total PSD-95 protein levels at DIV21 (**Fig. 4-3**). When cypin is unable to bind to the PDZ domains of PSD-95, total protein levels of PSD-95 are not significantly altered (**Fig. 4-3**), indicating that the interaction between cypin and PSD-95 mediates the change in PSD-95 expression. This result is surprising since we have shown that cypin decreases clustering of synaptic PSD-95 (Firestein et al. 1999). Hence, cypin alters synaptic and total PSD-95 protein levels in an opposite manner but both are dependent on PSD-95 binding.

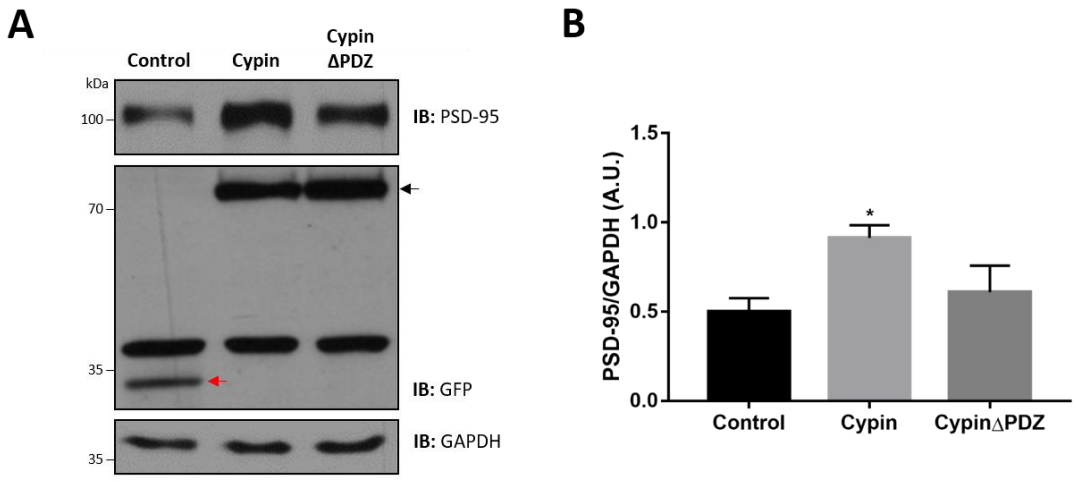

Figure 4-3. Cypin overexpression increases total PSD-95 levels. (A) Neurons were transduced at DIV10, and Western blotting was performed at DIV21. Representative blots show successful transduction as determined by probing with an antibody

against GFP. Black arrow indicates predicted size of GFP-tagged cypin protein (~78 kDa) and red arrow indicates predicted size of GFP (~28 kDa). The bands above GFP are due to a previous probing with an antibody against GAPDH (~37 kDa). (B) Densitometry analysis of PSD-95 protein levels normalized to GAPDH protein expression. Statistics were calculated by two-way ANOVA followed by Tukey's multiple comparisons test (n = 4 for all conditions; *p < 0.05).

Three different shRNA lentiviruses were developed to target cypin segments starting at base pairs 352, 404, and 941. Primary hippocampal neurons were transduced, and cypin knockdown was assessed by Western blot analysis. Transduction efficiency and cypin knockdown were consistently successful when targeting base pair 941 (labeled Cypin shRNA), and this shRNA was chosen for all future knockdown experiments. Hippocampal neurons were transduced on DIV10, and Western blot analysis performed on DIV21 lysates **(Fig. 4-4A)**. We observed a ~40% decrease in cypin protein levels after transduction **(Fig. 4-4B)**. We found a trend (p = 0.06) towards a decrease in total PSD-95 protein levels after cypin knockdown **(Fig. 4-4C)**.

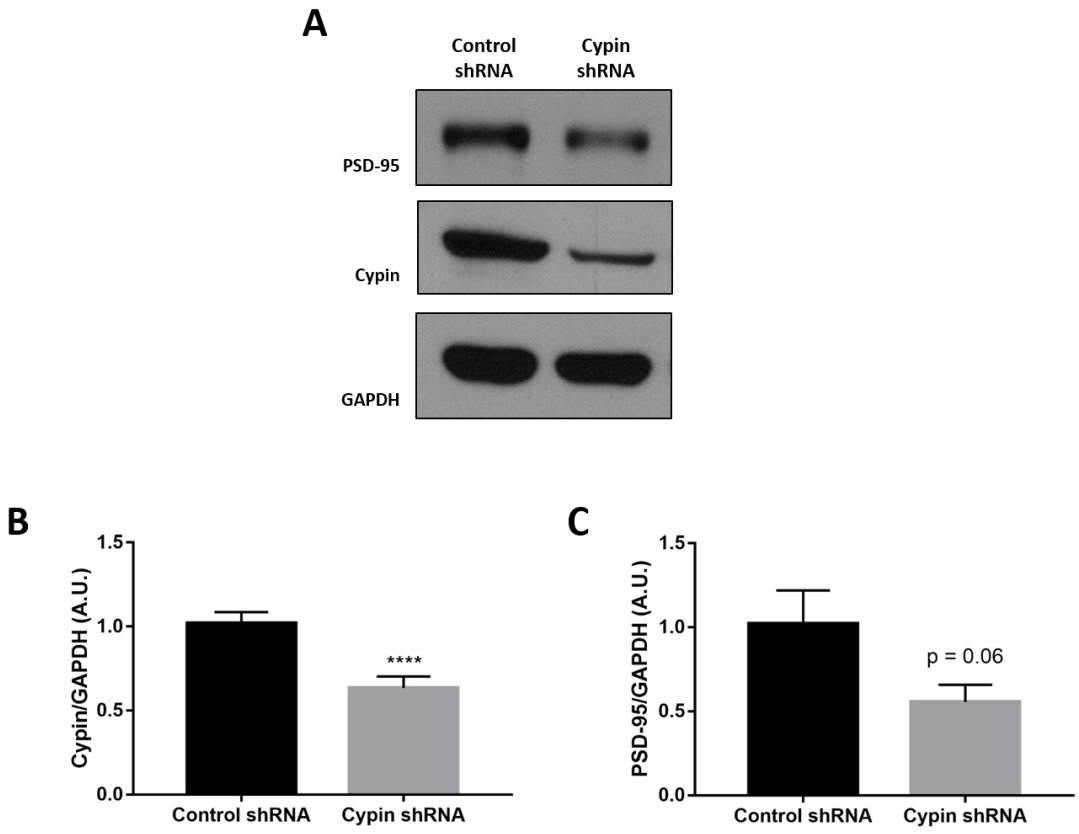

Figure 4-4. PSD-95 levels trend towards a decrease after cypin knockdown. (A) Neurons were transduced with shRNA lentiviral plasmids at DIV10 and Western blots performed at DIV21 to determine effect on cypin and PSD-95 levels. (B) Densitometric analysis of cypin protein normalized to GAPDH protein expression shows ~40% reduction in cypin protein levels (n=6, ****p < 0.0001 determined by paired t test. (C) Densitometric analysis of PSD-95 protein levels normalized to GAPDH shows that PSD-95 protein levels decrease after cypin knockdown (n=4, p = 0.06 determined by paired t test).

4.3.3 Cypin alters the subcellular distribution of PSD-95

Since cypin overexpression alters total PSD-95 protein levels, and we previously reported that cypin decreases the number of PSD-95 clusters (Firestein et al. 1999), we investigated whether synaptic PSD-95 protein levels change after cypin overexpression. We overexpressed cypin in cultures of hippocampal neurons at DIV10 and performed synaptosomal fractionation (Firestein et al. 1999; M. Chen et al. 2005) at DIV21. This technique allows us to isolate enriched fractions and analyze their composition. We found that when cypin was overexpressed, there was a significant decrease in PSD-95 present in synaptosomes and the postsynaptic density (PSD) fractions, where PSD-95 is typically enriched (Pak et al. 2001; **Fig. 4-5**). Synaptosomes are composed of the presynaptic terminal as well as the postsynaptic membrane and postsynaptic density (Bai and Witzmann 2007). Our findings are in agreement with our previous report (Firestein et al. 1999) and unpublished data from our group that show that cypin regulates synaptic clustering of PSD-95 and that the PDZ-binding motif of cypin is necessary for this effect. Interestingly, overexpression of cypin lacking the PDZ-binding motif results in an increase in PSD-95 levels in the PSD **(Fig. 4-5B)**.

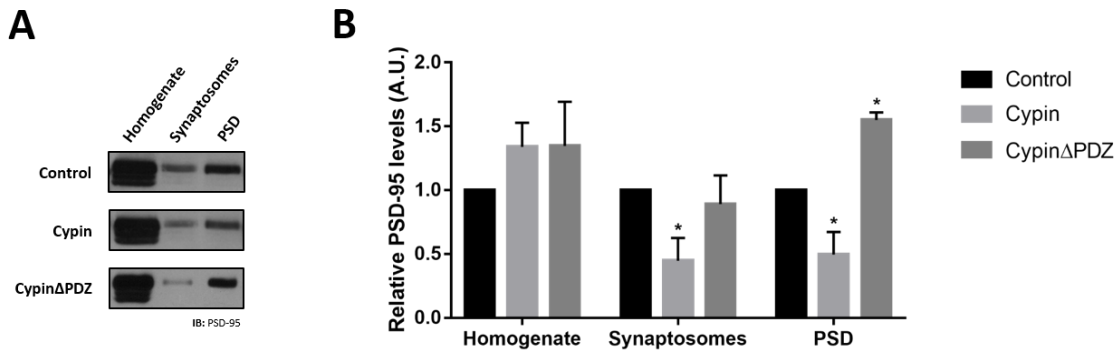

Figure 4-5. Cypin overexpression alters the subcellular distribution of PSD-95. (A) Representative blots show decreased levels of PSD-95 in synaptosomes and PSD of cultures overexpressing cypin when compared to control cultures. (B) Densitometric analysis of PSD-95 protein relative to the control condition shows decreased PSD-95 in synaptosomes and PSD after cypin overexpression (*$p < 0.05$). Statistics were calculated by two-way ANOVA followed by Dunnett's multiple comparison test (*n* = 5 for control, 5 for cypin and 3 for cypinΔPDZ).

We further investigated the effect of altering cypin levels on PSD-95 localization and performed synaptosomal fractionation after cypin knockdown. We found that there were no changes in PSD-95 localization after cypin knockdown when compared to the control knockdown **(Fig. 4-6)**. Since we only achieve a partial knockdown with this method, it is possible that the endogenous cypin that remains is sufficient to allow for correct PSD-95 localization, and hence, knockdown does not have a substantial effect on PSD-95 localization.

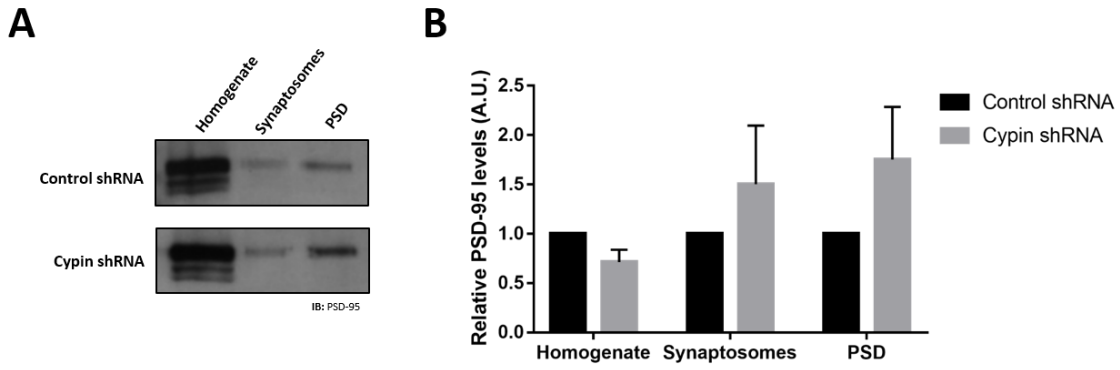

Figure 4-6. Cypin knockdown does not affect the subcellular distribution of PSD-95. (A) Representative blots and (B) densitometric analysis of PSD-95 protein levels in subcellular fractions after cypin knockdown. No statistical significance was found as calculated by two-way ANOVA followed by Sidak's multiple comparison test (n = 6 for all conditions).

4.3.4 Cypin overexpression decreases the number of dendritic spines

Dendritic spines are small protrusions in the membrane of dendrites that receive most of the excitatory synapses in the brain. The presence and absence of PSD-95 puncta are likely to correlate with spine and synapse formation and pruning (Cane et al. 2014). Since cypin overexpression results in a decrease in PSD-95 puncta and protein expression, we investigated the effect of altering cypin levels on the density and maturity of dendritic spines. We found that when cypin is overexpressed, the number of dendritic spines is reduced significantly when compared to the control condition **(Fig. 4-7)**. Moreover, when cypinΔPDZ is overexpressed, there is a trend towards a decrease in dendritic spines ($p = 0.06$), but this is not statistically different from the spine density found after cypin overexpression **(Fig. 4-7B)**. Hence, our results suggest that the PDZ-binding motif is only

partially necessary for the observed reduction in dendritic spines after cypin overexpression.

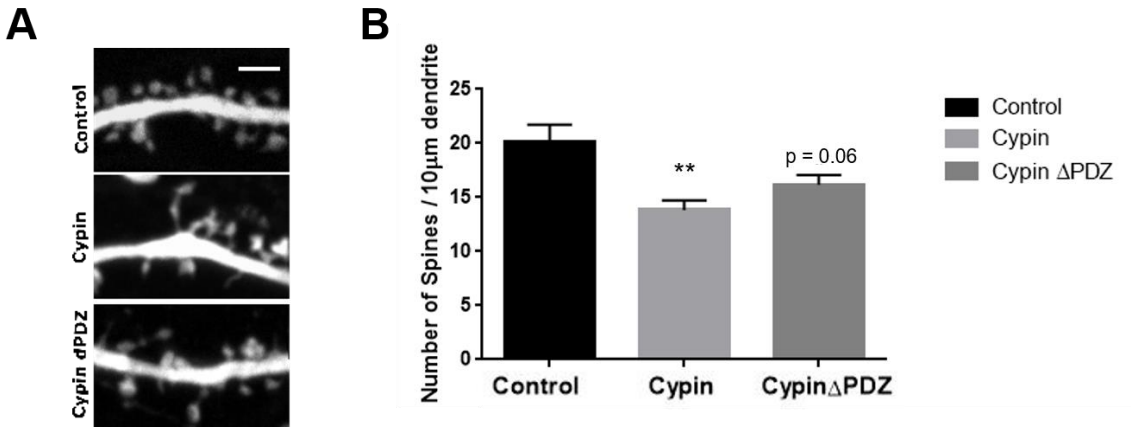

Figure 4-7. Cypin overexpression results in reduced spine density. (A) Representative mRFP images of dendritic segments from hippocampal neurons at DIV17. Scale bar is 2 µm. (B) Cypin overexpression results in a significant decrease in the density of dendritic spines. CypinΔPDZ overexpression results in a trend towards decreased spine density that is not statistically different from the spine density observed after cypin overexpression. Statistics calculated by one-way ANOVA followed by Tukey's multiple comparisons test (p < 0.01).**

4.3.5 Cypin overexpression increases synaptic transmission

We performed whole-cell patch-clamp recordings of miniature excitatory postsynaptic currents (mEPSCs) in hippocampal neurons. We transduced neurons with lentivirus to either overexpress or knockdown cypin on DIV14 and recorded mEPSCs at DIV21. Overexpression of cypin or cypinΔPDZ resulted in an increase in the frequency of mEPSCs **(Fig. 4-8B)** while their amplitude remained unchanged **(Fig. 4-8C)**. Interestingly, this suggests that this effect is independent of cypin binding to PSD-95 or PSD-95 family

members. This result is surprising given our findings regarding the PDZ-binding-dependent observed decrease in synaptic PSD-95 protein levels with cypin overexpression. A study by Béïque and colleagues showed that in PSD-95$^{-/-}$ (KO) mice, PSD-95 exhibits synapse specificity and the functional defects that result from its deletion can be restricted to only a subset of synapses (Béïque et al. 2006). We believe that it is possible that the synaptic defect that results from knocking down synaptic PSD-95 via cypin overexpression may affect a small population of synapses and that other members of the MAGUK family of proteins may compensate for decreases in synaptic PSD-95 localization.

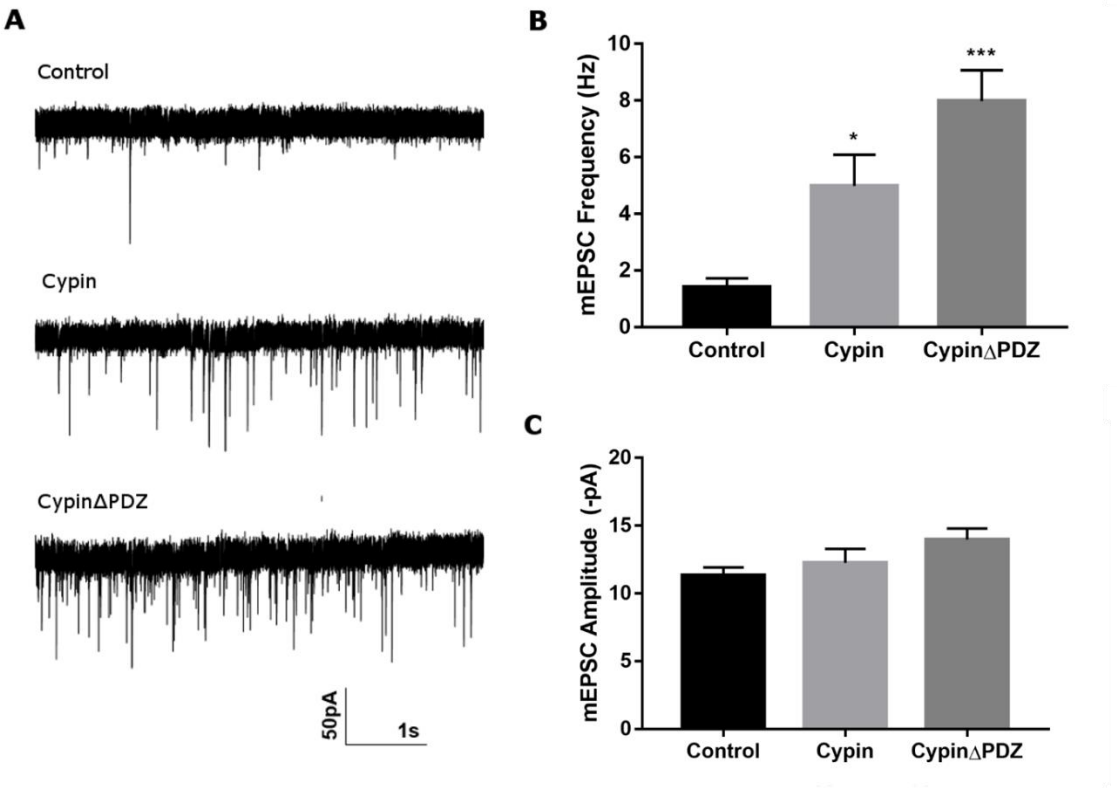

Figure 4-8. Overexpresion of cypin or cypinΔPDZ results in increased frequency of mEPSCs. (A) Representative traces of mEPSCs. (B) Overexpressing cypin (*p < 0.05) and cypinΔPDZ (*p < 0.001) increases the frequency of mEPSCs (C) The amplitude**

of mEPSCs remains unchanged after overexpression. Statistics calculated by one-way ANOVA followed by Tukey's multiple comparisons test (*n* = 12 for control, 15 for cypin and 15 for cypinΔPDZ).

When we knocked down cypin and recorded mEPSCs, we found that neither the frequency nor amplitude of mEPSCs changes **(Fig. 4-8)**. As with the changes in synaptic PSD-95 protein levels in subcellular fractions, it is possible that a partial cypin knockdown in dissociated hippocampal cultures is not sufficient to significantly change synaptic transmission.

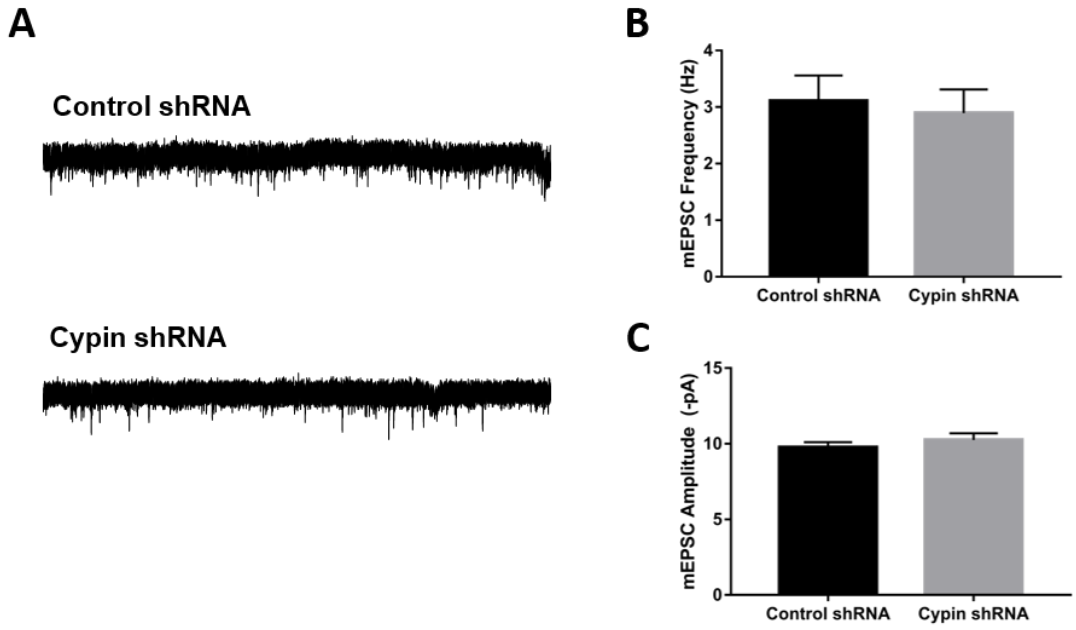

Figure 4-8. Cypin knockdown does not change the frequency or amplitude of mEPSCs. (A) Representative traces of mEPSCs. (B, C) The frequency and amplitude of mEPSCs remains unchanged after knockdown. No statistical significance as calculated by t test (*n* = 15 for control shRNA and *n* = 17 for cypin shRNA).

4.3.5 Cypin overexpression alters AMPAR function in neuronal circuits

To investigate whether cypin-promoted changes to PSD-95 protein levels and synaptic function affect AMPAR-mediated synaptic transmission, we cultured hippocampal neurons on MEAs and treated them with increasing amounts of the AMPAR antagonist CNQX on DIV15. Changing PSD-95 expression is known to influence the synaptic targeting and trafficking of glutamate receptors, resulting in alterations in the electrical activity of glutamatergic synapses (A. E. El-Husseini et al. 2000; Béïque et al. 2006; Keith and El-Husseini 2008; Yudowski et al. 2013). PSD-95 indirectly interacts with AMPAR subunits through stargazin and influences the efficiency of AMPAR trafficking (Bredt and Nicholl 2003; Vandenberghe, Nicoll, and Bredt 2005).

We found that networks that overexpress GFP (control) do not exhibit significant changes in the rate of spiking regardless of concentration of CNQX treatment **(Fig. 4-9A)**. This lack of dose-dependent response might be due to compensatory mechanisms within the network and the effect of NMDAR-mediated synaptic transmission. However, in networks that overexpress cypin, all CNQX concentrations significantly reduce the overall spike rate. Interestingly, this effect is not dependent on cypin binding to PSD-95 or its family members as overexpressing cypinΔPDZ results in a similar decrease in spike rate. These results suggest that there is a deficit in synaptic AMPAR expression and function in neuronal networks when cypin is overexpressed. Moreover, we found that the number of active electrodes was practically unchanged across conditions and treatments **(Fig. 4-9B)**, implying that these observed effects are due to deficits in synaptic transmission.

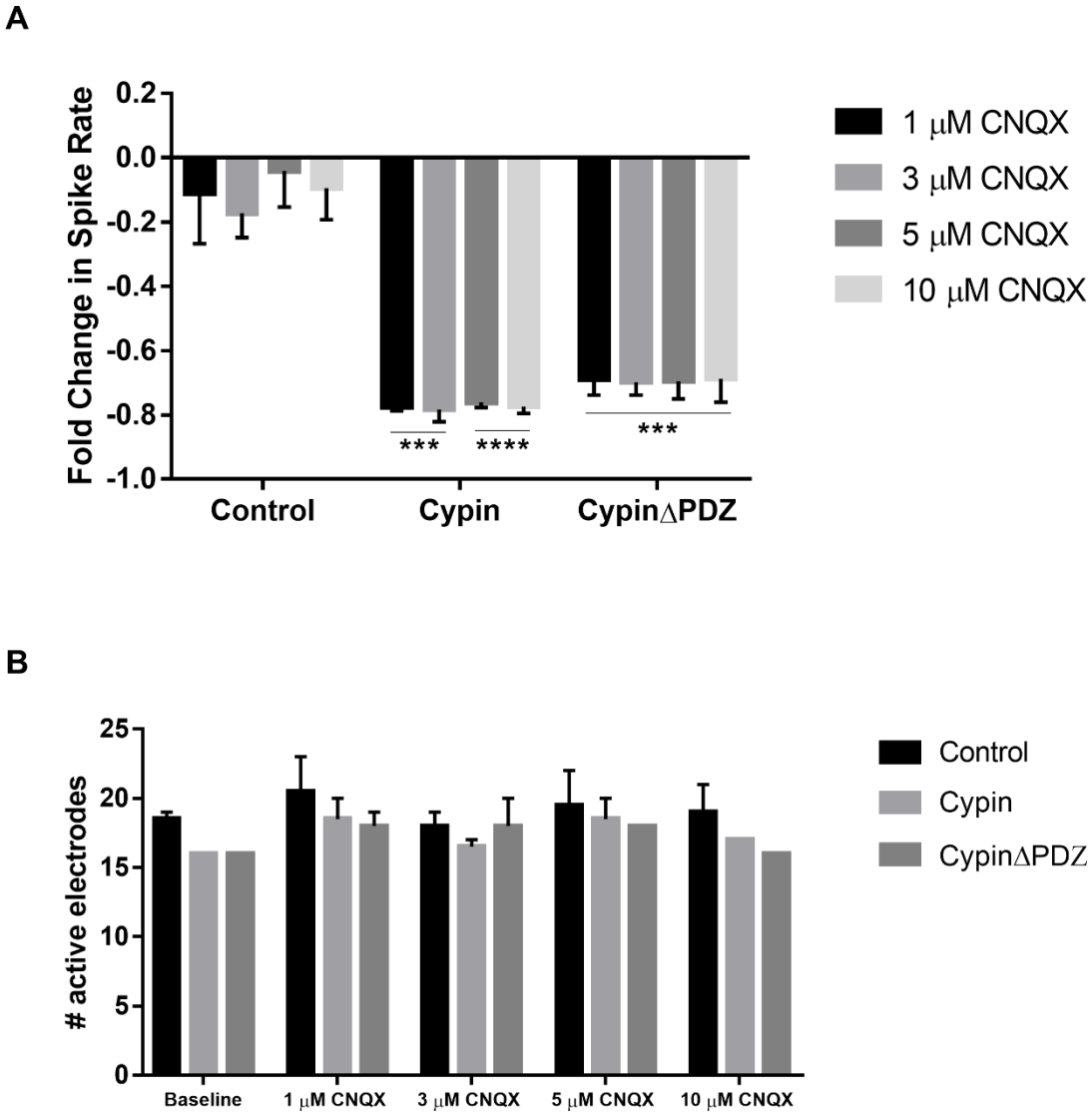

Figure 4-9. Networks overexpressing cypin exhibit a reduction in functional AMPARs. (A) Cypin or cypinΔPDZ overexpression decreases the amount of CNQX needed to block synaptic transmission in neuronal networks. (B) The number of active electrodes was consistent across all conditions. Statistics were calculated by two-way ANOVA followed by Tukey's multiple comparisons test (n = 2 for all conditions; ***$p < 0.001$ and ****$p < 0.0001$).

We measured the spiking variability in these networks after CNQX treatment. We used the Fano factor (FF) as a measure of the dispersion of the spike count distribution and found that it is significantly decreased after cypin or cypinΔPDZ overexpression regardless of the CNQX concentration the networks were treated with **(Fig. 4-10A)**. Interestingly, networks that overexpress GFP also exhibit a decrease in spike count variability after treatment with 3 μM and 5 μM CNQX, suggesting that the Fano factor decreases although spike rate remains unchanged. This underlies the value of studying variability in network responses as well as their overall activity to uncover differences that might be ignored otherwise.

In addition, we found that networks that overexpress cypin or cypinΔPDZ display a significant increase in the average interspike interval **(ISI; Fig. 4-10B)** that is accompanied by a significant decrease in the coefficient of variation **(CV; Fig. 4-10C)**. Hence, with a decrease in spike rate after CNQX treatment, cultures overexpressing cypin or cypinΔPDZ exhibit spikes that are temporally further apart, but the variability in this timing decreases and becomes more regular. In fact, when we look at the raw values of CV, we see that their CV at baseline is between 2.2 – 3.3, and decreases to near Poisson values (~1) after CNQX exposure.

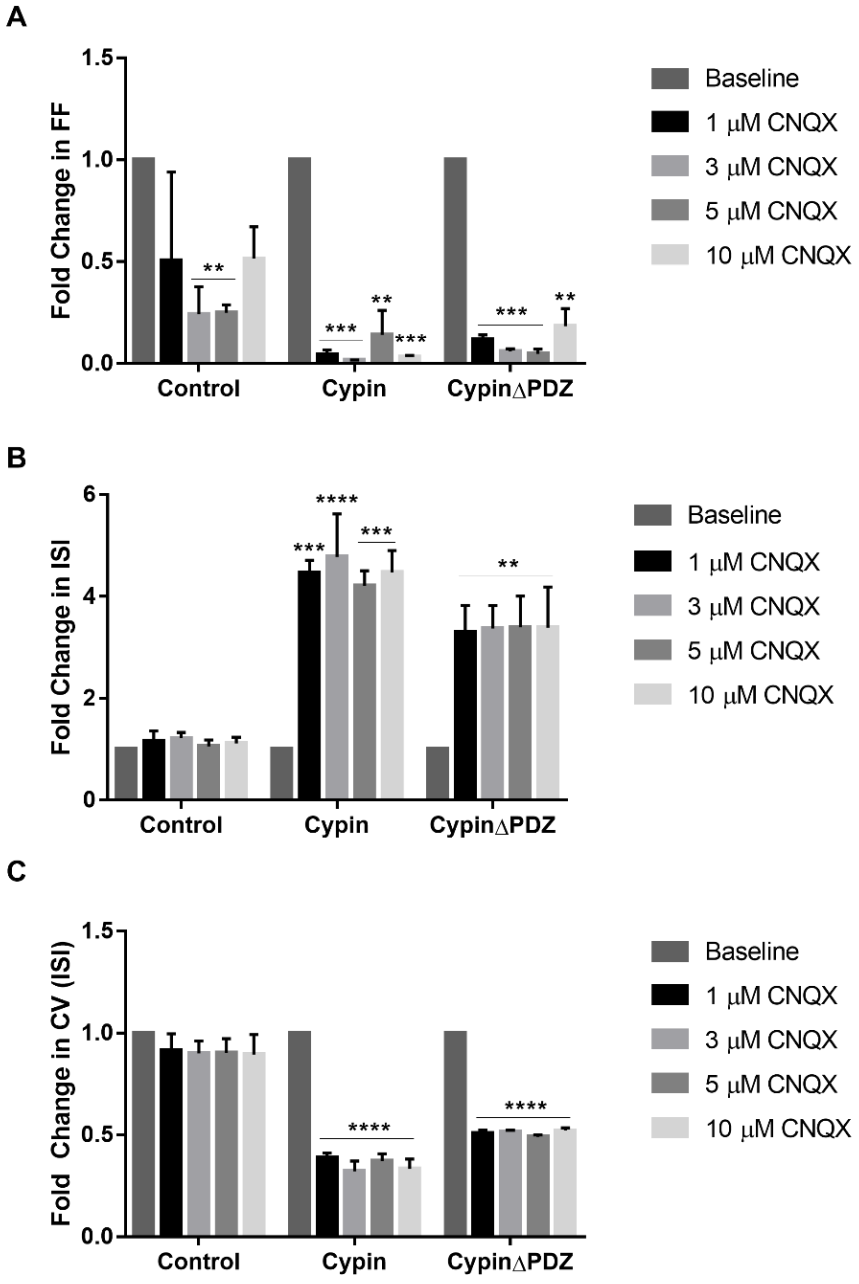

Figure 4-10. Spike variability is affected by CNQX treatment. (A) Spike count variability decreases after CNQX treatment in networks that overexpress cypin or cypinΔPDZ and in control networks after treatment with 3 or 5 μM CNQX. (B) Cypin or cypinΔPDZ overexpression result in a significant increase in ISI and (C) CV, regardless of CNQX concentration. Statistics were calculated by two-way

ANOVA followed by Dunnett's multiple comparisons test (n = 2 for all conditions; **p < 0.01, ***p < 0.001, and ****p < 0.0001).

We performed sorting based on spike waveforms to determine whether CNQX treatment affects the shapes of detected spikes. We first investigated the spike shapes at DIV15 before CNQX treatment **(Fig. 4-11)**. Our results show that the networks of all conditions exhibit a majority of negative spike shapes. In agreement with our results in Chapter 3, we observed that networks that overexpress cypin display spike shapes that are not found in the control condition with an overall larger proportion of non-negative peaks **(Fig. 4-11B)**.

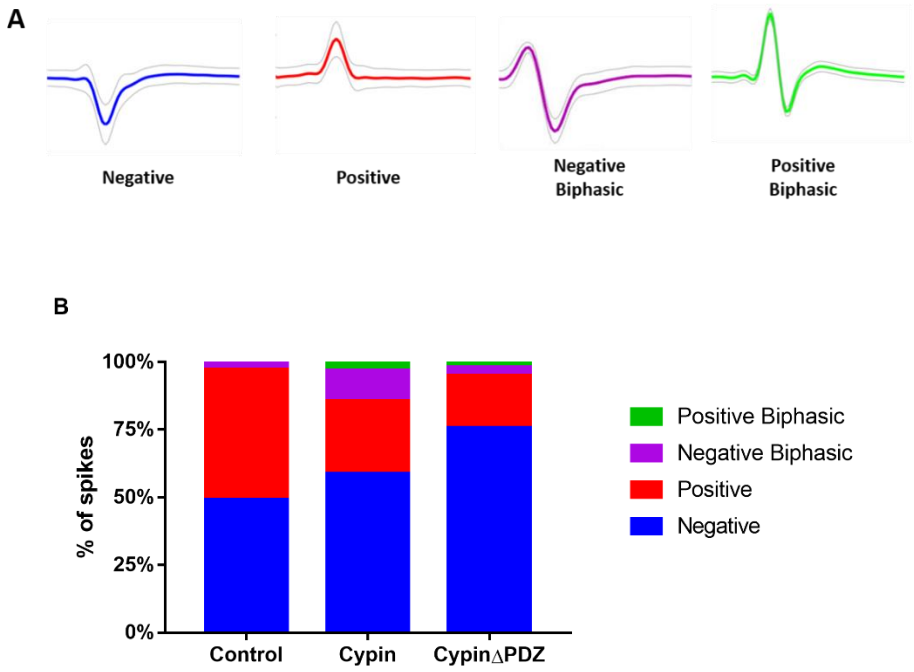

Figure 4-11. (A) Representative average spike waveforms observed. (B) Cypin overexpression results in more complex spike waveform distributions. Spike sorting was performed on DIV15 recordings prior to CNQX treatment.

We assessed the effect of blocking AMPAR function with CNQX on spike shapes. We found that networks that overexpress GFP **(Fig. 4-12A)** exhibit subtle changes in the distribution of spike shapes after CNQX treatment. At baseline, they exhibit a small proportion of negative biphasic spikes that then changes to a positive biphasic subset of spikes for the remainder of the experiment. Networks that overexpress cypinΔPDZ **(Fig. 4-12C)** display a complete loss of the subset of biphasic spikes observed before CNQX exposure and only exhibit a combination of negative and positive spikes that remains unchanged with CNQX treatment. Interestingly, networks that overexpress cypin **(Fig. 4-12B)** maintain the subset of negative biphasic spikes during the course of CNQX treatment, with the exception of treatment with 1 μM CNQX. These data suggest that although CNQX treatment results in a dramatic spike rate reduction and variability after cypin overexpression, the types of spikes that are produced and detected are largely unaffected by CNQX treatment.

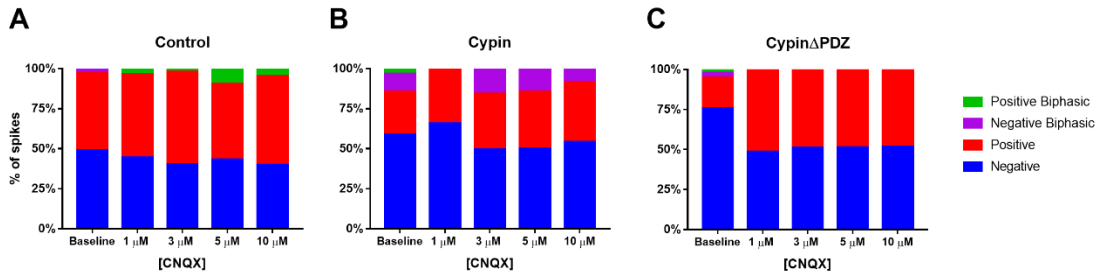

Figure 4-12. Spike waveforms after CNQX exposure. We assessed the distributions of spike shapes during the course of CNQX dosage for networks that overexpress (A) GFP, (B) cypin, and (C) cypinΔPDZ.

4.4 Discussion

In this chapter, we used biochemical and electrophysiological techniques to investigate the consequence of altering cypin levels on dendrite branching, PSD-95 protein levels, and synaptic function. Our group has published extensively on the role of cypin in dendrite branching at different developmental timepoints (Akum et al. 2004; Charych et al. 2006; M. Kwon et al. 2011; O'Neill et al. 2015). In the present work, we overexpressed cypin or cypinΔPDZ on DIV7 and measured changes to the dendritic arbor on DIV12. We found that overexpression of cypin increases the total number of dendrites by DIV12 and that this effect is not completely dependent on its ability to interact with PDZ domain-containing proteins. In addition, we found that cypin overexpression results in a significant increase in tertiary dendrites.

A recent study by our group (O'Neill et al. 2015) demonstrated that cypin overexpression increases primary and tertiary dendrites by DIV10, leading us to hypothesize that primary dendrites are pruned between DIV10-12. Moreover, we also previously reported that PSD-95 has a nonsynaptic and activity-independent function in hippocampal dendrites as it acts as a stop signal for proximal dendrite branching early in development (Charych et al. 2006). It is plausible that the interaction between cypin and PSD-95 influences dendrite branching between DIV10-12, causing the likely pruning of primary dendrites. This underlines the specificity and sometimes transient nature of these changes as well as the interplay between cypin and PSD-95 at different times in development.

The majority of this chapter focused on the effect of cypin overexpression or knockdown on PSD-95 protein levels and the functional consequence of this action. We

found that overexpressing cypin in hippocampal neurons results in an increase in total PSD-95 protein levels and that this increase is dependent on the PDZ-binding motif of cypin. Conversely, cypin knockdown resulted in a trend towards a decrease in total PSD-95 levels. Interestingly, total SAP102 protein levels are unaffected with either cypin or cypinΔPDZ overexpression (data not shown), suggesting that cypin influences PSD-95 protein levels specifically as opposed to generally affecting levels of any PDZ domain-containing protein. We performed synaptosomal fractionation and showed that cypin overexpression results in a decrease of PSD-95 protein levels in the synaptosomes and PSD fraction, in agreement with the finding of reduced PSD-95 synaptic clusters after cypin overexpression (Firestein et al. 1999). This suggests that cypin has a distinct effect on synaptic and nonsynaptic PSD-95 protein expression and redistribution.

The PSD exhibits constant remodeling and the dynamic recruitment of its constituents to the synapse and has been shown to be regulated by changes in synaptic activity (Ehlers 2003), post-translational modifications (Colledge et al. 2003; Catarino et al. 2013; Fukata et al. 2004; Perez de Arce et al. 2010), and local protein translation (Schuman, Dynes, and Steward 2006). Constitutive NMDAR hypofunction and hyperfunction results in altered protein expression of NMDAR and AMPAR subunits at the synapse (Balu and Coyle 2011). In addition, palmitoylation of PSD-95 controls its recruitment and removal at the synapse and influences retention of AMPARs (A. E. D. El-Husseini et al. 2002). Furthermore, activity-dependent degradation and ubiquitination have been reported for several constituents of the PSD, including PSD-95 (Colledge et al. 2003), and proteasomes can translocate to postsynaptic sites in response to synaptic activity (Bingol and Schuman 2006). Cypin interacts with a proteasome subunit, and hence, it may act to regulate the synaptic localization of PSD-95 via the proteasome. It is possible that cypin also inhibits

the proteasome-dependent degradation of nonsynaptic PSD-95, resulting in its increased expression. We explore this hypothesis in more detail in the next chapter.

We recorded miniature excitatory postsynaptic currents (mEPSCs) to determine if the cypin-promoted decrease in synaptic PSD-95 levels leads to alterations in synaptic transmission. We found that cypin overexpression increases the frequency but not the amplitude of mEPSCs and that this is independent of PSD-95-binding. This result was counterintuitive since others have shown that PSD-95 overexpression results in increased frequency of mEPSCs (A. E. El-Husseini et al. 2000; Béïque and Andrade 2003). Interestingly, it has been reported that knocking out PSD-95 results in a disruption of AMPAR function in only a subset of synapses (Béïque et al. 2006) and that acute inactivation of PSD-95 in culture results in an abrupt disruption of endogenous GluR2 subunits of AMPARs with no observed differences in NMDARs levels (Yudowski et al. 2013). These data suggest that compensation occurs and that NMDARs may be stabilized by a scaffolding protein other than PSD-95 at the synapse. A potential limitation of our study is that individual hippocampal neurons have varying levels of endogenous cypin, and hence, overexpression and knockdown of cypin may result in a range of effects in different populations. Our data suggest that the decrease in synaptic PSD-95 levels promoted by cypin overexpression may only affect a subset of synapses and that homeostatic mechanisms (Turrigiano and Nelson 2012) may result in increased synaptic transmission in a subset of neurons.

Finally, we assessed whether cypin overexpression affects AMPAR-mediated synaptic transmission in neuronal networks. We found that the overall spike rate of networks that overexpress cypin is dramatically decreased with addition of the AMPAR

antagonist CNQX, regardless of concentration. This suggests that cypin overexpression causes a reduction in functional AMPARs in these networks, in agreement with reports on AMPAR-mediated activity disruption as a result of decreasing PSD-95 levels (Yudowski et al. 2013; Béïque et al. 2006). This effect was not dependent on PSD-95 binding. In contrast, networks that overexpress GFP did not exhibit this change to activity with CNQX treatment. One explanation is that AMPAergic synaptic upscaling is triggered in the networks overexpressing GFP in the presence of CNQX. Reduced AMPAergic transmission through CNQX is sufficient to trigger upscaling directly as a compensatory response in cortical networks (Fong et al. 2015). Our results suggest that overexpression of cypin reduces the amount of functional AMPARs, further preventing homeostatic upscaling from being triggered. We did not study bursting or synchronization behavior in these networks because at this level of suppression of activity, the rates of bursting events were extremely low, and many times bursting was not present.

We found that the spike count variability (Fano factor) and variability of the interspike intervals (CV) of networks that overexpress cypin or cypinΔPDZ decrease as a function of their spike rate, suggesting that regularity of the firing patterns of these networks increases in the presence of CNQX. Interestingly, CNQX exposure between 3-5 μM decreases the variability of the spike count of networks that overexpress GFP but not the temporal distribution of the emitted spikes. It is important to note that it remains a possibility that at high levels of suppression of activity, the Fano factor is not a completely reliable measure when measured over a long window of time, as was done in this study. It is possible that by using a long window of time, subtle effects in spike count variability are missed.

Overall, the results shown in this chapter demonstrate that cypin-mediated alterations in PSD-95 protein levels result in changes to synaptic transmission that are independent of PSD-95 binding. Moreover, our data support previous evidence that cypin acts to redistribute PSD-95 and that this is dependent on the PDZ-binding motif of cypin. We believe that cypin and PSD-95 have balancing influences in the morphological and functional establishment of neuronal circuits.

4.5 Acknowledgements

I would like to thank Dr. Munjin Kwon for her work and collaboration on PSD-95 levels after cypin overexpression and cypin knockdown characterization, Mihir Patel for his collaboration in the dendrite branching studies, and Przemyslaw Swiatkowski for his work on mEPSCs recording.

Chapter 5: The interaction of cypin with the proteasome

5.1 Introduction

The continuous modification of synapses by activity and experience is believed to be essential for information storage in the brain (Lüscher et al. 2000; Yuste and Bonhoeffer 2001). Much of this remodeling takes place at the postsynaptic density (PSD) of excitatory synapses, a compartment containing glutamate receptors and signaling proteins assembled by a various scaffolding molecules (Morgan Sheng and Hoogenraad 2007). Changes in the molecular composition of the PSD are thought to mediate and accompany structural changes in response to activity and during synapse establishment and maturation (Lüscher et al. 2000; Ehlers 2003). These molecular changes can occur through the addition of new synaptic proteins (Schuman, Dynes, and Steward 2006), as well as by changes in stabilization or the removal of existing proteins (Ehlers 2003; Colledge et al. 2003).

PSD-95 (**p**ost**s**ynaptic **d**ensity protein **95**) is a major scaffolding protein at excitatory synapses, where it interacts with transmembrane receptors and channels, as well as signaling proteins. PSD-95 binds directly to NMDARs (Lin et al. 2004) and indirectly to AMPARs, through the transmembrane regulatory protein stargazin (Schnell et al. 2002; Vandenberghe, Nicoll, and Bredt 2005). Through interactions with these and other synaptic proteins, PSD-95 strongly influences receptor recruitment (Lin et al. 2004; X. Chen et al. 2011; Yudowski et al. 2013), dendritic spine maturation (A. E. El-Husseini et al. 2000; Pak et al. 2001), and synaptic transmission and scaling (Sun and Turrigiano 2011).

Cypin is a known cytosolic interactor of PSD-95 in the brain (Firestein et al. 1999). We have shown that cypin overexpression results in a decrease in PSD-95 synaptic

clustering (Firestein et al. 1999) and protein expression in rat hippocampal neurons. We now know that this is accompanied by an increase in total PSD-95 protein levels. A yeast two hybrid screen with cypin lacking the last four amino acids as bait identified the β7 subunit of the proteasome as a potential interactor of cypin, leading us to hypothesize that cypin regulates PSD-95 levels via the proteasome. Synaptic protein turnover is essential for the correct establishment and function of synapses (Ehlers 2003), and proteasome dysfunction has been implicated in the pathogenesis of many disease states (Um et al. 2010), including Alzheimer's disease, where proteasome inhibition is predicted to be involved in the synaptic defects that characterize it (Haynes et al. 2015; Gong, Radulovic, and Figueiredo-pereira 2016).

The ubiquitin-proteasome pathway is a major mechanism that controls protein abundance via exquisitely regulated protein degradation. It is involved and essential in many cellular processes, including cell cycle progression, signal transduction, metabolism, and protein quality control. In eukaryotic cells, proteins are tagged with polyubiquitin chains for degradation by the proteasome. The process of ubiquitination involves multiple steps and uses three classes of enzymes – E1, E2, and E3 – to active ubiquitin (E1), conjugate it (E2), and catalyze the transfer (E3) of ubiquitin to a recognized substrate.

The 26S proteasome is an ATP-dependent complex comprised of a catalytic (20S) particle and two regulatory (19S) particles, both of which are composed of sets of distinct subunits (Baumeister et al. 1998). The structure and function of the proteasome is highly conserved. The 20S proteasome is a cylindrical particle formed by four stacked heptameric rings: two inner rings composed of seven β subunits and two outer rings composed of seven α subunits. These subunits are expressed from distinct, yet related genes (Johnston

and Madura 2004). The 20S particle has three distinct peptidase activities that are produced by three different β subunits – β1, β2, and β5 – in the interior of the cylinder (M Groll et al. 1997). In contrast, the 19S regulatory particle consists of two distinct multiunit subcomplexes, the base and the lid, that are linked by the subunit Rpn10 (Glickman et al. 1999). The 19S proteasome is involved in the recognition, binding, deubiquitination, unfolding, and translocation of substrates to the proteolytic chamber of the 20S proteasome for degradation.

It is now generally accepted that PSD-95 is ubiquitinated and a target of the proteasome (Colledge et al. 2003; Bingol and Schuman 2004; Bianchetta et al. 2011; Tsai et al. 2012). Upon NMDAR stimulation, synaptic PSD-95 is ubiquitinated and degraded by the proteasome, resulting in a loss of synaptic AMPARs and long-term depression induction (Colledge et al. 2003). In addition, AMPAR stimulation leads to proteasome-dependent degradation of dendritic PSD-95 (Bingol and Schuman 2004). These studies have provided evidence that the ubiquitin-proteasome pathway plays an important role in synaptic remodeling and response. Here, we investigate the effects of the interaction between cypin and the β7 subunit of the proteasome, as a potential mechanism by which cypin regulates PSD-95 protein levels.

5.2 Materials and Methods

5.2.1 Co-immunoprecipitation

HEK293T cells were transfected with plasmids encoding RFP or RFP-tagged cypin using the calcium phosphate precipitation method (Munjin Kwon and Firestein 2013).

Cells were harvested 48 hours post-transfection in RIPA buffer (10 mM Tris-HCl pH 8.0, 1 mM EDTA, 0.5 mM EGTA, 1% Triton X-100, 0.1% sodium deoxycholate, 0.1% SDS, 140 mM NaCl, and 1 mM PMSF). Cell lysates were cleared for 1 hour and incubated with anti-β7 (Enzo Life Sciences) overnight at 4°C. Antibody-protein complexes were precipitated with Protein G Sepharose beads (GE Life Sciences) for 1 hour at 4 °C. Protein samples were resolved by SDS-PAGE, transferred to a PVDF membrane and probed for β7 and RFP to confirm the specific interaction.

5.2.2 ZsGreen transfection and fluorescence measurement

COS-7 cells were co-transfected with a ZsGreen-expressing proteasome sensor vector (pZsProSensor-1; Clontech Laboratories) and plasmids encoding either RFP or RFP-tagged cypin and cypin mutants using Lipofectamine 2000 (Invitrogen) according to the manufacturer's instructions. The proteasome sensor vector encodes a destabilized form of green fluorescent protein (ZsGreen) that is rapidly degraded by healthy proteasomes. Cells were fixed and immunostained 48 hours post-transfection, images were obtained at 600X with oil immersion, and ZsGreen fluorescence intensity was measured using ImageJ software (NIH).

5.2.3 $Ub^{G76V}GFP$ transfection and fluorescence measurement

HEK293T cells were co-transfected with $Ub^{G76V}GFP$ plasmid (Addgene) and plasmids encoding either RFP or RFP-tagged cypin using Lipofectamine 2000 (Invitrogen) according to the manufacturer's instructions. GFP fluorescence was measured 48 hours post-transfection at room temperature using a fluorescence plate reader at λ_{EX} = 485 and λ_{EM} = 530. A subset of cells were treated with 5 uM of the proteasome inhibitor

epoxomicin to validate the assay. All measurements were taken in PBS to prevent the cell culture medium from interfering with the fluorescence signal.

5.2.4 Western blotting

COS-7 cells were co-transfected with HA-tagged ubiquitin and plasmids encoding RFP or RFP-tagged cypin. Cells were harvested in RIPA buffer (10 mM Tris-HCl pH 8.0, 1 mM EDTA, 0.5 mM EGTA, 1% Triton X-100, 0.1% sodium deoxycholate, 0.1% SDS, 140 mM NaCl, and 1 mM PMSF) using Lipofectamine 2000 (Invitrogen) according to the manufacturer's instructions. Samples were spun at 7,500x*g* and 4 °C for 10 minutes, and supernatants were snap frozen in liquid nitrogen. Protein extracts (20 µg) were resolved by SDS-PAGE, transferred to a PVDF membrane, and probed for HA tag to identify ubiquitinated proteins. The membrane was also probed for actin as a protein loading control.

5.2.5 Measurement of proteasome activity

Extracts were prepared from COS-7 cells 48 hours after transfection with plasmids encoding RFP or RFP-tagged cypin. The chymotryptic-like activity of the proteasome in 20 µg of cell extracts was measured in the presence of the fluorogenic substrate Suc-Leu-Leu-Val-Tyr-AMC (Boston Biochem). The release of fluorescent AMC was measured at room temperature at an excitation wavelength of 360 nm and an emission wavelength of 425 nm for 60 minutes at 5-minute intervals. Proteasome-specific activity was calculated by subtracting values obtained in the presence of the proteasome inhibitor epoxomicin. All measurements were performed in duplicate.

5.2.6 Native gel analysis

Non-denaturing polyacrylamide gel electrophoresis (PAGE) was performed as described (Chandra et al. 2010) with some modifications. Briefly, protein lysates (70 μg) from HEK293T cells transfected with plasmids encoding either RFP or RFP-tagged cypin were separated and resolved for 3 hours (125V for 30 minutes and 150V for the remaining 2.5 hours) in steps of 3, 4, and 5% polyacrylamide. The gel was incubated with buffer containing Suc-LLVY-AMC for 20 minutes at 37 °C, and the fluorescence signal was visualized upon exposure to UV light. The enzymatic activity of the 20S core was stimulated by addition of 0.05% SDS.

5.3 Results

5.3.1 Cypin interacts with the β7 proteasome subunit in HEK293T cells

A yeast two hybrid screen with cypin lacking the last four amino acids as bait identified the β7 subunit of the proteasome as a potential interactor of cypin. To confirm this interaction in a mammalian cell line, we transfected HEK293T cells with a plasmid encoding RFP or RFP-tagged cypin and performed co-immunoprecipitation assays with an antibody against β7. HEK293T cells do not express endogenous cypin. We found that RFP-tagged cypin co-immunoprecipitates with the β7 subunit while RFP does not **(Fig. 5-1)**. We previously showed that cypin interacts with the β7 subunit in rat brain (Previtera and Firestein, unpublished results); hence, our results confirm that the interaction between cypin and the β7 subunit of the proteasome can take place in different cell types. Moreover, RFP-tagged cypin does not co-immunoprecipitate with the Rpt6 subunit of the

19S proteasome (data not shown), suggesting that its interaction with β7 is specific and it does not bind to all proteasome subunits.

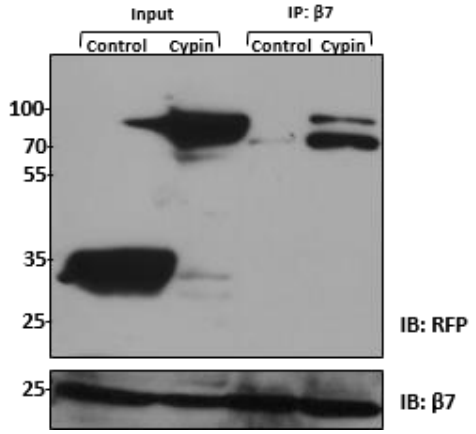

Figure 5-1. Cypin co-immunoprecipitates with the β7 subunit of the proteasome in HEK293T cells. We transfected cells with plasmids encoding RFP or RFP-tagged cypin and performed co-immunoprecipitation assay with a β7 antibody. RFP-tagged cypin, but not RFP, co-immunoprecipitates with the β7 subunit.

5.3.2 Cypin interferes with the degradation of ZsGreen

We used a reporter assay to investigate whether the interaction of cypin with a subunit of the proteasome results in the modulation of proteasome activity. We co-transfected COS-7 cells with a proteasome sensor plasmid and either RFP or RFP-tagged cypin, cypinΔPDZ or cypinΔ76-84 (amino acids 76-84 are necessary for zinc binding and guanine deaminase activity). The proteasome sensor plasmid encodes a form of ZsGreen, a green fluorescent protein, which is unstable and rapidly degraded by the proteasome. The ZsGreen C-terminus is fused to a degradation motif that targets it for removal by the 26S proteasome independent of its ubiquitination state. We measured ZsGreen fluorescence after co-transfection and found that overexpression of cypin or either cypin mutant

resulted in higher ZsGreen fluorescence levels when compared to levels in cells co-transfected with RFP **(Fig. 5-2)**. These data suggest that cypin interferes with the degradation of ZsGreen by the proteasome and that this effect is not dependent on its PDZ- or zinc-binding motifs.

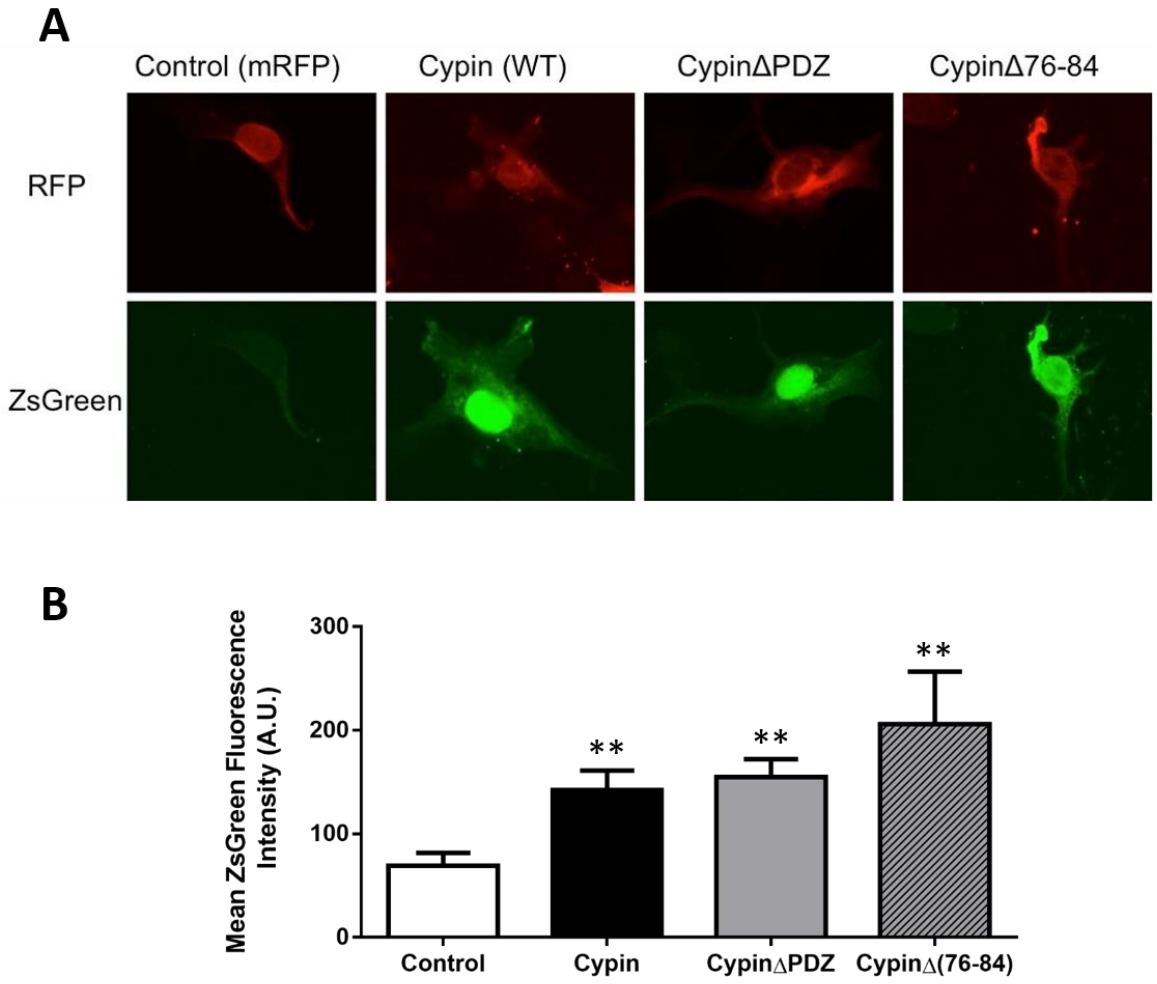

Figure 5-2. Cypin interferes with ZsGreen degradation. (A) COS-7 cells expressing cypin exhibit higher levels of ZsGreen fluorescence when compared to the control condition. Cells were fixed and immunostained 48 hours post-transfection, images were obtained at 600X with oil immersion, and (B) ZsGreen fluorescence intensity was measured. Statistics were calculated by one-way ANOVA followed by Dunnett's

multiple comparisons test (Data pooled from 3 independent experiments; **p<0.01 vs. control).

5.3.3 Cypin interferes with the degradation of $Ub^{G76V}GFP$

To further investigate whether cypin interferes with protein degradation, we employed a reporter plasmid that encodes a GFP-based substrate fused to ubiquitin, which is therefore targeted for degradation by the ubiquitin-proteasome system (Dantuma et al. 2000; Um et al. 2010). A ubiquitin monomer is covalently attached to GFP, avoiding its removal by deubiquitination machinery. Thus, the level of $Ub^{G76V}GFP$ protein is inversely proportional to the activity of the 26S proteasome. Accordingly, we found that $Ub^{G76V}GFP$ fluorescence was increased in the presence of the proteasome inhibitor epoxomicin to a degree similar to what has been reported (Um et al. 2010).

We co-transfected HEK293T cells with either RFP or RFP-tagged cypin together with $Ub^{G76V}GFP$ and found that the level of $Ub^{G76V}GFP$ fluorescence was higher in cells that were expressing both RFP-cypin and $Ub^{G76V}GFP$ than in those expressing RFP and $Ub^{G76V}GFP$ (**Fig. 5-3**). Although the covalently attached monoubiquitin cannot be removed from the substrate, it can be further polyubiquitinated and deubiquitinated. We performed Western blot analysis and confirmed that the increase in GFP fluorescence is a result of accumulated mono and polyubiquitinated substrate and not free GFP (data not shown). Our results suggest that cypin impairs the activity of the proteasome in cultured mammalian cells and that this is the case in the presence or absence of ubiquitination.

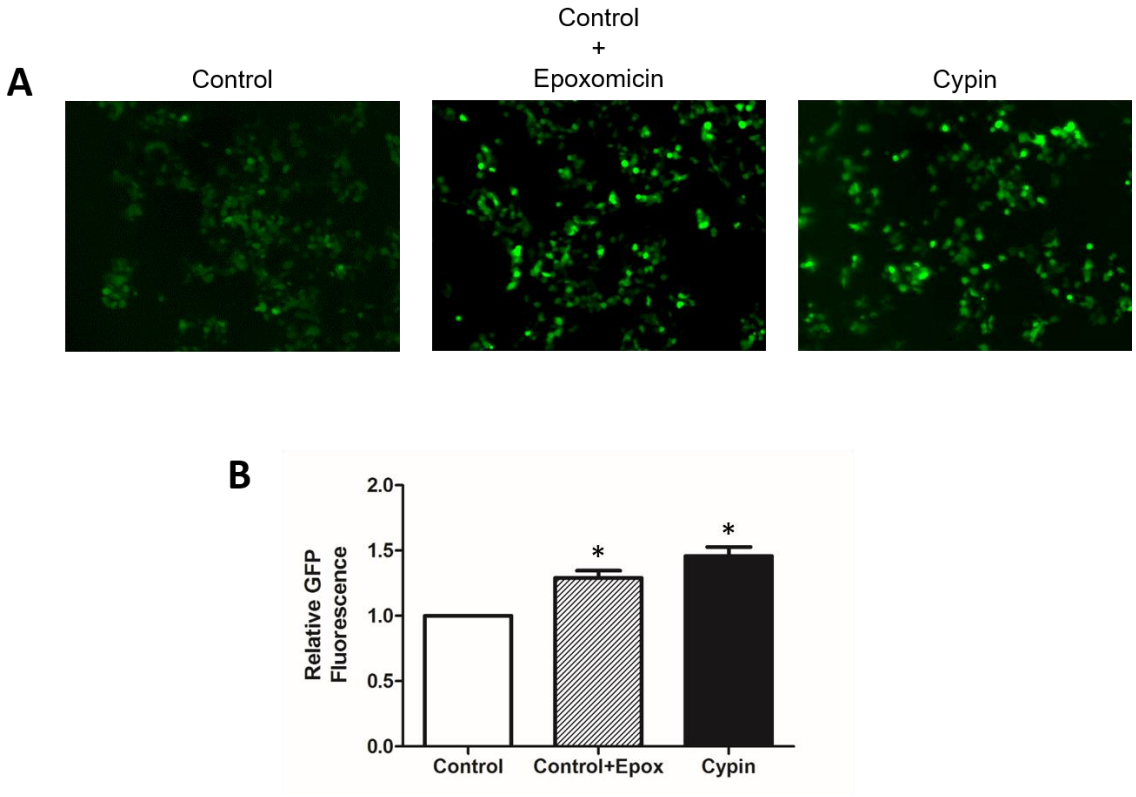

Figure 5-3. Cypin inhibits the degradation of $Ub^{G76V}GFP$. HEK293T cells were co-transfected with $Ub^{G76V}GFP$ and either RFP or RFP-tagged cypin. (A) Higher levels of $Ub^{G76V}GFP$ fluorescence were observed in the presence of epoxomicin and in the presence of cypin. (B) Fluorescence was measured using a fluorescence microplate reader. Statistics were calculated by one-way ANOVA followed by Dunnett's multiple comparisons test (Data pooled from 2 independent experiments; *p<0.05 vs. control).

5.3.4 Cypin overexpression increases accumulation of ubiquitinated proteins and decreases activity of the proteasome in mammalian cell lines

Next, we examined the effects of cypin overexpression on the peptidase activity of the proteasome in mammalian cell lines. We measured the chymotrypsin-like activity of

the proteasome using the widely used fluorogenic substrate Suc-LLVY-AMC and measured its hydrolysis in our cell lysates. We found that cypin overexpression resulted in a ~50% reduction in proteasome activity in COS-7 cells **(Fig. 5-4B)**. In addition, we co-transfected COS-7 cells with HA-tagged ubiquitin and RFP or RFP-tagged cypin and found that cypin overexpression results in an accumulation of ubiquitinated proteins in cell lysates **(Fig. 5-4A)**. Interestingly, when we examined this in HEK293T cells, we found that this accumulation of endogenous ubiquitinated proteins is not dependent on the PDZ- or zinc-binding motifs of cypin **(Fig. 5-4C)**. Together, our data suggest that cypin negatively modulates the peptidase activity of the proteasome, resulting in an accumulation of ubiquitin-tagged proteins, and that this effect is not specific to only one cell type.

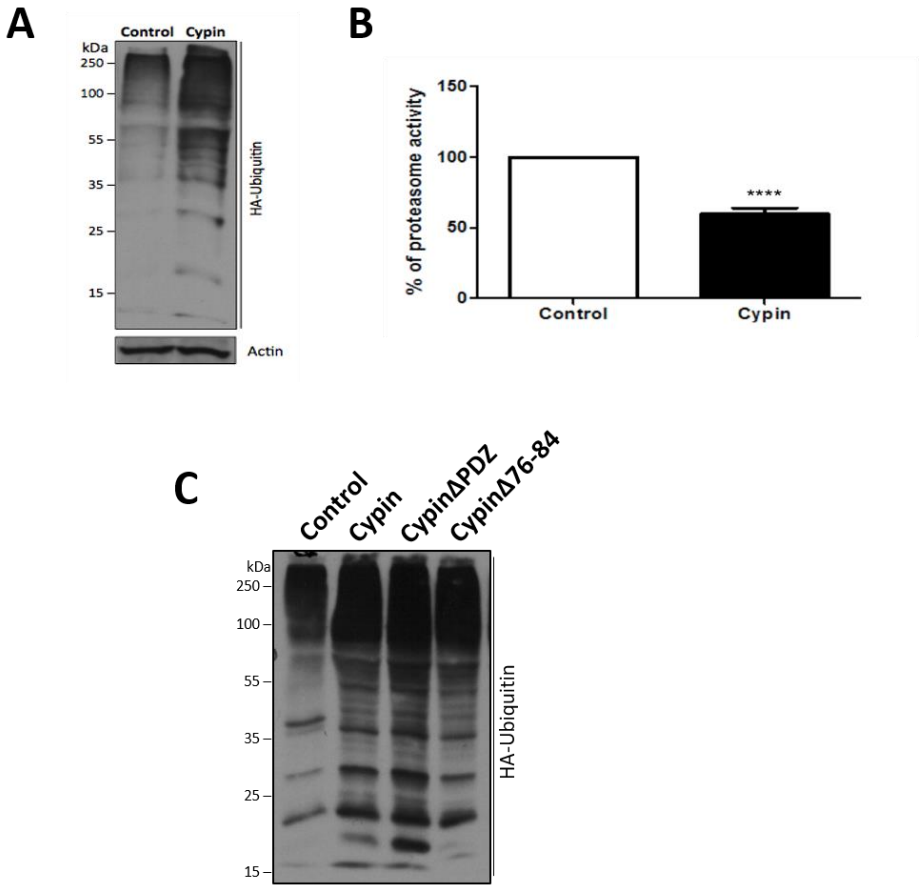

Figure 5-4. Cypin overexpression modulates proteasome activity. (A) Cypin overexpression results in an accumulation of ubiquitinated proteins in COS-7 cells and a (B) decrease in chymotrypsin-like activity of the proteasome (Data pooled from 2 independent experiments; ****p < 0.0001 calculated by Student's t test). (C) In HEK293T cells, overexpression of cypin or its mutants results in an accumulation of ubiquitinated proteins.

5.3.5 Proteasome assembly in the presence of cypin

To examine if the modulation of proteasome activity by cypin is a consequence of a defect in proteasome assembly or activity of intact proteasomes, we prepared lysates of

HEK293T cells overexpressing cypin and resolved lysate proteins in native polyacrylamide gels. In-gel hydrolysis of Suc-LLVY-AMC showed two bands corresponding to double-capped (19S + 20S + 19S) and single-capped (19S + 20S) proteasomes in lysates from cells overexpressing either RFP or cypin **(Fig. 5-5A)**. Free 20S particle was also detected but at a considerably lower level. These data suggest that cypin overexpression does not result in a significant decrease in intact functional proteasomes. After in-gel analysis, we transferred the proteins to PVDF membranes and subjected them to immunoblotting. We probed the membranes with antibodies against 20S (β7) and 19S (Rpt6) subunits and detected high amounts of these subunits at the level of single- and double-capped proteasomes **(Fig. 5-5B)**. Thus, cypin overexpression does not result in a significant increase in the proportion of free 20S particle, suggesting that cypin does not interfere with proteasome activity by affecting its integrity.

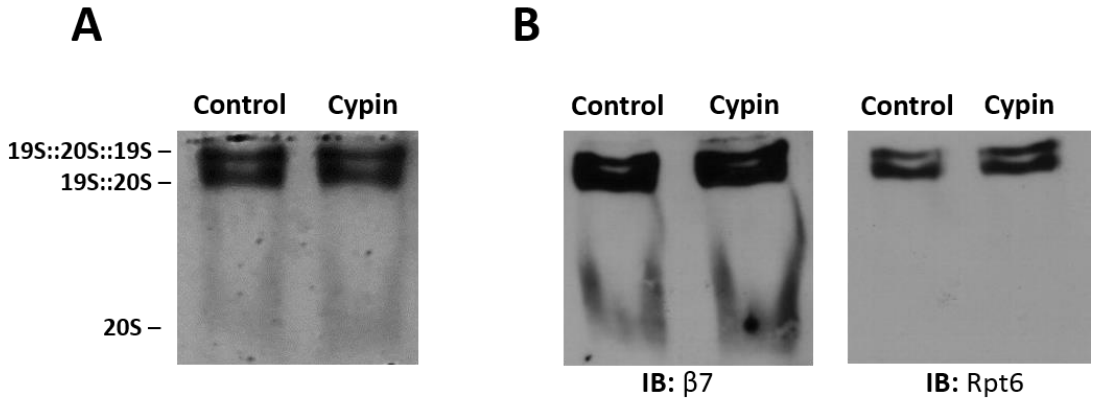

Figure 5-5. In-gel proteasome activity assay. (A) Lysate proteins were separated and resolved via non-denaturing PAGE, and the hydrolysis of Suc-LLVY-AMC was measured. (B) Proteins in the native gel were transferred to a PVDF membrane and probed with antibodies against 19S and 20S subunits.

5.3.6 Cypin overexpression increases PSD-95 ubiquitination

Cypin was originally identified as an interactor of the scaffolding protein PSD-95. In Chapter 4, we demonstrated that cypin overexpression results in an increase in total PSD-95 levels and a decrease in synaptic PSD-95 expression in hippocampal neurons. We now investigate if alterations in PSD-95 protein levels are a consequence of the interaction between cypin and resulting inhibition of the proteasome and its peptidase activity. We co-transfected HEK293T cells with plasmids encoding GFP-tagged PSD-95, HA-tagged ubiquitin, and RFP or RFP-tagged cypin or cypinΔPDZ. We then immunoprecipitated PSD-95 and assayed ubiquitination levels using Western blot analysis. We found that cypin overexpression resulted in an increase in PSD-95 ubiquitination **(Fig. 5-6)**. Interestingly, overexpression of cypinΔPDZ does not affect PSD-95 ubiquitination levels. Taken together with data from Chapter 4, our result suggests that cypin modulates PSD-95 levels via the proteasome and that this is dependent on interaction between cypin and PSD-95.

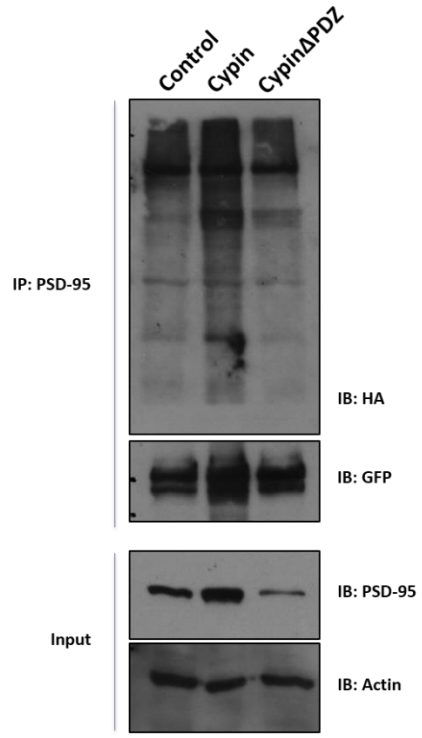

Figure 5-6. Cypin overexpression results in increased PSD-95 ubiquitination. HEK293 cells were co-transfected with plasmids encoding PSD-95-GFP, HA-Ubiquitin, and either RFP or RFP-tagged cypin or cypinΔPDZ. Cells lysates were subjected to immunoprecipitation, and immunoprecipitated proteins were resolved by SDS-PAGE and transferred to PVDF membrane. An increase in HA tag levels was observed exclusively when cypin is overexpressed. The membrane was probed for actin as a protein loading control.

5.4 Discussion

Cypin plays a role in the establishment and development of dendritic arbors (Akum et al. 2004; Charych et al. 2006; M. Kwon et al. 2011; O'Neill et al. 2015) and is an interactor of the scaffolding protein PSD-95 (Firestein et al. 1999). In the present study, we

propose a new role for cypin as a regulator of proteasome activity. We showed that cypin interacts with the β7 subunit of the proteasome. In addition, cypin overexpression decreases the chymotryptic-like activity of the proteasome and interferes with the degradation of two proteasome sensors. The degradation of the ZsGreen-expressing sensor is not dependent on ubiquitination. This is in line with the idea that cypin may act directly on the proteasome to inhibit its peptidase activity and not merely affect the ubiquitination level of proteasome targets.

Although the mechanism by which cypin interferes with proteasome activity was not elucidated, one possibility is that cypin disrupts correct proteasome assembly or stabilization through its interaction with β7. Proteasome activity can be modulated through interactions with subunits (Snyder et al. 2003; Lee, Lee, and Park 2012). For example, parkin, a widely studied protein implicated in Parkinson's disease, interacts with subunits in the 19S regulatory particle and promotes the activity and accelerates the assembly of the 26S proteasome (Um et al. 2010).

Assembly of the 26S proteasome is a highly orchestrated process that involves multiple steps and dedicated assembly chaperones (reviewed in: Murata, Yashiroda, and Tanaka 2009; Kunjappu, Hochstrasser, and Wolf 2014; Livneh et al. 2016). Assembly of the 20S proteasome begins with the formation of an α-ring, which the β–ring then uses as a scaffold for assembly. The β subunits are incorporated one by one, with β7 being incorporated last and completing the formation of a half 20S proteasome. The β7 subunit induces dimerization of two half proteasomes by inserting its C-terminal extension between the β1 and β2 subunits in the opposite β-ring. Thus, β7 has a stabilizing role in the formation of the catalytic proteasome, and truncation of its C-terminal extension

results in impaired proteasome activity and unstable proteasomes (Marques et al. 2007). Furthermore, most β subunits, including β7, are synthesized as precursors with N-terminal propeptides (Michael Groll et al. 1999), and upon complete proteasome assembly, the propeptides undergo autocatalytic cleavage (P. Chen and Hochstrasser 1996).

We do not know if cypin binds to the β7 propeptide. If it does, cypin could prevent its cleavage and interfere with the exposure of the catalytic site of the β subunits, thus resulting in decreased proteasome activity. Likewise, we do not know if cypin binds to other subunits in the 20S or 19S proteasome. β1 and β2 are two of the subunits that contain peptidase activity, and given their direct proximity to β7 in both rings, it is plausible that cypin may interfere with their proper assembly and function (Michael Groll et al. 1999). Although our preliminary results **(Fig. 5-6)** show that proteasome assembly is not disrupted in HEK293T cells upon cypin overexpression, further investigation is needed to confirm this, as well as to determine whether cypin interacts with other proteasome subunits or the β7 propeptide.

In line with our finding that cypin decreases proteasome activity, we further showed that cypin overexpression results in an accumulation of endogenous ubiquitinated proteins and that this accumulation is independent of the PDZ- and zinc-binding motifs of cypin. In addition, cypin overexpression increases the ubiquitination of PSD-95. This is in agreement with our finding that cypin overexpression results in an increase in total PSD-95 levels. PSD-95 is ubiquitinated by the E3 ligase Mdm2 (Bianchetta et al. 2011). Increased interaction between Mdm2 and PSD-95 enhances ubiquitination of PSD-95 but does not affect PSD-95 levels *in vivo* in mice with reduced cyclin-dependent kinase 5

(Cdk5) activity (Bianchetta et al. 2011). It has been proposed that Cdk5 regulates the distribution of Mdm2 in neurons and increases its levels at the postsynaptic density, where it ubiquitinates PSD-95 and promotes synapse elimination (Tsai et al. 2012).

We showed in Chapter 4 that the increase in total PSD-95 levels promoted by cypin overexpression is accompanied by a decrease in synaptic PSD-95 expression. It is plausible that Mdm2 or another E3 ligase ubiquitinates PSD-95 at the synapse, decreasing its expression in the PSD, while nonsynaptic PSD-95 is ubiquitinated but not degraded. We hypothesize that cypin alters proteasome activity and PSD-95 levels with the help of additional proteins since the proteasome activity of purified 20S does not change in the presence of GST-tagged cypin in a cell-free system (data not shown).

We have shown evidence to support the fact that cypin interferes with proteasome activity and mediates changes in PSD-95 levels via the proteasome. Additional studies will focus on identifying the mechanism by which cypin decreases the activity of the proteasome and how it relates to changes in synaptic dynamics. PSD-95 is an important component of the PSD and understanding the mechanism by which its expression and activity is regulated will give insight into the rearrangement and remodeling of the PSD.

5.5 Acknowledgements

I would like to thank Madeline Porter for her work with the ZsGreen proteasome sensor in COS-7 cells.

Chapter 6: Summary and Future Directions

Proper establishment and development of neuronal circuits is essential for healthy brain function and necessitates precise neuronal patterning and synaptic machinery. Our group identified cypin as a core regulator of dendrite branching in hippocampal neurons and an interactor of the scaffolding protein PSD-95. The goal of this dissertation is to enhance our understanding of the functional implications of altering cypin levels on PSD-95 protein and synaptic function.

In Chapters 2 and 3, we used microelectrode arrays to investigate neuronal network dynamics after overexpression of cypin or a mutant of cypin that cannot bind to PSD-95 or its family members (cypinΔPDZ). We established hippocampal cultures on MEAs and used lentiviral transduction to alter cypin levels. Specifically, in Chapter 2, we measured parameters that describe the global activity of the network, including spiking, bursting, and synchronized firing. We found that the trial-to-trial variability was high, and mean changes in these parameters were subtle, potentially due to averaging of small positive and negative changes. However, the overall spiking activity of our networks decreased over time, consistent with maturation of the networks.

In Chapter 3, we extended our analysis of network activity to the evaluation of spiking variability. Spiking variability is thought to be related to the clustered state of a network. Synaptic connections between excitatory neurons are thought to be clustered in functional subnetworks, rather than being uniform (Litwin-Kumar and Doiron 2012), and alterations in spiking variability can be related to activity level and underlie changes in the wiring of a network. We found that networks that overexpress cypin exhibit higher spike count variability than do control networks, as measured by the Fano factor, and that this

increase is dependent on initial level of activity. These data suggest that networks that overexpress cypin contain functional subnetworks that exhibit more fluctuations in firing rate over time.

We calculated the Fano factor for windows of 10 seconds; future studies should investigate changes in Fano factor using shorter windows of time, as longer windows might uncover variability patterns that takes place over short timescales. Moreover, we suggest the computation of the mean-matched Fano factor (Churchland et al. 2010), as it avoids artifacts related to large changes in mean spike rate and low trial counts. We calculated changes in temporal spike variability, as measured by the interspike interval (ISI) and the coefficient of variation. We found that cypin overexpression results in an increase in the ISI by DIV21. Overall, only networks that overexpress cypin exhibit significant changes in spiking variability. Thus, we were able to detect changes that were not detected using traditional global activity parameters.

We performed spike sorting based on waveform shapes and found that networks that overexpress cypin display a wider distribution of spike shapes over time. Interestingly, we found that networks that overexpress cypin exhibit a proportion of negative triphasic spikes, which is not found for any of the other conditions on DIV21. Recordings from planar MEAs typically exhibit field potentials dominated by negative peaks, which are thought to reflect inward currents recorded mainly from axons and excitable soma. In contrast, positive field potentials are associated with outward currents from dendrites (Fendyur et al. 2011). Negative spikes that are characterized by positive components have been associated with electrodes that are in close vicinity to dendritic segments (Csicsvari et al. 1999). Hence, it is conceivable to assume that the enhanced dendritic arbor

promoted by cypin overexpression influences the distribution of spike shapes observed. For this analysis, we pooled the spike waveform data for all spikes in a given condition at a given timepoint. Future studies should investigate changes in spike waveforms for individual electrodes to determine specific changes in spike shape over time, as they relate to the spatial arrangement of the network.

In Chapter 4, we examined the effect of altering cypin expression on total and synaptic PSD-95 levels and synaptic transmission. We found that cypin overexpression results in an increase of total PSD-95 levels and a decrease in synaptic PSD-95 levels and that this effect is dependent on cypin binding to PSD-95 family members. Moreover, cypin overexpression results in decreased dendritic spine density that is only partially dependent on PSD-95 family member binding to cypin. Cypin overexpression also results in increased frequency of miniature excitatory postsynaptic currents (mEPSCs), with no changes in amplitude. Interestingly, this increase in frequency is independent of binding to PSD-95 family members.

Other MAGUKs, such as SAP102 and PSD-93, are also highly enriched in the PSD. RNAi-mediated knockdown of PSD-93 or PSD-95 results in reduced number of AMPAR-containing synapses with no reduction in the number of AMPAR in the remaining synapses. Moreover, simultaneous knockdown of PSD-95, PSD-93, and SAP102 results in large decreases in AMPAR- and NMDAR-mediated synaptic transmission due to a reduction in synapses containing glutamate receptors with no change to number of dendritic spines or the strength of the remaining functional synapses (Levy et al. 2015). PSD-95 is necessary, but not sufficient, for synaptic scaling in cortical neurons, and PSD-93 supports scaling up and down of activity (Sun and Turrigiano 2011). These studies

support the role of homeostatic regulation after loss of PSD-95 via cypin overexpression and present the possibility that other MAGUKs compensate for the loss of PSD-95. We have shown that cypin overexpression does not change SAP102 levels, but future studies should elucidate whether expression of other MAGUKs is affected by changes in cypin protein levels.

We complemented this finding with an evaluation of changes in AMPAR-mediated synaptic transmission in neuronal networks. We found that the activity of the networks that overexpress cypin is silenced at much lower concentrations of the AMPAR antagonist CNQX when compared to networks that overexpress GFP. This reduction in activity is not dependent on binding to PSD-95 or its family members. Our data suggest that global overexpression of cypin in neuronal networks decreases the amount of functional AMPARs and may prevent synaptic upscaling from being triggered. Upward synaptic scaling can be triggered by reduced spiking and by chronically blocking AMPARs (Fong et al. 2015). Future studies should focus on investigating whether NMDAR-mediated synaptic transmission is affected after cypin overexpression. However, we found the present experiments to be technically challenging since the health of the cultures deteriorates due to viral transduction followed by multiple recordings to assess activity at different concentrations of the antagonist.

In Chapter 5, we propose a new role for cypin as a regulator of the proteasome. We show that cypin interacts with the β7 subunit of the proteasome in HEK293T cells and inhibits the chymotryptic-like activity of the proteasome. Moreover, cypin interferes with the degradation of two proteasome sensors. Cypin overexpression results in an accumulation of endogenous ubiquitinated proteins and an increase in ubiquitination of

PSD-95. We hypothesize that cypin acts via the proteasome to promote the degradation of synaptic PSD-95 while nonsynaptic PSD-95 is ubiquitinated but not degraded. Future studies should focus on elucidating the mechanism by which cypin interferes with proteasome activity and investigating the effect of cypin on proteasome activity and assembly in hippocampal neurons.

The correct establishment of neuronal networks requires proper spatiotemporal regulation of dendrite branching and synaptic protein turnover. Proteasome-dependent protein degradation has been implicated as a key process in synaptic plasticity (Ehlers 2003). We have shown evidence to support the fact that cypin alters PSD-95 levels in a proteasome-dependent manner. Moreover, we show that cypin overexpression affects spiking variability and AMPAR-mediated synaptic transmission. The next logical step is to extend this work and investigate how cypin affects neuronal circuitry and proteasome-mediated processes *in vivo*.

REFERENCES

Akum, Barbara F, Maxine Chen, Samuel I Gunderson, Gary M Riefler, Monica M Scerri-Hansen, and Bonnie L Firestein. 2004. "Cypin Regulates Dendrite Patterning in Hippocampal Neurons by Promoting Microtubule Assembly." *Nature Neuroscience* 7 (2): 145–52. doi:10.1038/nn1179.

Bai, Fengju, and Frank A Witzmann. 2007. "Synaptosome Proteomics." *Sub-Cellular Biochemistry* 43. NIH Public Access: 77–98. http://www.ncbi.nlm.nih.gov/pubmed/17953392.

Balu, Darrick T., and Joseph T. Coyle. 2011. "Glutamate Receptor Composition of the Post-Synaptic Density Is Altered in Genetic Mouse Models of NMDA Receptor Hypo- and Hyperfunction." *Brain Research* 1392: 1–7. doi:10.1016/j.brainres.2011.03.051.

Baumeister, W, J Walz, F Zuhl, and E Seemuller. 1998. "The Proteasome: Paradigm of a Self-Compartmentalizing Protease." *Cell* 92 (3): 367–80. doi:S0092-8674(00)80929-0 [pii].

Becchetti, Andrea, Francesca Gullo, Giuseppe Bruno, Elena Dossi, Marzia Lecchi, and Enzo Wanke. 2012. "Exact Distinction of Excitatory and Inhibitory Neurons in Neural Networks: A Study with GFP-GAD67 Neurons Optically and Electrophysiologically Recognized on Multielectrode Arrays." *Frontiers in Neural Circuits* 6 (September): 63. doi:10.3389/fncir.2012.00063.

Béïque, Jean-Claude, and Rodrigo Andrade. 2003. "PSD-95 Regulates Synaptic Transmission and Plasticity in Rat Cerebral Cortex." *The Journal of Physiology* 546 (Pt 3): 859–67. doi:10.1113/jphysiol.2002.031369.

Béïque, Jean-Claude, Da-Ting Lin, Myoung-Goo Kang, Hiro Aizawa, Kogo Takamiya, and

Richard L Huganir. 2006. “Synapse-Specific Regulation of AMPA Receptor Function by PSD-95.” *Proceedings of the National Academy of Sciences* 103 (51): 19535–40. doi:10.1073/pnas.0608492103.

Bianchetta, Michael J, Tukiet T Lam, Stephen N Jones, and Maria a Morabito. 2011. “Cyclin-Dependent Kinase 5 Regulates PSD-95 Ubiquitination in Neurons.” *The Journal of Neuroscience : The Official Journal of the Society for Neuroscience* 31 (33): 12029–35. doi:10.1523/JNEUROSCI.2388-11.2011.

Biffi, Emilia, Giulia Regalia, Andrea Menegon, Giancarlo Ferrigno, and Alessandra Pedrocchi. 2013. “The Influence of Neuronal Density and Maturation on Network Activity of Hippocampal Cell Cultures: A Methodological Study.” *PloS One* 8 (12): e83899. doi:10.1371/journal.pone.0083899.

Bingol, Baris, and Erin M Schuman. 2006. “Activity-Dependent Dynamics and Sequestration of Proteasomes in Dendritic Spines.” *Nature* 441 (7097): 1144–48. doi:10.1038/nature04769.

Bingol, Baris, and Erin M. Schuman. 2004. “A Proteasome-Sensitive Connection between PSD-95 and GluR1 Endocytosis.” *Neuropharmacology* 47 (5): 755–63. doi:10.1016/j.neuropharm.2004.07.028.

Blatt, Wiseman, and Domany. 1996. “Superparamagnetic Clustering of Data.” *Physical Review Letters* 76 (18): 3251–54. doi:10.1103/PhysRevLett.76.3251.

Bredt, D, and R a Nicholl. 2003. “AMPA Receptor Trafficking at Excitatory Synapses.” *Neuron* 40 (2): 361–79. doi:10.1016/S0896-6273(03)00640-8.

Brewer, G J, M D Boehler, R A Pearson, A A DeMaris, A N Ide, B C Wheeler, Gaiarsa J L and

Ben Ari Y Barbin G, Pollard H, et al. 2009. "Neuron Network Activity Scales Exponentially with Synapse Density." *Journal of Neural Engineering* 6 (1). IOP Publishing: 14001. doi:10.1088/1741-2560/6/1/014001.

Brewer, Gregory J., Michael D. Boehler, Torrie T. Jones, and Bruce C. Wheeler. 2008. "NbActiv4 Medium Improvement to Neurobasal/B27 Increases Neuron Synapse Densities and Network Spike Rates on Multielectrode Arrays." *Journal of Neuroscience Methods* 170 (2): 181–87. doi:10.1016/j.jneumeth.2008.01.009.

Cane, Michele, Bohumil Maco, Graham Knott, and Anthony Holtmaat. 2014. "The Relationship between PSD-95 Clustering and Spine Stability In Vivo" 34 (6): 2075–86. doi:10.1523/JNEUROSCI.3353-13.2014.

Carrel, Damien, Yangzhou Du, Daniel Komlos, Norell M Hadzimichalis, Munjin Kwon, Bo Wang, Linda M Brzustowicz, and Bonnie L Firestein. 2009. "NOS1AP Regulates Dendrite Patterning of Hippocampal Neurons through a Carboxypeptidase E-Mediated Pathway." *The Journal of Neuroscience : The Official Journal of the Society for Neuroscience* 29 (25): 8248–58. doi:10.1523/JNEUROSCI.5287-08.2009.

Catarino, Tatiana, Luís Ribeiro, Sandra D Santos, and Ana Luísa Carvalho. 2013. "Regulation of Synapse Composition by Protein Acetylation: The Role of Acetylated Cortactin." *Journal of Cell Science* 126 (Pt 1): 149–62. doi:10.1242/jcs.110742.

Chandra, Abhishek, Li Chen, Huiyan Liang, and Kiran Madura. 2010. "Proteasome Assembly Influences Interaction with Ubiquitinated Proteins and Shuttle Factors." *Journal of Biological Chemistry* 285 (11): 8330–39. doi:10.1074/jbc.M109.076786.

Chao, T C, and C M Chen. 2005. "Learning-Induced Synchronization and Plasticity of a

Developing Neural Network." *Journal of Computational Neuroscience* 19 (3): 311–24. doi:10.1007/s10827-005-2653-4.

Charych, Erik I, Barbara F Akum, Joshua S Goldberg, Rebecka J Jörnsten, Christopher Rongo, James Q Zheng, and Bonnie L Firestein. 2006. "Activity-Independent Regulation of Dendrite Patterning by Postsynaptic Density Protein PSD-95." *The Journal of Neuroscience : The Official Journal of the Society for Neuroscience* 26 (40): 10164–76. doi:10.1523/JNEUROSCI.2379-06.2006.

Chater, Thomas E, and Yukiko Goda. 2014. "The Role of AMPA Receptors in Postsynaptic Mechanisms of Synaptic Plasticity" 8 (November): 1–14. doi:10.3389/fncel.2014.00401.

Chen, H., and B. L. Firestein. 2007. "RhoA Regulates Dendrite Branching in Hippocampal Neurons by Decreasing Cypin Protein Levels." *Journal of Neuroscience* 27 (31): 8378–86. doi:10.1523/JNEUROSCI.0872-07.2007.

Chen, M., Kenyatta G. Lucas, Barbara F. Akum, Gaithri Balasingam, Tamara M. Stawicki, Janine M. Provost, Gary M. Riefler, Rebecka J. Jörnsten, and Bonnie L. Firestein. 2005. "A Novel Role for Snapin in Dendrite Patterning: Interaction with Cypin." *Molecular Biology of the Cell* 16 (11). American Society for Cell Biology: 5103–14. doi:10.1091/mbc.E05-02-0165.

Chen, Ping, and Mark Hochstrasser. 1996. "Autocatalytic Subunit Processing Couples Active Site Formation in the 20S Proteasome to Completion of Assembly" 86: 961–72.

Chen, X., C. D. Nelson, X. Li, C. A. Winters, R. Azzam, A. A. Sousa, R. D. Leapman, H. Gainer, M. Sheng, and T. S. Reese. 2011. "PSD-95 Is Required to Sustain the Molecular Organization of the Postsynaptic Density." *Journal of Neuroscience* 31 (17): 6329–38.

doi:10.1523/JNEUROSCI.5968-10.2011.

Chiappalone, Michela, Alessandro Vato, Luca Berdondini, Milena Koudelka-Hep, and Sergio Martinoia. 2007. "Network Dynamics and Synchronous Activity in Cultured Cortical Neurons." *Int J Neural Syst* 17 (2): 87–103. doi:10.1142/S0129065707000968.

Christodoulou, Chris, and Guido Bugmann. 2001. "Coefficient of Variation (CV) vs Mean Interspike Interval (ISI) Curves: What Do They Tell Us about the Brain?" *Neurocomputing*, 1141–49.

Christodoulou, Chris, and Aristodemos Cleanthous. 2011. "Does High Firing Irregularity Enhance Learning?" *Neural Computation* 23: 656–63. doi:10.1162/NECO_a_00090.

Churchland, Mark M, Byron M Yu, John P Cunningham, Leo P Sugrue, Marlene R Cohen, Greg S Corrado, William T Newsome, et al. 2010. "Stimulus Onset Quenches Neural Variability: A Widespread Cortical Phenomenon." *Nature Neuroscience* 13 (3). Nature Publishing Group: 369–78. doi:10.1038/nn.2501.

Colledge, Marcie, Eric M. Snyder, Robert A. Crozier, Jacquelyn A. Soderling, Yetao Jin, Lorene K. Langeberg, Hua Lu, Mark F. Bear, and John D. Scott. 2003. "Ubiquitination Regulates PSD-95 Degradation and AMPA Receptor Surface Expression." *Neuron* 40 (3): 595–607. doi:10.1016/S0896-6273(03)00687-1.

Csicsvari, J, H Hirase, a Czurkó, a Mamiya, and G Buzsáki. 1999. "Oscillatory Coupling of Hippocampal Pyramidal Cells and Interneurons in the Behaving Rat." *The Journal of Neuroscience : The Official Journal of the Society for Neuroscience* 19 (1): 274–87.

Dantuma, N P, K Lindsten, R Glas, M Jellne, and M G Masucci. 2000. "Short-Lived Green Fluorescent Proteins for Quantifying Ubiquitin/proteasome-Dependent Proteolysis in

Living Cells." *Nature Biotechnology* 18 (5): 538–43. doi:10.1038/75406.

Dotti, C G, C a Sullivan, and G a Banker. 1988. "The Establishment of Polarity by Hippocampal Neurons in Culture." *The Journal of Neuroscience : The Official Journal of the Society for Neuroscience* 8 (4): 1454–68. doi:10.1016/0012-1606(89)90269-8.

Eden, Uri T., and Mark A. Kramer. 2010. "Drawing Inferences from Fano Factor Calculations." *Journal of Neuroscience Methods* 190 (1). Elsevier B.V.: 149–52. doi:10.1016/j.jneumeth.2010.04.012.

Ehlers, Michael D. 2003. "Activity Level Controls Postsynaptic Composition and Signaling via the Ubiquitin-Proteasome System." *Nature Neuroscience* 6 (3): 231–42. doi:10.1038/nn1013.

Eisenman, Lawrence N, Christine M Emnett, Jayaram Mohan, Charles F Zorumski, and Steven Mennerick. 2015. "Quantification of Bursting and Synchrony in Cultured Hippocampal Neurons." *Journal of Neurophysiology*, jn.00079.2015. doi:10.1152/jn.00079.2015.

El-Husseini, A E, E Schnell, D M Chetkovich, R A Nicoll, and D S Bredt. 2000. "PSD-95 Involvement in Maturation of Excitatory Synapses." *Science (New York, N.Y.)* 290 (5495): 1364–68. doi:10.1126/science.290.5495.1364.

El-Husseini, Alaa El Din, Eric Schnell, Srikanth Dakoji, Neal Sweeney, Qiang Zhou, Oliver Prange, Catherine Gauthier-Campbell, Andrea Aguilera-Moreno, Roger A. Nicoll, and David S. Bredt. 2002. "Synaptic Strength Regulated by Palmitate Cycling on PSD-95." *Cell* 108 (6): 849–63. doi:10.1016/S0092-8674(02)00683-9.

Eytan, Danny, Amir Minerbi, Noam Ziv, and Shimon Marom. 2004. "Dopamine-Induced

Dispersion of Correlations between Action Potentials in Networks of Cortical Neurons." *Journal of Neurophysiology* 92 (3): 1817–24. doi:10.1152/jn.00202.2004.

Fendyur, Anna, Noa Mazurski, Joseph Shappir, and Micha E. Spira. 2011. "Formation of Essential Ultrastructural Interface between Cultured Hippocampal Cells and Gold Mushroom-Shaped MEA- Toward 'IN-CELL' Recordings from Vertebrate Neurons." *Frontiers in Neuroengineering* 4. Frontiers: 14. doi:10.3389/fneng.2011.00014.

Firestein, Bonnie L, Jay E Brenman, Chiye Aoki, Ana M Sanchez-Perez, Alaa El-Din El-Husseini, and David S Bredt. 1999. "Cypin: A Cytosolic Regulator of PSD-95 Postsynaptic Targeting." *Neuron* 24 (3): 659–72. doi:10.1016/S0896-6273(00)81120-4.

Fong, Ming-fai, Jonathan P Newman, Steve M Potter, and Peter Wenner. 2015. "Upward Synaptic Scaling Is Dependent on Neurotransmission rather than Spiking." *Nature Communications* 6. Nature Publishing Group: 6339. doi:10.1038/ncomms7339.

Fukata, Masaki, Yuko Fukata, Hillel Adesnik, Roger A Nicoll, David S Bredt, and San Francisco. 2004. "Identification of PSD-95 Palmitoylating Enzymes University of California at San Francisco" 44: 987–96.

Gambazzi, Luca, Ozgun Gokce, Tamara Seredenina, Elena Katsyuba, Heike Runne, Henry Markram, Michele Giugliano, and Ruth Luthi-carter. 2010. "Diminished Activity-Dependent BDNF Expression Underlies Cortical Neuron Microcircuit Hypoconnectivity Resulting from Exposure to Mutant Huntingtin Fragments." *The Journal of Pharmacology and Experimental Therapeutics* 335 (1): 13–22. doi:10.1124/jpet.110.167551.

Geraerts, Martine, Sofie Willems, Veerle Baekelandt, Zeger Debyser, and Rik Gijsbers. 2006.

"Comparison of Lentiviral Vector Titration Methods." *BMC Biotechnology* 6 (1): 34. doi:10.1186/1472-6750-6-34.

Glickman, M H, D M Rubin, H Fu, C N Larsen, O Coux, I Wefes, G Pfeifer, et al. 1999. "Functional Analysis of the Proteasome Regulatory Particle." *Molecular Biology Reports* 26 (1–2): 21–28. http://www.ncbi.nlm.nih.gov/pubmed/10363642.

Gold, Carl, Darrell A Henze, Christof Koch, and György Buzsáki. 2006. "On the Origin of the Extracellular Action Potential Waveform: A Modeling Study." *Journal of Neurophysiology* 95 (5): 3113–28. doi:10.1152/jn.00979.2005.

Gong, Bing, Miroslav Radulovic, and Maria E Figueiredo-pereira. 2016. "The Ubiquitin-Proteasome System : Potential Therapeutic Targets for Alzheimer ' S Disease and Spinal Cord Injury" 9 (January): 1–16. doi:10.3389/fnmol.2016.00004.

Gramowski, A, D Schiffmann, and G W Gross. 2000. "Quantification of Acute Neurotoxic Effects of Trimethyltin Using Neuronal Networks Cultured on Microelectrode Arrays." *Neurotoxicology* 21 (3): 331–42. http://www.ncbi.nlm.nih.gov/pubmed/10894123.

Groll, M, L Ditzel, J Löwe, D Stock, M Bochtler, H D Bartunik, and R Huber. 1997. "Structure of 20S Proteasome from Yeast at 2.4 A Resolution." *Nature* 386 (6624): 463–71. doi:10.1038/386463a0.

Groll, Michael, Wolfgang Heinemeyer, Sibylle Jager, Tobias Ullrich, Matthias Bochtler, Dieter Wolf, and Robert Huber. 1999. "The Catalytic Sites of 20S Proteasomes and Their Role in Subunit Maturation : A Mutational and Crystallographic Study" 96 (September): 10976–83.

Gross, G, Barry K. Rhoades, Hassan M.E. Azzazy, and Ming-Chi Wu. 1995. "The Use of

Neuronal Networks on Multielectrode Arrays as Biosensors." *Biosensors and Bioelectronics* 10 (6–7). Elsevier: 553–67. doi:10.1016/0956-5663(95)96931-N.

Gullo, Francesca, Andrea Maffezzoli, Elena Dossi, Marzia Lecchi, and Enzo Wanke. 2012. "Classifying Heterogeneity of Spontaneous up-States: A Method for Revealing Variations in Firing Probability, Engaged Neurons and Fano Factor." *Journal of Neuroscience Methods* 203 (2). Elsevier B.V.: 407–17. doi:10.1016/j.jneumeth.2011.10.014.

Gullo, Francesca, Irene Manfredi, Marzia Lecchi, Giorgio Casari, Enzo Wanke, and Andrea Becchetti. 2014. "Multi-Electrode Array Study of Neuronal Cultures Expressing Nicotinic Î²2-V287L Subunits, Linked to Autosomal Dominant Nocturnal Frontal Lobe Epilepsy. An in Vitro Model of Spontaneous Epilepsy." *Frontiers in Neural Circuits* 8 (July). Frontiers: 87. doi:10.3389/fncir.2014.00087.

Hales, Chadwick M, John D Rolston, and Steve M Potter. 2010. "How to Culture, Record and Stimulate Neuronal Networks on Micro-Electrode Arrays (MEAs)." *Journal of Visualized Experiments : JoVE*, no. 39: 1–7. doi:10.3791/2056.

Harris, Kenneth D, Rodrigo Quian Quiroga, Jeremy Freeman, and Spencer L Smith. 2016. "Improving Data Quality in Neuronal Population Recordings." *Nature Neuroscience* 19 (9). Nature Research: 1165–74. doi:10.1038/nn.4365.

Haynes, Kathryn A., Thuy K. Smith, Collin J. Preston, and Ashok N. Hegde. 2015. "Proteasome Inhibition Augments New Protein Accumulation Early in Long-Term Synaptic Plasticity and Rescues Adverse Aβ Effects on Protein Synthesis." American Chemical Society. doi:10.1021/ACSCHEMNEURO.5B00068.

Hernandez, Kristina, Przemyslaw Swiatkowski, Mihir V. Patel, Chen Liang, Natasha R.

Dudzinski, Linda M. Brzustowicz, and Bonnie L. Firestein. 2016. “Overexpression of Isoforms of Nitric Oxide Synthase 1 Adaptor Protein, Encoded by a Risk Gene for Schizophrenia, Alters Actin Dynamics and Synaptic Function.” *Frontiers in Cellular Neuroscience* 10 (February). doi:10.3389/fncel.2016.00006.

Johnston, Jennifer A., and Kiran Madura. 2004. “Rings, Chains and Ladders: Ubiquitin Goes to Work in the Neuron.” *Progress in Neurobiology* 73 (4): 227–57. doi:10.1016/j.pneurobio.2004.05.004.

Kapucu, Fikret E, Jarno M A Tanskanen, Jarno E Mikkonen, Laura Ylä-Outinen, Susanna Narkilahti, and Jari A K Hyttinen. 2012. “Burst Analysis Tool for Developing Neuronal Networks Exhibiting Highly Varying Action Potential Dynamics.” *Frontiers in Computational Neuroscience* 6 (June): 38. doi:10.3389/fncom.2012.00038.

Kapucu, Fikret Emre, Meeri E-L Mäkinen, Jarno M A Tanskanen, Laura Ylä-Outinen, Susanna Narkilahti, and Jari A K Hyttinen. 2016. “Joint Analysis of Extracellular Spike Waveforms and Neuronal Network Bursts.” *Journal of Neuroscience Methods* 259 (February): 143–55. doi:10.1016/j.jneumeth.2015.11.022.

Karra, Daniela, and Ralf Dahm. 2010. “Transfection Techniques for Neuronal Cells.” *The Journal of Neuroscience : The Official Journal of the Society for Neuroscience* 30 (18): 6171–77. doi:10.1523/JNEUROSCI.0183-10.2010.

Keith, Dove, and Alaa El-Husseini. 2008. “Excitation Control: Balancing PSD-95 Function at the Synapse.” *Frontiers in Molecular Neuroscience* 1 (March): 4. doi:10.3389/neuro.02.004.2008.

Knoblauch, Andreas. 2012. “What Is Signal and What Is Noise ?” *Realclimate.Org*, no. May

2004: 1–13.

Köller, H, M Siebler, C Schmalenbach, and H W Müller. 1990. “GABA and Glutamate Receptor Development of Cultured Neurons from Rat Hippocampus, Septal Region, and Neocortex.” *Synapse (New York, N.Y.)* 5 (1): 59–64. doi:10.1002/syn.890050105.

Konopaske, Glenn T., Nicholas Lange, Joseph T. Coyle, and Francine M. Benes. 2014. “Prefrontal Cortical Dendritic Spine Pathology in Schizophrenia and Bipolar Disorder.” *JAMA Psychiatry* 71 (12). American Medical Association: 1323. doi:10.1001/jamapsychiatry.2014.1582.

Kuebler, ES, and JP Thivierge. 2014. “Spiking Variability: Theory, Measures and Implementation in Matlab.” *Tqmp.Org*, 131–42. http://www.tqmp.org/Content/vol10-2/p131/p131.pdf.

Kulkarni, Vaishali A., and Bonnie L. Firestein. 2012. “The Dendritic Tree and Brain Disorders.” *Molecular and Cellular Neuroscience* 50 (1). Elsevier Inc.: 10–20. doi:10.1016/j.mcn.2012.03.005.

Kunjappu, Mary J, Mark Hochstrasser, and Dieter H Wolf. 2014. “Biochimica et Biophysica Acta Assembly of the 20S Proteasome ☆ α β β α.” *BBA - Molecular Cell Research* 1843 (1). Elsevier B.V.: 2–12. doi:10.1016/j.bbamcr.2013.03.008.

Kutzing, Melinda K., Vincent Luo, and Bonnie L. Firestein. 2011. “Measurement of Synchronous Activity by Microelectrode Arrays Uncovers Differential Effects of Sublethal and Lethal Glutamate Concentrations on Cortical Neurons.” *Annals of Biomedical Engineering* 39 (8): 2252–62. doi:10.1007/s10439-011-0319-0.

———. 2012. “Protection from Glutamate-Induced Excitotoxicity by Memantine.” *Annals of Biomedical Engineering* 40 (5): 1170–81. doi:10.1007/s10439-011-0494-z.

Kutzing, Melinda K, Christopher G Langhammer, Vincent Luo, Hersh Lakdawala, and Bonnie L Firestein. 2010. “Automated Sholl Analysis of Digitized Neuronal Morphology at Multiple Scales.” *Journal of Visualized Experiments : JoVE*, no. November: 2–7. doi:10.3791/2354.

Kwon, M., J. R. Fernandez, G. F. Zegarek, S. B. Lo, and B. L. Firestein. 2011. “BDNF-Promoted Increases in Proximal Dendrites Occur via CREB-Dependent Transcriptional Regulation of Cypin.” *Journal of Neuroscience* 31 (26): 9735–45. doi:10.1523/JNEUROSCI.6785-10.2011.

Kwon, Munjin, and Bonnie L. Firestein. 2013. “DNA Transfection: Calcium Phosphate Method.” In , 107–10. doi:10.1007/978-1-62703-444-9_10.

Langhammer, Christopher G., Michelle L. Previtera, Eric S. Sweet, Simranjeet S. Sran, Maxine Chen, and Bonnie L. Firestein. 2010. “Automated Sholl Analysis of Digitized Neuronal Morphology at Multiple Scales: Whole Cell Sholl Analysis versus Sholl Analysis of Arbor Subregions.” *Cytometry Part A* 77 A (12): 1160–68. doi:10.1002/cyto.a.20954.

Lee, Kwang Min, Jongwon Lee, and Chul-seung Park. 2012. “Cereblon Inhibits Proteasome Activity by Binding to the 20S Core Proteasome Subunit Beta Type 4.” *Biochemical and Biophysical Research Communications* 427 (3). Elsevier Inc.: 618–22. doi:10.1016/j.bbrc.2012.09.108.

Lei, Hong, Carolina E. Reisenman, Caroline H. Wilson, Prasad Gabbur, and John G.

Hildebrand. 2011. “Spiking Patterns and Their Functional Implications in the Antennal Lobe of the Tobacco Hornworm Manduca Sexta.” *PLoS ONE* 6 (8). doi:10.1371/journal.pone.0023382.

Levy, Jonathan, Xiaobing Chen, Thomas Reese, and Roger A. Nicoll. 2015. “Synaptic Consolidation Normalizes AMPAR Quantal Size Following MAGUK Loss” 6 (2): 356–72. doi:10.1007/s12671-013-0269-8.Moving.

Lin, Y., V. Arvydas Skeberdis, A. Francesconi, M.V.L. Bennett, and R.S. Zukin. 2004. “Postsynaptic Density Protein-95 Regulates NMDA Channel Gating and Surface Expression.” *Journal of Neuroscience* 24 (45): 10138–48. doi:10.1523/JNEUROSCI.3159-04.2004.

Litwin-Kumar, Ashok, and Brent Doiron. 2012. “Slow Dynamics and High Variability in Balanced Cortical Networks with Clustered Connections.” *Nature Neuroscience* 15 (11). Nature Publishing Group: 1498–1505. doi:10.1038/nn.3220.

Livneh, Ido, Victoria Cohen-kaplan, Chen Cohen-rosenzweig, Noa Avni, and Aaron Ciechanover. 2016. “The Life Cycle of the 26S Proteasome : From Birth , through Regulation and Function , and onto Its Death.” *Cell Research* In Press (8). Nature Publishing Group: 869–85. doi:10.1038/cr.2016.

Lüscher, C, R A Nicoll, R C Malenka, and D Muller. 2000. “Synaptic Plasticity and Dynamic Modulation of the Postsynaptic Membrane.” *Nature Neuroscience* 3 (6): 545–50. doi:10.1038/75714.

Malenka, Robert C., and Mark F. Bear. 2004. “LTP and LTD: An Embarrassment of Riches.” *Neuron* 44 (1): 5–21. doi:10.1016/j.neuron.2004.09.012.

Marques, A.J., Christoph Glanemann, Paula C Ramos, and R.J. Dohmen. 2007. "The C-Terminal Extension of the beta7 Subunit and Activator Complexes Stabilize Nascent 20 S Proteasomes and Promote Their Maturation *" 282 (48): 34869–76. doi:10.1074/jbc.M705836200.

Massobrio, Paolo, Jacopo Tessadori, Michela Chiappalone, and Mirella Ghirardi. 2015. "In Vitro Studies of Neuronal Networks and Synaptic Plasticity in Invertebrates and in Mammals Using Multielectrode Arrays." *Neural Plasticity* 2015. doi:10.1155/2015/196195.

Migaud, M, P Charlesworth, M Dempster, L C Webster, a M Watabe, M Makhinson, Y He, et al. 1998. "Enhanced Long-Term Potentiation and Impaired Learning in Mice with Mutant Postsynaptic Density-95 Protein." *Nature* 396 (6710): 433–39. doi:10.1038/24790.

Morefield, S I, E W Keefer, K D Chapman, and G W Gross. 2000. "Drug Evaluations Using Neuronal Networks Cultured on Microelectrode Arrays." *Biosensors & Bioelectronics* 15 (7–8): 383–96. http://www.ncbi.nlm.nih.gov/pubmed/11219752.

Moreno-Bote, Rub??n. 2014. "Poisson-Like Spiking in Circuits with Probabilistic Synapses." *PLoS Computational Biology* 10 (7). doi:10.1371/journal.pcbi.1003522.

Murata, Shigeo, Hideki Yashiroda, and Keiji Tanaka. 2009. "Molecular Mechanisms of Proteasome Assembly" 10 (fEbRuARy). doi:10.1038/nrm2630.

Myers, L, and M J Sirois. 2006. "Differences between Spearman Correlation Coefficients." *Encyclopedia of Statistical Sciences* 12 (1): 1–2. doi:10.1002/0471667196.ess5050.pub2.

O'Neill, Kate M, Barbara F Akum, Survandita T Dhawan, Munjin Kwon, Christopher G Langhammer, and Bonnie L Firestein. 2015. "Assessing Effects on Dendritic

Arborization Using Novel Sholl Analyses." *Frontiers in Cellular Neuroscience* 9 (July): 285. doi:10.3389/fncel.2015.00285.

Obien, Marie Engelene J, Kosmas Deligkaris, Torsten Bullmann, Douglas J. Bakkum, and Urs Frey. 2015. "Revealing Neuronal Function through Microelectrode Array Recordings." *Frontiers in Neuroscience* 9 (JAN): 423. doi:10.3389/fnins.2014.00423.

Pak, Daniel T S, Soyoung Yang, Sheila Rudolph-Correia, Eunjoon Kim, and Morgan Sheng. 2001. "Regulation of Dendritic Spine Morphology by SPAR, a PSD-95-Associated RapGAP." *Neuron* 31 (2): 289–303. doi:10.1016/S0896-6273(01)00355-5.

Perez de Arce, Karen, Karen Perez de Arce, Lorena Varela-Nallar, Olivia Farias, Alejandra Cifuentes, Paulina Bull, Brian A Couch, Anthony J Koleske, Nibaldo C Inestrosa, and Alejandra R Alvarez. 2010. "Synaptic Clustering of PSD-95 Is Regulated by c-Abl through Tyrosine Phosphorylation." *The Journal of Neuroscience : The Official Journal of the Society for Neuroscience* 30 (10). NIH Public Access: 3728–38. doi:10.1523/JNEUROSCI.2024-09.2010.

Ponce-Alvarez, Adrián, Bjørg Elisabeth Kilavik, and Alexa Riehle. 2010. "Comparison of Local Measures of Spike Time Irregularity and Relating Variability to Firing Rate in Motor Cortical Neurons." *Journal of Computational Neuroscience* 29 (1–2): 351–65. doi:10.1007/s10827-009-0158-2.

Quian Quiroga, Rodrigo. 2004. "Spike Sorting — University of Leicester." http://www2.le.ac.uk/centres/csn/research-2/spike-sorting.

Quiroga, R Quian, Z Nadasdy, and Y Ben-Shaul. 2004. "Unsupervised Spike Detection and Sorting with Wavelets and Superparamagnetic Clustering." *Neural Computation* 16 (8):

1661–87. doi:10.1162/089976604774201631.

Raichman, Nadav, and Eshel Ben-Jacob. 2008. "Identifying Repeating Motifs in the Activation of Synchronized Bursts in Cultured Neuronal Networks." *Journal of Neuroscience Methods* 170 (1): 96–110. doi:10.1016/j.jneumeth.2007.12.020.

Rey, Hernan G., Matias J. Ison, Carlos Pedreira, Antonio Valentin, Gonzalo Alarcon, Richard Selway, Mark P. Richardson, and Rodrigo Quian Quiroga. 2015. "Single-Cell Recordings in the Human Medial Temporal Lobe." *Journal of Anatomy* 227 (4): 394–408. doi:10.1111/joa.12228.

Rey, Hernan Gonzalo, Carlos Pedreira, and Rodrigo Quian Quiroga. 2015. "Past, Present and Future of Spike Sorting Techniques." *Brain Research Bulletin* 119. Elsevier Inc.: 106–17. doi:10.1016/j.brainresbull.2015.04.007.

Scaglione, A., K. A. Moxon, J. Aguilar, and G. Foffani. 2011. "Trial-to-Trial Variability in the Responses of Neurons Carries Information about Stimulus Location in the Rat Whisker Thalamus." *Proceedings of the National Academy of Sciences of the United States of America* 108 (36): 14956–61. doi:10.1073/pnas.1103168108.

Schnell, Eric, Max Sizemore, Siavash Karimzadegan, Lu Chen, David S Bredt, and Roger A Nicoll. 2002. "Direct Interactions between PSD-95 and Stargazin Control Synaptic AMPA Receptor Number." *Proceedings of the National Academy of Sciences of the United States of America* 99 (21): 13902–7. doi:10.1073/pnas.172511199.

Schuman, Erin M, Joseph L Dynes, and Oswald Steward. 2006. "Synaptic Regulation of Translation of Dendritic mRNAs." *The Journal of Neuroscience* 26 (27): 7143–46. doi:10.1523/jneurosci.1796-06.2006.

Selinger, Jonathan V., Joseph J. Pancrazio, and Guenter W. Gross. 2004. "Measuring Synchronization in Neuronal Networks for Biosensor Applications." *Biosensors and Bioelectronics* 19 (7): 675–83. doi:10.1016/S0956-5663(03)00267-7.

Shadlen, M N, and W T Newsome. 1994. "Noise, Neural Codes and Cortical Organization." *Current Opinion in Neurobiology* 4 (4): 569–79. http://www.ncbi.nlm.nih.gov/pubmed/7812147.

Sheng, M. 2001. "Molecular Organization of the Postsynaptic Specialization." *Proceedings of the National Academy of Sciences of the United States of America* 98 (13): 7058–61. doi:10.1073/pnas.111146298.

Sheng, Morgan, and Casper C Hoogenraad. 2007. "The Postsynaptic Architecture of Excitatory Synapses: A More Quantitative View." *Annual Review of Biochemistry* 76: 823–47. doi:10.1146/annurev.biochem.76.060805.160029.

Snyder, Heather, Kwame Mensah, Catherine Theisler, Jack Lee, Andreas Matouschek, and Benjamin Wolozin. 2003. "Aggregated and Monomeric Alpha-Synuclein Bind to the S6' Proteasomal Protein and Inhibit Proteasomal Function" 278 (14): 11753–59. doi:10.1074/jbc.M208641200.

Softky, W R, and C Koch. 1993. "The Highly Irregular Firing of Cortical Cells Is Inconsistent with Temporal Integration of Random EPSPs." *The Journal of Neuroscience : The Official Journal of the Society for Neuroscience* 13 (1): 334–50. http://www.ncbi.nlm.nih.gov/pubmed/8423479.

Softky, William R. 1992. "Cortical Cells Should Fire Regularly , But Do Not." *Neural Computation* 646: 643–46. doi:10.1162/neco.1992.4.5.643.

Sun, Qian, and Gina G Turrigiano. 2011. “PSD-95 and PSD-93 Play Critical But Distinct Roles in Synaptic Scaling Up and Down.” *The Journal of Neuroscience : The Official Journal of the Society for Neuroscience* 31 (18): 6800–6808. doi:10.1523/JNEUROSCI.5616-10.2011.

Sweet, E. S., M. L. Previtera, J. R. Fernandez, E. I. Charych, C.-Y. Tseng, M. Kwon, V. Starovoytov, J. Q. Zheng, and B. L. Firestein. 2011. “PSD-95 Alters Microtubule Dynamics via an Association With EB3.” *Journal of Neuroscience* 31 (3): 1038–47. doi:10.1523/JNEUROSCI.1205-10.2011.

Tau, Gregory Z, and Bradley S Peterson. 2010. “Normal Development of Brain Circuits.” *Neuropsychopharmacology* 35 (1): 147–68. doi:10.1038/npp.2009.115.

Tsai, Nien Pei, Julia R. Wilkerson, Weirui Guo, Marina A. Maksimova, George N. Demartino, Christopher W. Cowan, and Kimberly M. Huber. 2012. “Multiple Autism-Linked Genes Mediate Synapse Elimination via Proteasomal Degradation of a Synaptic Scaffold PSD-95.” *Cell* 151 (7). Elsevier Inc.: 1581–94. doi:10.1016/j.cell.2012.11.040.

Tseng, C.-Y., and B. L. Firestein. 2011. “The Role of PSD-95 and Cypin in Morphological Changes in Dendrites Following Sublethal NMDA Exposure.” *Journal of Neuroscience* 31 (43): 15468–80. doi:10.1523/JNEUROSCI.2442-11.2011.

Turrigiano, Gina G., and Sacha B. Nelson. 2012. “Homeostatic Plasticity in the Nervous System.” *Neural Plasticity* 2012. doi:10.1155/2012/913472.

Um, J. W., E. Im, H. J. Lee, B. Min, L. Yoo, J. Yoo, H. Lubbert, et al. 2010. “Parkin Directly Modulates 26S Proteasome Activity.” *Journal of Neuroscience* 30 (35): 11805–14. doi:10.1523/JNEUROSCI.2862-09.2010.

Vandenberghe, Wim, Roger A Nicoll, and David S Bredt. 2005. “Stargazin Is an AMPA

Receptor Auxiliary Subunit." *Proceedings of the National Academy of Sciences of the United States of America* 102 (2): 485–90. doi:10.1073/pnas.0408269102.

Vetter, Philipp, Arnd Roth, Michael Häusser, Paolo Medini, Anna L Huguenard, Shannon M Fernando, D Ashley Monks, Dale R Sengelaub, Debora Ledergerber, and Matthew Evan Larkum. 2012. "Propagation of Action Potentials in Dendrites Depends on Dendritic Morphology Propagation of Action Potentials in Dendrites Depends on Dendritic Morphology," 926–37.

Vogel, A. 2005. "Increase of Neuronal Response Variability at Higher Processing Levels as Revealed by Simultaneous Recordings." *Journal of Neurophysiology* 93 (6): 3548–59. doi:10.1152/jn.01288.2004.

Wagenaar, Daniel A, Jerome Pine, and Steve M Potter. 2006. "An Extremely Rich Repertoire of Bursting Patterns during the Development of Cortical Cultures." *BMC Neuroscience* 7 (1): 11. doi:10.1186/1471-2202-7-11.

Weir, Keiko, Oriane Blanquie, Werner Kilb, Heiko J Luhmann, and Anne Sinning. 2014. "Comparison of Spike Parameters from Optically Identified GABAergic and Glutamatergic Neurons in Sparse Cortical Cultures." *Frontiers in Cellular Neuroscience* 8 (January): 460. doi:10.3389/fncel.2014.00460.

White, B., L. F. Abbott, and J. Fiser. 2012. "Suppression of Cortical Neural Variability Is Stimulus- and State-Dependent." *Journal of Neurophysiology* 108 (9): 2383–92. doi:10.1152/jn.00723.2011.

Yudowski, Guillermo A., Olav Olsen, Hillel Adesnik, Kurt W. Marek, and David S. Bredt. 2013. "Acute Inactivation of PSD-95 Destabilizes AMPA Receptors at Hippocampal

Synapses." *PLoS ONE* 8 (1): 1–9. doi:10.1371/journal.pone.0053965.

Yuste, R, and T Bonhoeffer. 2001. "Morphological Changes in Dendritic Spines Associated with Long-Term Synaptic Plasticity." *Annual Review of Neuroscience* 24: 1071–89. doi:10.1146/annurev.neuro.24.1.1071.